Regulating electrolyte solvation structure by metal-organic framework for high-performance rechargeable aqueous zinc batteries

September 2021

Huijun Yang

Regulating electrolyte solvation structure by metal-organic framework for high-performance rechargeable aqueous zinc batteries

Graduate School of Systems and Information Engineering
University of Tsukuba

September 2021

Huijun Yang

ABSTRACT

The great pressure on environment pollution and limited fossil fuel energy call for a clean, sustainable, and renewable energy supply, where energy storage systems maximum its energy utilization efficiency. Among the extensive family of energy storage systems, rechargeable zinc (Zn) batteries emerge as an extremely safe and low-cost choice, especially in comparison with the current rechargeable lithium-ion batteries. The advantages of rechargeable Zn batteries lie in the high abundance of Zn element, accessible to aqueous electrolyte and safe operation. However, since its initial research on 18th century, the progress on Zn anode reversibility, Zn dendrite manipulation and its short lifespan remain sluggish. In this thesis, we contribute to reveal the Zn battery failure mechanism and propose an effective electrolyte solvation structure regulation strategy to enhance Zn anode stability.

The major concern lies in the thermodynamic instability of Zn metal anode in aqueous environment. The free water molecular in bulk electrolyte and the electric double layer would corrode Zn anode during static and electrochemical working period. The strong water activity, especially the released water molecular from the de-solvation process, where happened in electric double layer region prior to final redox reaction process, would significantly cause the Zn anode morphology change, surface passivation and poor reversibility. One effective approach is developing highly concentrated aqueous electrolyte to coordinate most of water molecular and eliminate the fraction of free water molecular. However, this strategy would simultaneously cause burden in cost and physical property in saturated electrolyte. Inspired by renowned application of metal-organic frameworks (MOFs) for gas and solution separation, herein, we demonstrated MOF as ionic sieve coating/membrane

for tailoring the electrolyte solvation structure.

Firstly, we thoroughly studied the Zn metal degradation mechanism from the perspective of water passivation. Based on the general knowledge on electrolyte solvation structure, we proposed a zeolitic imidazolate (ZIF-7) coating on Zn anode surface to shield the attack of water molecular. As a front surface layer, the small pore size distribution (2.94 Å) can effectively block the directional migration of large ion-pairs under the electric field and then completed a partial de-solvation process in the interface of ZIF-7 layer. Raman spectra revealed a highly coordinated ion-pairs and suppressed water activity, which indicates a super-concentrated electrolyte solvation structure on Zn anode front surface. Benefitting the ZIF-7 front layer, the reversibility of Zn metal is significantly enhanced owing to round-edged electrodeposit morphology and neat surface without considerable side-products. In aspect of electrochemical behaviors, the ZIF-7 protected Zn anode enables the progress of symmetric cell lifespan to 3000 hours at 0.5 mA cm^{-2}/0.5 mAh cm^{-2} and a high cyclic stability over 600 cycles for Zn-MnO_2 battery with capacity retention of 88.9%. This approach was proved effective, and the concept can be probably extended to other types of metal-ion battery, not just in plating/stripping process of metal anode, but also for electrode reversibility.

To resolve the poor behaviors of high-current density of Zn anode and fast-charging Zn battery, we developed a multifunctional MOF membrane for Zn-I_2 battery. The highly efficient redox couples of Zn/Zn^{2+} and triiodide/iodide (I_3^-/I^-) in aqueous electrolyte has a prospect for scale-up application because of their high element abundance. Moreover, the liquid-liquid conversion mechanism also favors fast-charging. However, this promising system faced severe bottlenecks such as shuttle effect of soluble iodine species, poor Zn anode reversibility and their complex interplay on Zn anode surface. In this thesis, we contribute to reveal the interplay

between diffused iodine species with Zn anode surface in aqueous electrolyte environment by Raman and micro-IR spectroscopy characterizations. Our proposed functional Zn-BTC ($Zn_3(BTC)_2$) membrane, not only resolved the free migration of iodine species (negative electrode), but also favors Zn anode stability (positive electrode). Based on the synergistic effect on both iodine negative and Zn positive electrodes, our proposed rechargeable Zn-I_2 with Zn-BTC membrane significantly improved the cyclic life to 6000 cycles under high current density (1920 mA g^{-1}) and high cell reversibility with a high average Coulombic efficiency over 99.65%. Our study carried out a systematical analysis on battery degradation mechanism and proposed an efficient strategy to resolve these shortcomings.

Our original findings highlight the negative role of strong water activity for Zn anode degradation mechanism and contribute to a MOF coating/membrane strategy to resolve the related concerns. We believe that the comprehensive study in this dissertation would enlighten more insight and discovery in future better Zn batteries.

TABLE OF CONTENTS

LIST OF FIGURES

LIST OF TABLES

Chapter 1. General introduction

1.1 Shift from fossil fuel energy to renewable energy

The employment of fossil fuel energy greatly improved the productivity, economic development, and people life.[1-2] A wide spectrum of machine based on fossil fuel energy such as vehicle, aircraft and ships have been invented and utilized.[3] Even nowadays, fossil fuel energy remains a critical role in various industries and our daily life. However, the global increase in the use of and reliance on fossil fuel energy accelerated the consumption and triggered the energy crisis (**Figure 1.1**). First, the limited storage of fossil fuel energy is estimated to be incapable to satisfy the requirement of current industry development.[4] Moreover, as a natural wealth, the uneven distribution of fossil fuel energy would easily induce military conflict, which remains one of the greatest threats for people life.[5] Most importantly, the extensive consumption of fossil fuel energy causes serious environmental pollution in land, air, and lake, which cannot be overlooked nowadays. Thus, people anticipate a sustainable, durable, green, and cost-effective renewable energy to replace the fossil fuel energy. Among them, renewable energy such as solar, wind and biomass were considered as one of the most promising candidates.[6]

In consideration of the difficulty of directly powering electric devices by renewable energy, how to develop efficient energy storage became one of the most challenging problems. **Figure 1.2** shows the multi-function of energy storage system to equip with the renewable energy.[7] First of all, most of renewable energy can be stored in power station and transported to factories, office buildings, commercial facilities and homes. In detail, static energy storage devices play a vital role in alleviating the burden of powerhouse. Therefore, this part has higher demand in cost,

safety, and service life, but less interest in high-energy-density. Other mobile energy storage devices, which employ in electric vehicles and portable electronic devices urge a high-energy-density system for long-term use. Especially, the development of electric vehicles from previous gasoline vehicles significantly enlarged the market of energy storage systems. In all, the development of energy storage devices become the hotspot in the related field and require a good integration from the perspective of energy, chemistry, materials, and engineering.[8-10]

Figure 1.1 The extensive utilization of fossil fuel energy triggered the energy crisis owing to the limited storage, and environmental concerns. Pictures are harvested from https://theconversation.com/co-shortage-why-cant-we-just-pull-carbon-dioxide-out-of-the-air-99255(July.2018);https://sustainablejapan.jp/2019/09/26/uniting-behind-the-science-to-step-up-ambition-by-2020/42530;https://www.harmees.com/articles/view/501314.html(Sept.2019);https://www.assignmentpoint.com/business/economics/energy-crisis-definition-causes.html.

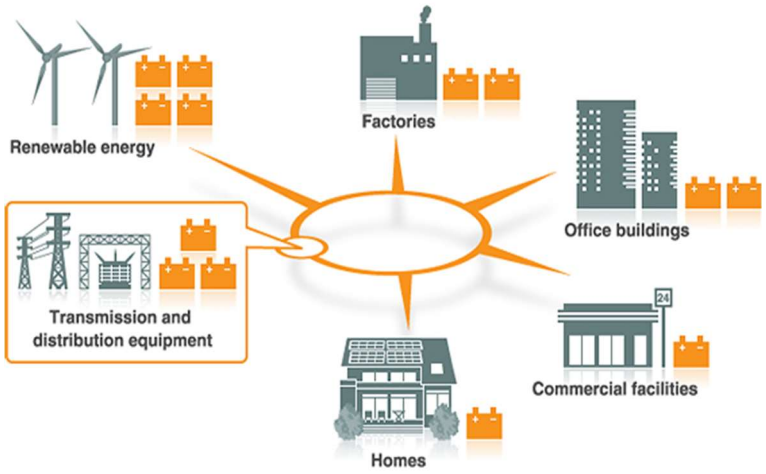

Figure 1.2 The development of energy storage systems can maximum the energy utilization efficiency. Picture is harvested from https://tr.nec.com/en_TR/global/environment/energy/nec_aes/index.html.

1.2 Energy storage systems: batteries and applications

Energy storage systems function as the carrier for better energy transmission and distribution. The emergence and application of energy storage systems greatly reshaped people life.[11] Among them, rechargeable batteries have several overwhelming advantages in terms of high-energy-density and long cyclic life. With the continuous development in materials and electrolytes, more and more types of rechargeable batteries were invented and applied. Rechargeable battery generally consists of two electrode materials to reversibly store ion, electrolyte for ion transport and separator for avoiding short-circuit. One of the most representative is lithium-ion battery, which has been widely employed in our daily life. LIB system generally consists of electrode materials to store lithium ion (Li^+), electrolyte for Li^+ transport and separator for avoiding short-circuit.[12-13] Herein, I give a brief introduction of LIB including its development and application. The rapid development of LIB was dependent on a series of important invention of graphite anode and lithium transitional metal oxide cathodes, discovery of ethylene carbonate-based (EC)

carbonate ester electrolytes.[14] After significant progress on optimizations, LIB was commercialized and dominated lots of market in energy storage field.[15-17] As shown in **Figure 1.3**, LIB power most of 3C portable electronic (computer, mobile phone and digital camera), electric vehicle, and some special purpose (aerospace and military). However, the extensive employment of LIB nowadays induced some concerns. First of all, LIB confronted severe safety concerns because of the extreme flammable organic electrolyte and reactive oxygen release from the cathodes.[18] The great number of reports about catching fire or explosion from electric vehicles caused panic among users. Moreover, the significant dependence on mineral resources, especially expensive cobalt and lithium triggered the price increase.[19] Therefore, the research shift to more safe and cost-effective battery system become the hotspot for researchers all over the world.

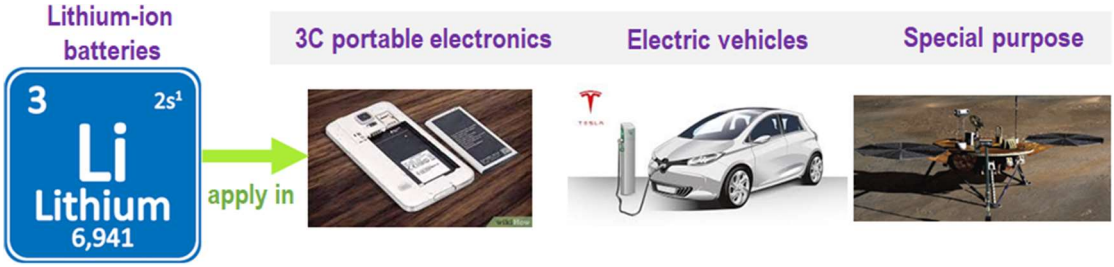

Figure 1.3 Basic property of lithium element and the application of lithium-ion battery electronic devices. Pictures are harvested from https://www.wikihow.com/Choose-a-Mobile-Phone-Battery(May.2021);https://www.phoneworld.com.pk/morris-garage-is-ready-to-launch-first-ever-ev-in-pakistan-by-2021/(June.2020);https://www.nasa.gov/mission_pages/phoenix/main/index.html(Aug.2008).

As one of the eldest batteries, zinc (Zn) battery also has a dominant market in energy field, especially in primary battery (**Figure 1.4**).[20] The normal operation of Zn battery involves the migration of Zn ion (Zn^{2+}) in the bulk electrolyte and redox reaction in positive electrode, and plating/stripping process on Zn anode. However,

the uncontrollable Zn dendrite growth made it unsatisfactory cyclic life.[21-23] Most of application of Zn battery are still stopped at primary battery. Primary battery means one-time use without recharging, which is different from secondary battery with repeated charging and discharging process. Primary battery is designed and used for an extensive requirement in portable electronic devices and some household appliances. The dominated (90%) market of primary batteries nowadays caused severe environmental concerns owing to the frequent discards of primary battery. The most typical primary Zn battery is a dry cell which offers a direct electric current from the controlled reaction from Zn anode and manganese dioxide (MnO_2). The employment of alkaline gel electrolyte prevents the leakage of electrolyte. The cell composes of a carbon rod for electron transport from MnO_2 electrode, which gives it name of Zn-carbon battery. The cell provides about 1.5 volts (V) which can satisfy most of electronic devices after more cells connected in series or in parallel. Recently, the research based on Zn flow battery also arises considerable interests owing to its safety and low-cost. Zn flow battery based on aqueous electrolyte involved a plating/stripping process on Zn negative electrode and a redox reaction in positive electrolyte such as chlorine, bromine, and iodine couples in aqueous electrolyte. The flow electrolyte not only greatly addressed the concern of Zn dendrite growth, but also favors the reaction kinetics of positive electrodes. Based on safe aqueous electrolytes, we can participate its bright future with continuous progress in both scientific and engineering aspect. Moreover, Zn battery can also satisfy some flexible purposes. In all, the development of promising Zn battery can benefit the efficiency of people life.[24]

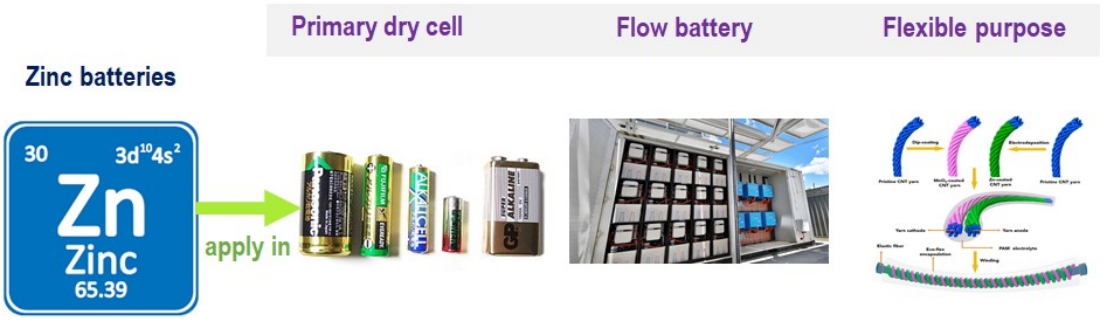

Figure 1.4 Basic property of Zn element and the application of Zn battery in primary dry cell, flow battery and flexible purpose. Pictures are harvested from https://www.electroniclinic.com/what-is-battery-types-of-battery-primary-and-secondary-cells/(Mar.2020);https://www.sciencemag.org/news/2018/10/new-generation-flow-batteries-could-eventually-sustain-grid-powered-sun-and-wind(Oct.2018);http://www.yhcl2016.com/xinwenzixun/9.html.

1.3 History of Zn battery from primary to secondary

Before in-depth research on Zn battery, we have to well acquainted with the development history and its study direction (**Figure 1.5**). The first electrical battery in people life can be dated back to the invention of voltaic pile in 1799.[25] The voltaic pile was stacked by Zn foil (negative electrode) and copper foil (positive electrode), which were separated by cloth absorbing with brine solution (electrolyte). Since that, researchers gradually developed lots of concepts to describe the electrochemistry, such as water electrolysis into oxygen (O_2) and hydrogen (H_2) and the discovery of reactive metals (sodium, potassium, and calcium, etc.). Then, the Daniell cell was invented by changing the electrolyte into copper (II) sulfate ($CuSO_4$) solution by mitigating hydrogen evolution in voltaic pile.[26] Daniell cell can deliver ca. 1.10 volt (V) based on the redox couples of Zn and Cu in $CuSO_4$ electrolyte. Owing to the reliable performance, Daniell cell was widely employed in telegraph networks prior to the invention of Leclanché cell in 1868.[27]

The Leclanché cell soon dominated battery market because of its widespread application in portable electronics. The cell design replaced the electrolyte into ammonium chloride (NH_4Cl) solution, and positive electrode into MnO_2. The extensive application in small electronic devices not only made it more mature, but also became the forerunner of the famous Zn-carbon cell. The Zn-carbon cell was modified by zinc chloride ($ZnCl_2$) addition into electrolyte, which enabled a working platform increasing from 1.4 to 1.5 V. After that, the modified Zn-MnO_2 cell in alkaline electrolyte based on Leclanché cell was developed. Because of no liquid electrolyte, the dry cell avoided electrolyte spilling and then achieved great commercial success.[28]

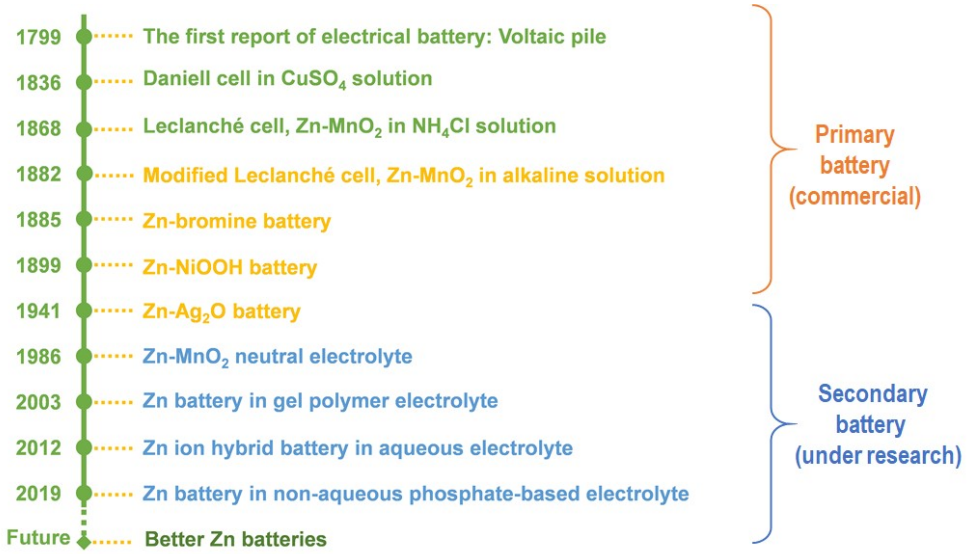

Figure 1.5 History of Zn battery from primary to rechargeable.

Besides the cell based on MnO_2 cathode, other types of primary cells were still under development. For example, Zn-Ni cell composed of Zn plate, NiOOH cathode and alkaline electrolyte and contributed a high voltage of 1.6 V.[29] Since its development in 1899, the application of Zn-Ni cell has exceeded over 100 years and was expected as a competitive alternative compared with lead-acid batteries or nickel-cadmium batteries. However, one of the major concerns lies in the severe self-discharge rate of Zn-Ni cell and poor reversibility of Zn metal anode. After that,

primary silver-oxide battery was invented, which used silver oxide as cathode and Zn as anode. Because of its constant nominal voltage, Zn-Ag primary cell obtained large market and commercial success.

Even up to now, the dry cell and Zn-Ag cell still serves in our daily life.[30] To reduce the dependence on resource, researchers try to develop a high-efficient rechargeable batteries and concentrates on the poor reversibility of Zn metal. Compared with conventional alkaline electrolyte, most of neutral aqueous electrolyte has a dynamic stability with Zn metal and provides a choice for reversible Zn plating/stripping.[31] Then, most of rechargeable Zn batteries with advanced aqueous electrolytes were proposed and developed. However, the major concerns of dendrite growth and severe hydrogen evolution reaction remain challenges for future researchers. We anticipate the final development of a better Zn battery with long lifespan, high-energy-density, and high security (**Figure 1.5**).[32-38]

1.4 Advantages of Zn ion battery

After the introduction of brief history of Zn battery development, here I would like to highlight the motivation of research on Zn battery. Firstly, Zn metal anode has a very high specific capacity based on volume because of its high metal density. On the contrary, the representative reactive metals have attractive high specific capacities based on mass (**Figure 1.6a**).[39] The development of Zn batteries favors the devices with high demands on volumetric energy density. Secondly, Zn metal operation is very convenient in the air environment owing to its stable property (**Figure 1.6b**).[40] Compared with alkaline metals, the air-stable property enables it convenient operation in the air ambient. Moreover, when it paired with aqueous electrolyte, the Zn battery becomes a highly safe system (**Figure 1.6c**). In comparison, reactive metals such as lithium and sodium were highly sensitive to air environment, facing severe safety

issues in practical applications. Lastly, Zn metal is also very cheap and suitable for large-scale operation (**Figure 1.6d**).[41]

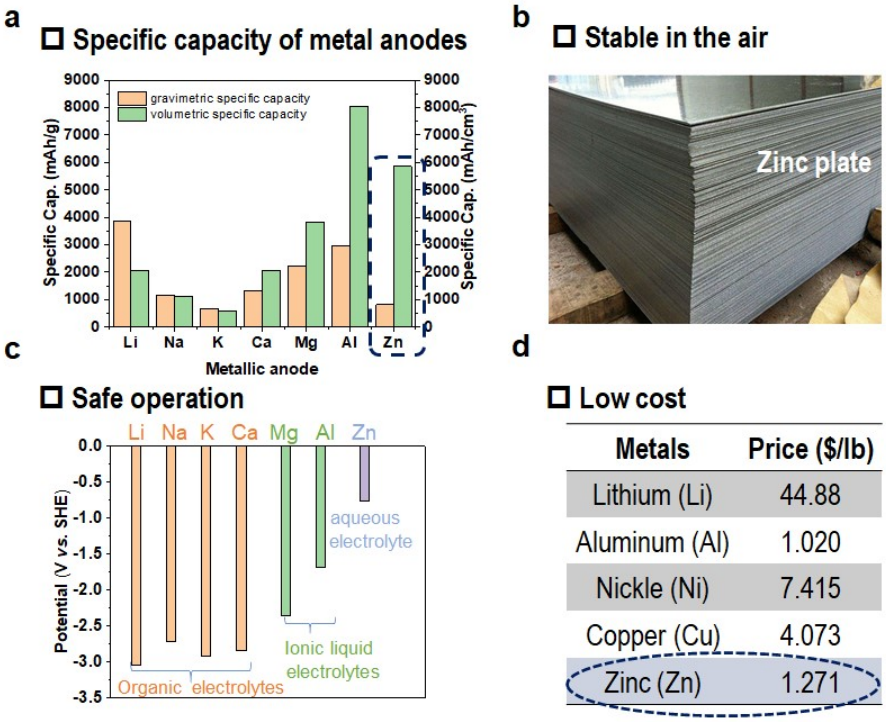

Figure 1.6 Advantages of Zn ion battery. (a) High specific capacity based on volume. (b) Stable property in the air. (c) Safe operation in aqueous electrolyte. (d) Low-cost of Zn metal. Picture in (b) is from https://www.okchem.com/product/al_powder-coated-galvanized-mild-steel-plate_60814268397_11386711.html.

1.5 The problems of Zn batteries: electrolyte issue

However, the development of Zn batteries confronted significant problems, mainly attributed to electrolytes. The metal anodes involved severe side-reaction with electrolytes, leaving side-product accumulation and inhomogeneous metal deposition. The enlarged over-potential of electrodes would degrade cell performance. Reactive metal anodes such as lithium, sodium, magnesium, and aluminum cannot survived in typical aqueous electrolyte and involved severe hydrogen evolution reaction.

Fortunately, our research target, Zn metal anode survived in the aqueous electrolyte owing to its moderate operation potential, -0.76 V versus standard hydrogen electrode. The employment of aqueous electrolyte made it an extremely safe choice for energy storage devices. Moreover, aqueous electrolyte also benefits the Zn battery system a low-cost and green choice. However, its long-term plating/stripping Zn metal anode in rechargeable batteries faced negative issues of side-reaction and Zn dendrite growth. The Zn battery study required scientific understating on the failure mechanism and effective strategy to resolve these problems.

Herein, I would like to clearly illustrate the failure mechanism of Zn metal anode in different types of electrolytes. Firstly, the acid electrolyte was not suitable for long-term working of Zn metal anode owing to its fast hydrogen evolution[42] (**Figure 1.7a**). In fact, most efforts in previous study were paid on alkaline electrolyte in primary battery such as dry cell in our daily life. Zn would be reacted with hydroxide anion and become into zinc tetra hydroxide anion. However, the poor reversibility would cause severe dendrite growth and shape change even with the common strategies of Al_2O_3 or SiO_2 layers (**Figure 1.7b**).[42] In recent years, most of attention was paid in neutral electrolyte (pH: 6~7), leaving relatively mild side-reaction with Zn anode (**Figure 1.7c**).[43] However, the repeated Zn plating/stripping process would also corrode Zn anode in neutral electrolyte. In brief, the water molecular corrosion can be mainly divided into two parts. One is the free water molecular, which exists in the bulk electrolyte and absorbs on the Zn anode surface. The lengthy soaking of Zn anode in aqueous electrolyte would automatically cause uneven morphology and side-product accumulation. Besides, before Zn^{2+} ion transfer and deposition, desolvation process would inevitably release some reactive water molecule within the electric double layer (EDL). This electrochemical corrosion would significantly exacerbate Zn anode, which is accompanied by the dendrite formation and shape

change with larger specific surface areas. Lots of literatures reported a wide spectrum of effective strategy to enhance the Zn anode performance.

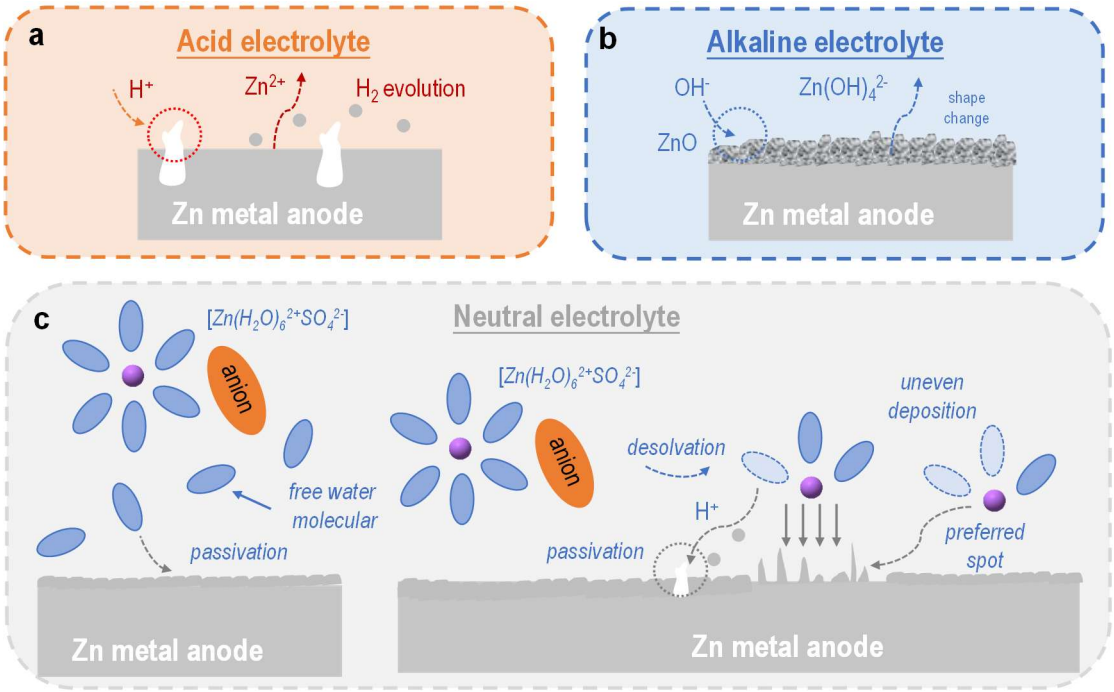

Figure 1.7 The problems of Zn in different types of aqueous electrolytes (a) Obvious metal dissolution in acid electrolyte and hydrogen evolution reaction. (b) Severe dendrite growth and shape change of Zn metal working in alkaline electrolyte. (c) Zn dendrite growth and surface passivation reaction from strong water activity.

1.6 Effective electrolyte strategies for Zn anode protection

One of the most of effective strategy is using water-in-salt electrolyte, which was developed by a famous scholar Prof. Chunsheng Wang.[44] By creating a highly concentrated aqueous electrolyte, the water molecule was highly coordinated with salt and the water activity was significantly suppressed, as the NMR result revealed (**Figure 1.8a**). This method was proved effective for homogeneous and reversible Zn deposition (**Figure 1.8b-c**). Following reports proved adding diluents would inherits the benefits of water-in-salt electrolyte system but effectively decrease the salt concentration.[44]

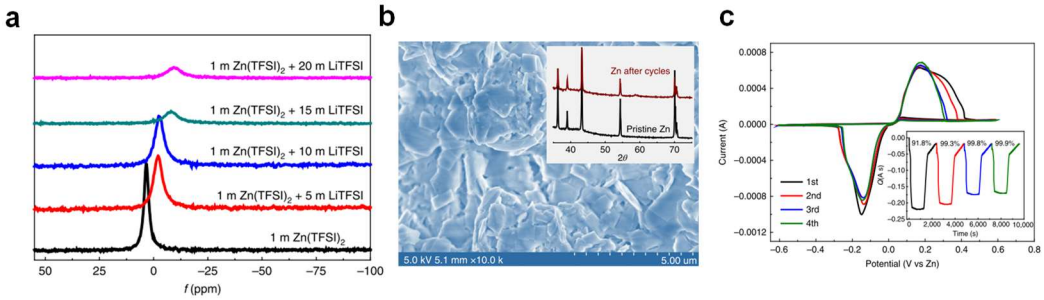

Figure 1.8 Zn behaviors in highly concentrated aqueous electrolyte.[44] (a) Nuclear magnetic resonance spectroscopy results. (b) SEM images of Zn electrodeposit. (c) Coulombic efficiency of Zn electrodeposit.

1.7 Motivation and targets of this dissertation

1.7.1 Motivation of this dissertation

The continuous boosting demands in electric devices for urges a high-efficient, low-cost, long-life energy storage system. The present commercial Li-ion batteries dominated most of battery sales but facing several major concerns such as safety concerns, high-cost and limited minder sources. As a competitive alternative, rechargeable Zn batteries are considered as a safe and sustainable choice among a wide-spectrum rechargeable battery. Besides, the high abundance of Zn element and high energy density also make it a promising candidate for next-generation rechargeable batteries. However, the adoption of rechargeable Zn batteries still has several challenges, such as poor Zn reversibility and dendrite growth. In this dissertation, we attributed these related problems of Zn metal to strong water activity in aqueous electrolyte and contributed to an effective strategy to suppress water activity.

In brief, the water molecular released from de-solvation process would corrode Zn metal. The related issues generally were tackled by introducing high concentration of salts to coordinate water molecular and suppress water activity. However, this

approach not only causes an economic burden in electrolyte costs, but also degrades the physical properties (ionic conductivity and viscosity) of electrolytes. Herein, we bypass this strategy and adopt another concept to regulate electrolyte solvation structure. Based on a simple and low-cost approach, we indeed improve the electrochemical behaviors of Zn batteries.

1.7.2 Outline of this dissertation

This dissertation composes of five chapters as following:

Chapter 1 presents a general introduction of the dissertation. In this chapter, a detailed background of Zn batteries and the development history are illustrated. The content covers the challenges for Zn batteries and the failure mechanism of Zn metal in different types of electrolytes. Finally, we propose our strategy and method of regulating electrolyte solvation structure.

Chapter 2 covers the experimental section of Chapter 3 and 4, separately.

Chapter 3 systematically discussed the reactive water releasing from de-solvation process and its side-effect for Zn metal anode. Based on the in-depth understanding on electrolyte solvation structure, we proposed an effective electrolyte solvation structure regulation approach. The method using MOF materials bypasses the disadvantages (poor ionic conductivity and high viscosity) for conventional high concentrated aqueous electrolyte. We the proved the MOF with abundant pores and caves can be employed to accommodate ion-pairs of electrolytes and reject migration of most of large ion-pairs. Raman spectroscopy revealed that water activity in ZIF-7 channels was highly suppressed and the Zn^{2+}-H_2O ion-pairs was signficantly enhanced. It indicates that ZIF-7 channels realized a super-saturated electrolyte in ZIF-7 channels in battery working period. Benefitted from supersaturated front surface on Zn anode surafec, the lifespan of symmetric Zn half cell was promoted to

3000 hours at 0.5 mA cm^{-2} without obvious voltage fluctiation. The lifespan of Zn-MnO_2 battery was also prolonged up to 600 cycles, with a high capacity-retention of 88.9%. However, this approach cannot satisfy for high-rate and fast-charging batteries.

Therefore, we modified the MOF channel to larger pore size, which can accomodate larger ion-pairs in Chapter 4. In this work, we demonstrate a multifunctional Zn-BTC membrane for Zn-I_2 battery system and contributed to reveal the electrode degradation mechanism. For the Zn metal anode protection, the Zn-BTC channel realized a fully CIP solvation mode, which enables highly reversible Zn electrodeposit and improve the current density to 5 mA cm^{-2}. For cathode, the liquid-liquid conversion mechanism favors fast-charging property. Moreover, the Zn-BTC membrane was proved effective to shield the shuttle of iodine active species.

In all, this dissertation concentrates on the electrolyte solvation structure regulation by MOF strategy and demonstrates two types of representative aqeuous Zn batteries. One is rechargeable Zn-MnO_2 battery, which is not only the successor of primary dry cell, but also is one of the most promising for high-energy aqueous batteries. Another is aqueous Zn-I_2 battery, which can satisfy for fast-charging demands. We anticipate that this concept can be widely extended to other types aqueous and non-aqueous rechargeable batteries.

Chapter 5 belongs to the general conclusion and perspective for next-step research in the future.

Chapter 2. Experimental section

2.1 Experimental section of Chapter 3

2.1.1 Preparation of ZIF-7 layer

ZIF-7 powder was prepared according to the previous literatures.[45] In brief, 0.528 g zinc acetate dehydrate ($Zn(CH_3COO)_2.H_2O$) mixed with 1.180 g benzimidazole and then dissolved into deionized water (300 mL). After string for 3 hours, the homogeneous milky solution was aging for 1 day until the ZIF-7 crystals fully precipitated. After removing by ethanol and deionized water for at least three times, the as-prepared ZIF-7 powder was then dispersed in ethanol for 3 days under room temperature. The ethanol was then replenished for 3 times before the centrifugation. The as-received ZIF-7 powder was dried at 80°C for 12 hours to remove absorbed solvent and transferred to vacuum oven for further activating at 180°C overnight. The activated ZIF-7 powder was mixed with poly vinylidene fluoride (PVDF)/dimethylformamide (DMF) solution in mass ratio of 3:1. The as-obtained slurry after stirring then was casted on Zn plate surface by a doctor blading method. The as-prepared MOF-coated Zn plate was moved to vacuum oven to remove the absorbed solvent prior to use.

2.1.2 Preparation of MnO_2 cathode

Electrolytic manganese dioxide (EMD) was also prepared by previous reports.[46] The MnO_2 cathode was prepared by mixing 70 wt% MnO_2 powder, 20 wt% Super P (conductive carbon), and 10 wt% poly(tetrafluoroethylene) (PTFE, suspension, 12 wt%) in water. Then, the large-area freestanding MnO_2 electrode was cut into pellets with diameter of 6 mm and pressed onto Ti mesh (diameter: 8 mm). The electrode was

moved to vacuum oven overnight to remove solvents prior to use. The weight load of MnO_2 content was ca. 4.2 mg cm^{-2}.

2.1.3 Preparation of electrolyte

Zinc sulfate ($ZnSO_4.7H_2O$) was dissolved into the deionized water solution to obtain the baseline $ZnSO_4$ electrolyte (2 mol) for Zn symmetric cells. Some solutions with $ZnSO_4$ concentration gradient ranging from 0.4 mol to 3.3 mol (saturated) are prepared for Raman spectroscopy characterization. Manganese sulfate ($MnSO_4.7H_2O$) was added into 2 mol $ZnSO_4$ electrolyte to prepare 2 mol $ZnSO_4$+0.2 mol $MnSO_4$ for Zn-MnO_2 cells.

2.1.4 Electrochemical measurements

All coin-type CR-2032 cells (Hohsen Corp) in this thesis were assembled and tested in ambient environment. The galvanostatic discharge/charge electrochemical characterizations of symmetric Zn half coin cells (Zn plate diameter: 8 mm) were carried out to evaluate the Zn reversibility of plating/stripping. Zn half cells were assembled by Zn plate (thickness: 200 μm), glass fiber separator with 50 μL of $ZnSO_4$ electrolyte (2 mol). Zn-MnO_2 cells were assembled by Zn plate, glass fiber separator with 40 μL of electrolyte (2 mol $ZnSO_4$+0.2 mol $MnSO_4$) and MnO_2 cathode. The galvanostatic discharge/charge measurements were conducted under voltage control (0.8~1.9 V) in battery tester system HJ1001SD8.

2.1.5 Characterizations

(1) SEM: The SEM observations were conducted on a LEO Gemini Supra machine, and SEM pictures were harvested with an accelerating voltage of 5 kV. The cycled Zn cells were disassembled under ambient environment and the Zn anode and cathode

were took out. The as-obtained Zn plates were rinsed by dimethoxyethane (DME) solutions for three times to wash precipitated components. Then the Zn electrodes were moved to vacuum chamber to remove solvent. The dried electrodes were then carefully transferred into SEM sample chamber. The Zn plates are not highly sensitive to ambient environment and short-time exposure to air would not damage their morphology and component. Similarly, the powder samples were also carried out to obtain SEM images without special treatment.

(2) X-ray Diffraction (XRD): X-ray diffraction measurement was carried out on a Bruker D8 Advanced diffractometer. The powder and electrodes samples were pretreated similarly to that for SEM observation.

(3) Raman Measurements (Micro-Raman): The Raman spectra measurement was carried out by a JASCO microscope. The scattered light then was collected in a backscattering geometry along the same optical path as the pumping laser. The liquid solutions are conducted by common procedures. For the MOF sample, MOF/Zn composites were taken apart from symmetric Zn battery after cycling (10 cycles at 0.5 mA cm^{-2}). Then the small amount of liquid electrolyte on the surface of MOF/Zn composite was wiped dry by clean tissue. The depth of Raman spectroscopy is also micro-scale (ca. 0.5~3.0 μm), which ensures the collected Raman spectra comes from the inner layer of MOF/Zn composite.

(4) Micro-infrared (IR): FTIR characterization was conducted on IRT-5200 Infrared Microscope spectrometer.

2.2 Experimental section of Chapter 4

2.2.1 Preparation of MOF membrane (Zn-BTC)

Zn-BTC powder was synthesized using a solvent thermal method according to

previous literatures.[47-48] In brief, 1.275 g zinc nitrate hexahydrate ($Zn(NO_3)_2 \cdot 6H_2O$) mixed with 0.3 g 1,3,5-benzenetricarboxylic acid (H_3BTC) and then totally dissolved into 75 mL of DMF solution. The solution was stirred and maintained 88°C in an oil bath over 16 hours. The received homogeneous milk solution was cleaned by centrifugation and replenished for 3 times in DMF solution before the final centrifugation. The as-obtained Zn-BTC powder was dried at 80°C for 12 hours to remove absorbed solvent and transferred to vacuum oven for further activating at 180°C overnight. The activated Zn-BTC powder was stirred with PVDF/DMF solution in mass ratio of 3:1. The slurry was uniformly cast on glass fiber separator by common doctor blading method. The as-prepared Zn-BTC membrane was transferred into vacuum oven to remove the absorbed solvent prior to use.

2.2.2 Electrode and electrolyte preparation

The $ZnSO_4 \cdot 7H_2O$ was dissolved into the deionized water to obtain the 2 mol $ZnSO_4$ solution for Zn symmetric cells. Some solutions with $ZnSO_4$ concentration gradient ranging from 1.0 to 3.3 mol (saturated) are prepared for Raman spectroscopy characterization. The catholyte contained 0.5 mol $ZnSO_4$, 1 mol LiI and 0.1 mol I_2. The anolyte contained 0.5 mol $ZnSO_4$ and 0.5 mol Li_2SO_4. Ketjen black (KB) carbon was mixed with PTFE binder in mass ratio of 4:1 and then compressed on carbon paper current collector. The loading of KB is ca. 1.5~2 mg cm^{-2} with a diameter of 5 mm.

2.2.3 Electrochemical measurements

All coin-type CR-2032 cells (Hohsen Corp) in this thesis were assembled and tested under ambient environment. The galvanostatic discharge/charge electrochemical tests of symmetric Zn half-cells (diameter: 8 mm) were conducted to

evaluate the Zn plating/stripping performance. Half cells were assembled by Zn plate (thickness: 200 μm), glass fiber separator or Zn-BTC membrane with 50 μl of electrolyte. The Zn-BTC membrane was tightly adhere to Zn surface after rolling. The areal capacity of plating/stripping was controlled by the current density and time during each process. Zn-I_2 cells were assembled by Zn foil, glass fiber or Zn-BTC membrane and KB carbon cathode with 30 μL catholyte. The galvanostatic discharge/charge measurements were conducted under potential control (0.6~1.6 V) using the battery tester system HJ1001SD8 under ambient environment. The redox couple of I^-/I_3^- was studied by Cyclic voltammetry (CV), ranging from 0.04 to 0.24 mV/s.

2.2.4 Characterizations

All the characterizations used in this chapter is similar to that in Chapter 3. Please refer to 2.1.5.

Chapter 3. Constructing a super-saturated electrolyte front surface for stable rechargeable aqueous zinc batteries

3.1 Introduction

The chapter 1 has well illustrated the significance of developing high-performance Zn batteries. Recently, the research hotspot of shifting Zn battery from primary to rechargeable was considered as a safe and environmentally friendly choice.[49-50] In comparison, rechargeable Zn battery can considerably promote the efficiency of materials and reduce the waste. By a thorough analysis, we find out that the most essential point lies in the Zn anode reversibility to satisfy long-term cycling. The service life of Zn battery system is fully determined by the dendrite growth and the time for short-circuit.[51] Zn metal is an amphoteric metal, which cannot survive long-term cycling in concentrated acid or alkaline electrolytes. Most of primary Zn battery in commercial market exploited alkaline electrolyte because of benign electrochemical compatibility with cathodes. However, its unstable thermodynamic property triggers severe self-corrosion and self-discharge, which cannot sustain its rechargeability.

Recently, most of attention focused on neutral electrolytes with pH value ranging from 4.5~6.5, which can effectively improve the thermodynamic stability of Zn metal anode. Typical, the simple and cost-effective $ZnSO_4$ electrolyte becomes one of the most appropriate choices, which was prepared by dissolving low-cost $ZnSO_4.7H_2O$ salt into water solution. However, the neutral $ZnSO_4$ electrolyte still consists of lots of free water molecular, which exists in both bulk electrolyte and the region for de-solvation process. In short, the corrosion happened on Zn anode surface can be mainly divided into two major parts (**Figure 3.1**). One aspect lies in the large amount

of free water molecular in the bulk electrolyte, which usually absorbs in the Zn anode surface. The intrinsic thermodynamic instability of Zn and its long-term soaking in $ZnSO_4$ electrolyte would trigger side-reaction and morphology change.[52] Besides, Zn anode during working period also suffers from the reactive water molecular, which is released during de-solvation period. The solvated ion-pairs undergo a final de-solvation process prior to Zn^{2+} ion transfer and diffusion (**Figure 3.2**).[53] Generally, a typical charge-transfer reaction contains three necessary steps during the metallic Zn electrodeposit process. Firstly, the solvated ion-complexes situating near to the electrodes need to de-solvate and release many activated water molecules. Finally, Zn^{2+} would receive electron and complete deposition process beneath SEI layer. The released water molecular within electric double layer becomes the major concerns for Zn anode failure after cycling. The strong water activity remains a critical factor and negatively deconstruct the Zn anode. In all, both the static and active water molecular poses a significant concern for Zn anode stability and urges an effective strategy in electrolyte regulation.

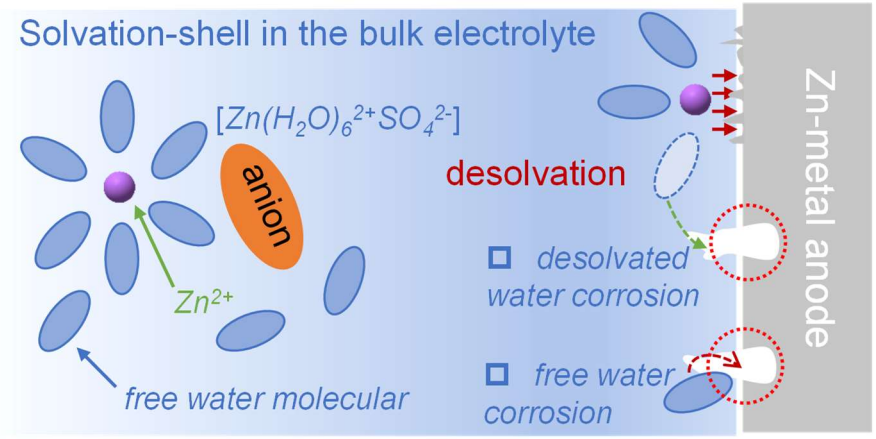

Figure 3.1 Schematic illustration of passivation process of water molecular on Zn anode surface.

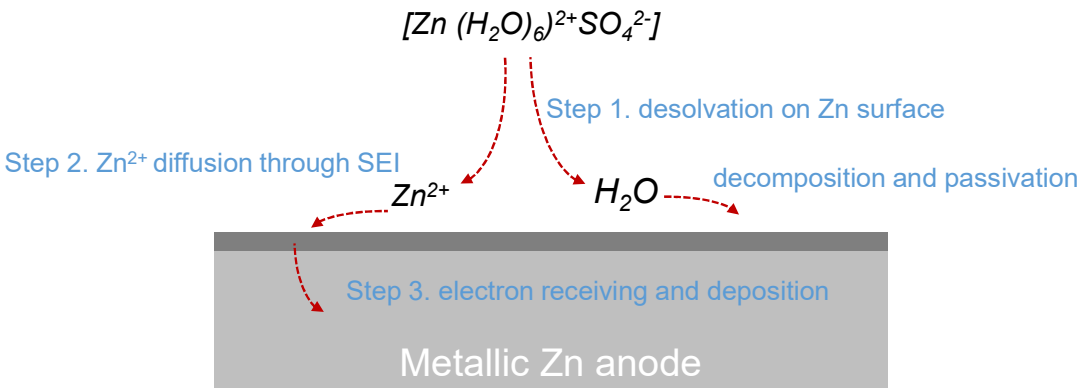

Figure 3.2 Typical process for charge-transfer reaction during the metallic Zn electrodeposit process.

A common approach is dissolving high concentrated salt into aqueous electrolyte, where most of water molecular is coordinated with cations. However, most of Zn salts have limited solubility (<5 mol) in water solution, except $ZnCl_2$ salt.[54-55] However, the complex solvation structure and its strong corrosion make it unfavorable choice for practical applications. By suppressing water activity, Wang et al. proposed a high concentrated aqueous electrolyte, consisting of 1 mol $Zn(TFSI)_2$ and 20 mol LiTFSI ($TFSI^-$: bis(trifluoromethanesulfonyl)imide).[44] In the concentrated electrolyte, most of water molecular are surrounded by cations and significantly suppress the hydrogen evolution. Moreover, this electrolyte enables a high reversible Zn anode plating/stripping process without obvious dendrite formation. However, the strategy of using high concentrated salt negatively caused high-cost and poor physical properties (high viscosity and low ionic conductivity). Herein, we summarized a table to compare the cost of Zn salts and LiTFSI (**Table 3.1**). Compared with expensive $Zn(TFSI)_2$ and $Zn(OTF)_2$ salt, the adoption of $ZnSO_4$ inherits the advantage of Zn batteries in low-cost. Up to now, developing a simple and cost-effective approach remain a significant challenge for high-performance rechargeable Zn batteries.[56] In this work, we contributed to demonstrate an effective electrolyte solvation structure regulation by interphase construction.[57]

Table 3.1 Information of the price and supplier of the common salts used in previous reports.

Zn salts	CAS Number	Price ($ per 1 g)	Supplier
$ZnSO_4.7H_2O$	7446-20-0	0.363	Sigmaaldrich
Zinc di[bis(trifluoromethylsulfonyl)imide] $Zn(TFSI)_2$	168106-25-0	61.3	Sigmaaldrich
Zinc trifluoromethanesulfonate $Zn(OTf)_2$	54010-75-2	4.83	Sigmaaldrich
$ZnCl_2$	7646-85-7	0.729	Sigmaaldrich
Lithium bis(trifluoromethanesulfonyl)imide LiTFSI	90076-65-6	6.88	Sigmaaldrich

3.2 Basic understanding on electrolyte solvation shell

Except $ZnCl_2$ aqueous solution, most of Zn salt solutions share a similar rule for solvation. In this work, we carefully studied the solvation structure $ZnSO_4$ solutions. In $ZnSO_4$ solutions, only a small fraction of water molecular is coordinated with Zn^{2+}, in a solvation shell because of low solubility of $ZnSO_4$ (53.8 g/100 g H_2O).[58] According to the classic Werner's theory on coordinated compounds containing two spheres of zones, there are typically inner sphere (coordination sphere) and outer sphere (ionization sphere). When $ZnSO_4$ dissolve into water, the tightly coordinated ion associations are firmly attached by coordinate bonds in the inner sphere. When the groups are loosely separated, the outer-sphere presents another ion associations by removing one water molecular. The common $ZnSO_4$ solution consists of two typical solvation mode, namely ($[Zn^{2+}(H_2O)_6{\cdot}SO_4^{2-}]$ and $[Zn^{2+}(H_2O)_5{\cdot}OSO_3^{2-}]$).[59] The solvation of $ZnSO_4$ into aqueous solution obeys the classic Eigen-Tamm (ET)

mechanism, which involves a two-step model for revealing the existence of solvated species in $ZnSO_4$ solutions (Equation 1 and 2).[60] As **Figure 3.3** schematically illustrated, these two species reached a dynamic equilibrium. In dilute $ZnSO_4$ solutions, Zn^{2+} exists as a hexahydrate, namely solvent separated ion pair (SSIP, $[Zn^{2+}(H_2O)_6{\cdot}SO_4^{2-}]$) in the outer-sphere. Increasing the $ZnSO_4$ concentration would evolve the ion-pair into a contact ion pair (CIP, $[Zn^{2+}(H_2O)_5{\cdot}OSO_3^{2-}]$) in the inner-sphere by loss of one water of hydration.[60]

$$Zn^{2+}_{(aq)}+SO_4^{2-}{}_{(aq)}\leftrightarrow[Zn^{2+}(H_2O)_6{\cdot}SO_4^{2-}]\leftrightarrow[Zn^{2+}(H_2O)_5{\cdot}OSO_3^{2-}] \quad \text{Equation 1}$$

$$[Zn^{2+}(H_2O)_6{\cdot}SO_4^{2-}]\leftrightarrow[Zn^{2+}(H_2O)_5{\cdot}OSO_3^{2-}]+H_2O \quad \text{Equation 2}$$

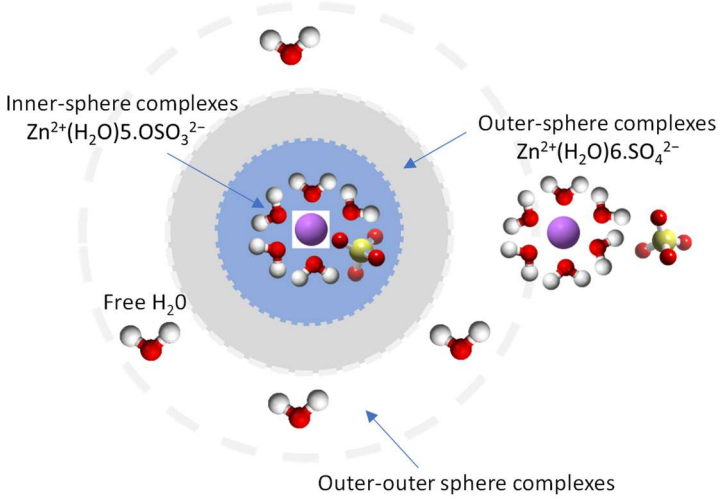

Figure 3.3 Schematic structure of ZnSO4 aqueous solutions.

In this work, we are inspired by the concept of developing highly aggressive electrolyte solvation structure (highly concentrated electrolyte). To overcome the disadvantages of high-cost salts and poor physical properties, we proposed a novel concept by constructing a super-concentrated electrolyte front surface on Zn anode surface. In detail, we dedicated to resolve the reactive water, which released in the region near to Zn surface. We the selected MOF as a functional coating on Zn anode surface to filtering aqueous electrolyte. As a non-conductive and highly adhered coating on Zn anode surface, the solvated ion-pairs have to de-solvate prior to migrating through MOF channels. Thanks to the limited pore size of MOF channels,

we assume that the large ion-pairs have to remove the water molecular when finally reaching the Zn anode front surface. Moreover, the tight adhere between Zn anode and MOF layer avoids the solvation of Zn^{2+} ion with water molecular one again.

Herein, we schematically depicted the working mechanism of MOF layer. In blank group with bare Zn anode and pristine $ZnSO_4$ electrolyte (2 mol $ZnSO_4$ in aqueous solution), Zn anode surface involves water decomposition, where water molecular generally derives from the de-solvation of $[Zn^{2+}(H_2O)_6{\cdot}SO_4^{2-}]$ (**Figure 3.4a**). The reactive water molecular would corrode Zn anode surface, with obvious hydrogen evolution and decomposition product accumulation. However, in the assistance of MOF layer, the major ion-pairs are rejected to migrate through the MOF channel until partial de-solvation process (**Figure 3.4b**). Therefore, Zn anode surface undergoes less water molecular attack and obtain good reversibility.

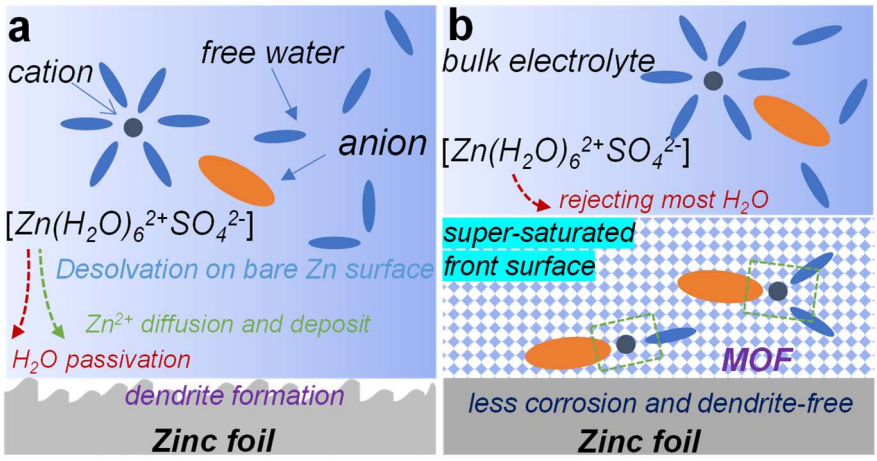

Figure 3.4 Schematic illustration de-solvation process happened on Zn anode surface. (a) In blank group with bare Zn anode and pristine $ZnSO_4$ electrolyte. (b) In experimental group with MOF-coated Zn anode and pristine $ZnSO_4$ electrolyte, where MOF serves an artificial layer for de-solvation process.

3.3 Preparation of ZIF-7 coating on Zn anode

In this work, we selected zeolitic imidazolate framework ZIF-7 as the pristine

material owing to its small size ca. 2.94 Å. The majority of MOF materials are sensitive to water environment and cannot maintain pristine structure after long-term soaking into aqueous electrolytes. Herein, ZIF-7 was selected as host materials because of its superior stability against water environment. The preparation method of ZIF-7 powder is introduced in Chapter 2.1. As shown in **Figure 3.5a**, ZIF-7 has a uniform pore size and caves, which serves as place to sieve and store electrolyte ion pairs. The XRD patterns of ZIF-7 is consistent with that from literature (**Figure 3.5b**).[61] We then checked its morphology by SEM observation, which shown uniform and highly ordered particles (**Figure 3.5c**).

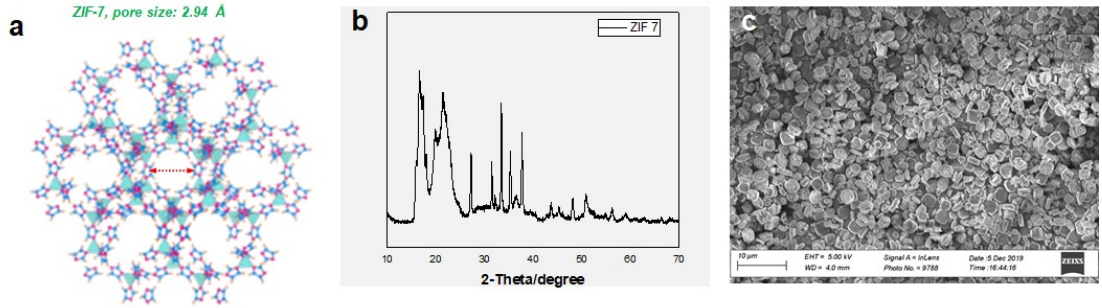

Figure 3.5 XRD and SEM characterization of as-synthesized ZIF-7 powder. (a) Schematic structure with size windows (ca. 2.94 Å). (b) XRD characterization; (b) SEM images.

We then reactivated the ZIF-7 pores by maintaining 160ºC for 24 hours in vacuum oven. This process is inevitable to remove the absorbed solvents.[45] After that, we prepared ZIF-7 coating by mixing ZIF-7 materials with PVDF slurry in DMF (mass ratio 3:1) and then dripped on Zn foil surface. The Zn foil with ZIF-7 coating then were transferred to remove the DMF solvent and form a robust ZIF-7 coating. The SEM images of ZIF-7 coated Zn anode were collected, where the typical uniform morphology of ZIF-7 particle was still well-maintained (**Figure 3.6**).

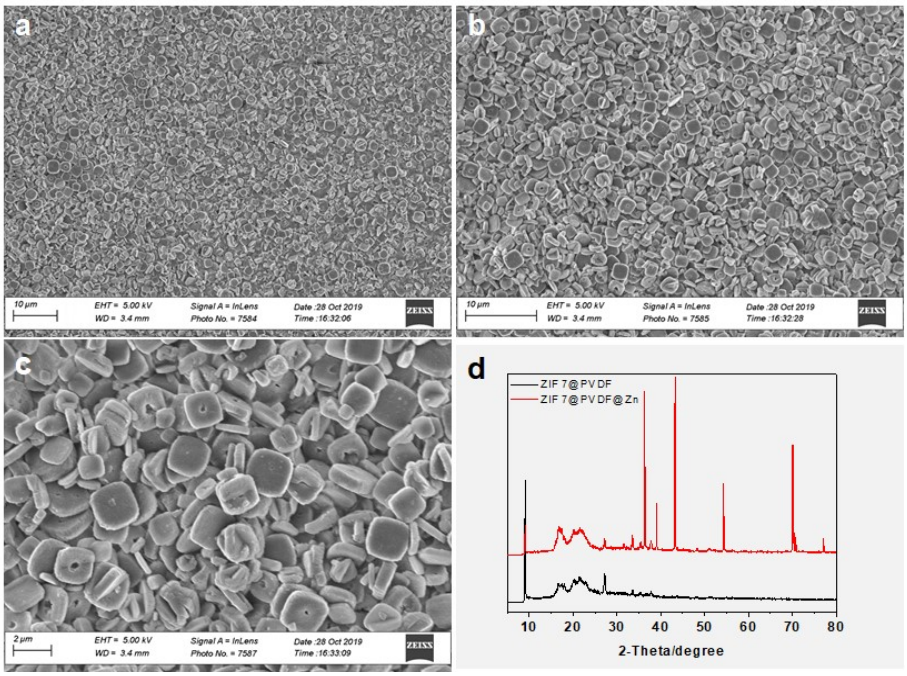

Figure 3.6 SEM and XRD characterization of ZIF-7-coated Zn. (a-c) SEM images of ZIF-7-coated Zn surface; (d) XRD of ZIF-7 layer and ZIF-7-coated Zn.

3.4 Raman spectroscopy study on electrolyte solvation structure

Raman spectroscopy characterization is employed to reveal the electrolyte solvation structure. We firstly studied the solvation structure of liquid electrolytes with different salt concentrations. The limit solubility of $ZnSO_4{\cdot}7H_2O$ in aqueous solution enables a saturated $ZnSO_4$ solutions (3.3 mol). Therefore, a series of solutions with $ZnSO_4$ concentration gradient (0.4, 0.8, 1.6, 2.0, 3.3 mol) were separately studied to reveal the evolution of Raman peak.

To study the Raman vibration trend of $[Zn^{2+}(H_2O)_6{\cdot}SO_4^{2-}]$ and $[Zn^{2+}(H_2O)_5{\cdot}OSO_3^{2-}]$, we carefully selected the Raman spectra peaks of ν-SO_4^{2-}, Zn-OH_2 vibration and O-H stretch vibration. The $ZnSO_4{\cdot}7H_2O$ presents a clear peak at 984.6 cm^{-1}, which is attributed to ν-SO_4^{2-} band (**Figure 3.7**).[62] Its dissolving into aqueous electrolyte displays a red-shift to 983~985 cm^{-1} for ν-SO_4^{2-} band.[63] The ν-SO_4^{2-} band can be split into configuration in SSIP (lower frequency at 983.5 cm^{-1})

and CIP (higher frequency at 988.0 cm^{-1}) (**Figure 3.8a**). With the increase of concentration, the ion-pairs evolve from SSIP to CIP, resulting into a closer interaction. For v-SO_4^{2-} band, the Raman spectra exhibits a blue shift with the salt concentration increasing. We then compared the related peak in ZIF-7 channel, where remarkably displays a sharp peak locating on 992 cm^{-1}. The significant blue shift indicates a highly coordinated ion-pairs, which indicates a unique solvation structure.[64]

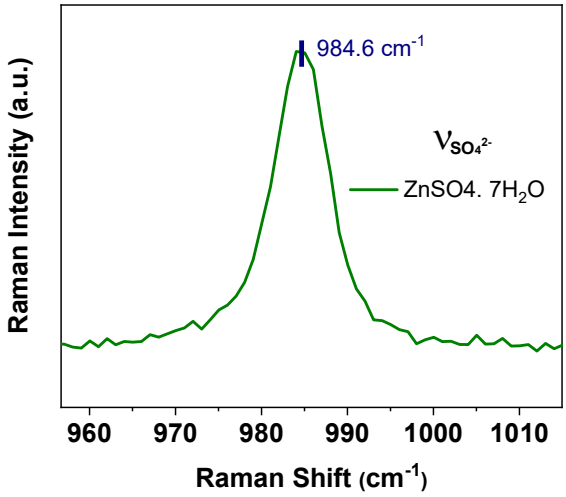

Figure 3.7 Raman spectroscopy of $\boldsymbol{v}$-SO_4^{2-} band from $ZnSO_4$.7H2O powder, where distinct peak located on 984.6 cm^{-1}.

Figure 3.8b demonstrates Zn-O vibration consisting of Zn-OH_2 vibration centering at ca. 390 cm^{-1}, and [Zn^{2+}.OSO_3^{2-}] ligand mode at 260 cm^{-1}.[62] The Zn-OH_2 vibration is widely existed in both [$Zn^{2+}(H_2O)_6{\cdot}SO_4^{2-}$] and [$Zn^{2+}(H_2O)_5{\cdot}OSO_3^{2-}$]. With the increase of salt concentration increases, more water molecular are coordinated with Zn^{2+} into SSIP and CIP mode. Therefore, the peak intensity strengthens, but does not make change for peak location. We then studied the [Zn^{2+}.OSO_3^{2-}] ligand mode, which can be assigned to the inner-sphere complexes ion-pair. With $ZnSO_4$ salt concentration increase and more ion-pairs evolving into CIP mode, the [Zn^{2+}.OSO_3^{2-}] peak intensifies and confirms a more constrict ion-pairs. We

then observe the intensity of [Zn^{2+}.OSO_3^{2-}] peak in ZIF-7 channel is significantly strengthened, which indicates more CIP mode in the unique electrolyte solvation structure.[63]

The O-H stretch vibration also provides important proof for revealing electrolyte solvation structure (**Figure 3.8c**). The broad O-H vibration can be split into HOH-OH_2 stretch and HOH-OSO_3^{2-}. In detail, the HOH-OH_2 stretch locating at 3264~3304 cm^{-1} exhibits a blue-shift and a depressed peak intensity as the increase of salt concentration, which substantiates suppressed interaction between water molecular.[65] Besides, the peak intensity of HOH-OSO_3^{2-} band enhanced with the salt concentration, because of the abundance of [$Zn^{2+}(H_2O)_5$·OSO_3^{2-}]. The detection in ZIF-7 channel reveals a highly suppressed HOH-OH_2 stretch and a dominated HOH-OSO_3^{2-} vibration. These results indicate a minority water molecular and highly coordinated ion-pairs in ZIF-7 pores.[60]

Based on the highly aggressive ion-pairs in ZIF-7 channel, we want to compare its solvation structure with that in highly concentrated electrolyte (saturation, 3.3 mol). The saturated $ZnSO_4$ solution is composed of SSIP (56%) and CIP (44%), which indicates large amount of free water molecular in the bulk electrolyte (**Figure 3.9a**). Moreover, the water released from SSIP and CIP solvation structure during de-solvation process would induce severe water passivation on Zn anode surface. The evolution of spectra in ZIF-7 channel indicates a unique solvation structure, which displays even closer ion-pairs than that in saturated electrolyte. Moreover, this special solvation structure only exists in ZIF-7 channel, where de-solvation process is completed in the interface. By removing water molecular and allowing suitable ion-pairs migrating through ZIF-7 channel, we harvest a super-concentrated front layer near Zn anode surface and does not destruct the electrolyte solvation structure in bulk electrolyte. The constrained solvated ion-pair can be simply depicted as

H_2O-Zn^{2+}·OSO_3^{2-}, near one water coordinated with Zn^{2+} (**Figure 3.9b**). The size of H_2O-Zn^{2+}·OSO_3^{2-} can be calculated as ca. 2.71 Å, which is smaller than ZIF-7 channel (2.94 Å). Therefore, in theory, this unique ion-pair can migrate through ZIF-7 channel.[66]

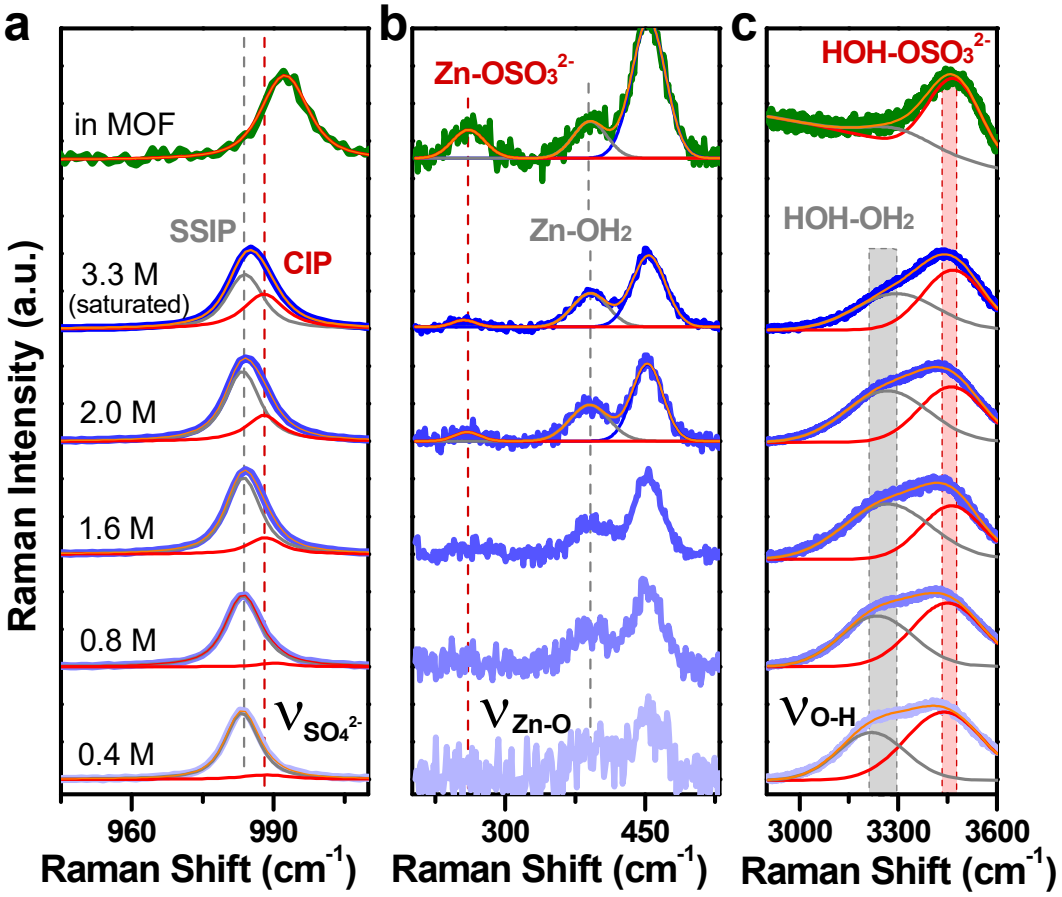

Figure 3.8 Raman spectroscopy characterization for ZnSO4 solutions with a concentration gradient and the interaction in ZIF-7 channel. (a) The ***ν***-SO_4^{2-} stretch band. (b) Zn-O stretch bond consisting of Zn-OH_2 and [Zn^{2+}.OSO_3^{2-}] band. (c) The O-H stretch vibration consisting of HOH-OH_2 stretch and HOH-OSO_3^{2-}.

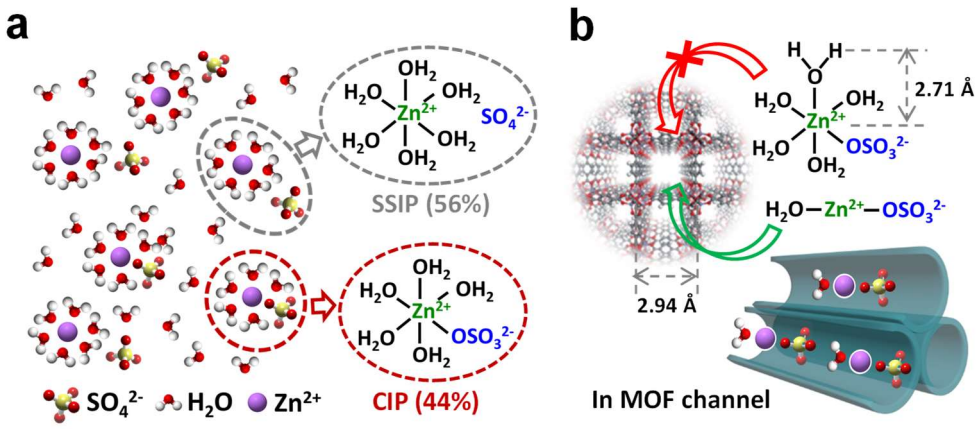

Figure 3.9 (a) The two different types of solvation structures in saturated $ZnSO_4$ aqueous solutions. (b) Schematic picture of our proposed highly aggressive ion-pairs of H2O-Zn^{2+}.OSO_3^{2-} transporting in the ZIF-7 channels..

3.5 Study on Zn anode reversibility

We then carried out electrochemical characterization to study the Zn anode reversibility by symmetric Zn||Zn cells. The blank group consists of two Zn plates and a glass fiber separator, where Zn dendrite growth during repeated plating/stripping process would easily penetrate through the glass fiber (**Figure 3.10a**). In our proposed concept, we demonstrated ZIF-7 layer to protect Zn anode. As discussed before, the ZIF-7 coating on Zn anode maintained a super-concentrated ion-pair to ensure the benign stability (**Figure 3.10b**).

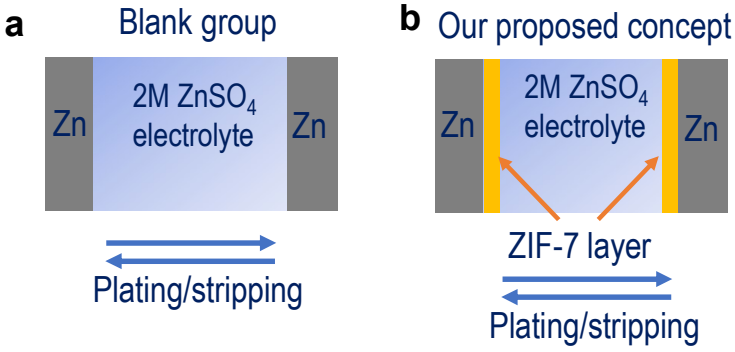

Figure 3.10 Schematical illustration of symmetrical Zn||Zn cells. (a) Blank group with bare Zn plate. (b) Our proposed experimental with ZIF-7 coated Zn plate.

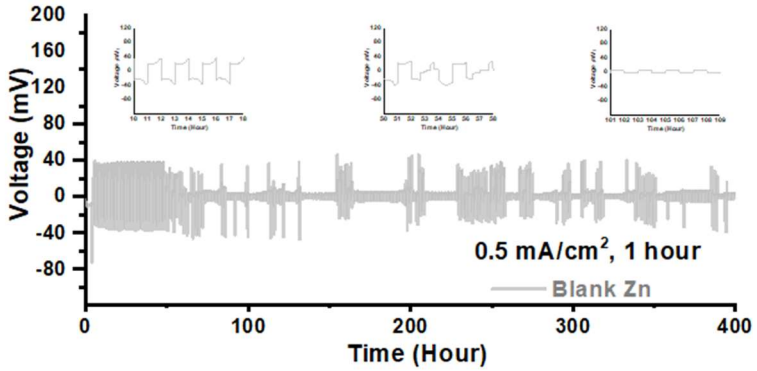

Figure 3.11 Symmetric Zn||Zn cell with bare Zn plates in control group.

Symmetric Zn||Zn cells were performed under the test condition of 0.5 mA cm^{-2}/0.5 mAh cm^{-2} in conventional 2 M $ZnSO_4$ electrolyte. In the control group, the voltage evolution maintained a stable profile only at the beginning time and soon fluctuated only after 55 hours (**Figure 3.11**). The instable profile indicates uncontrollable Zn dendrite growth on bare Zn anode. Soon, the symmetric Zn||Zn cell is short-circuit owing to the final Zn dendrite piercing through the glass fiber.[67]

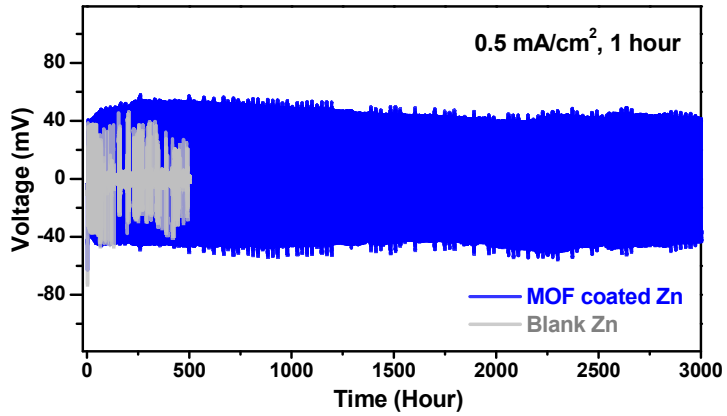

Figure 3.12 Symmetric Zn||Zn cells with ZIF-7 coated Zn in experimental group.

For the ZIF-7 coated Zn anode, the voltage maintained an ultra-stable profile over 3000 hours (125 days) without noticeable fluctuation (**Figure 3.12**). In comparison with the lifespan of 55 hours in blank group, the ZIF-7 coated Zn enables a 55-times increase of cyclic life for Zn anode stability. Moreover, we have a closer observation on the evolution of over-potential (**Figure 3.13**). The over-potential maintained at 40 mV even after 3000 hours.

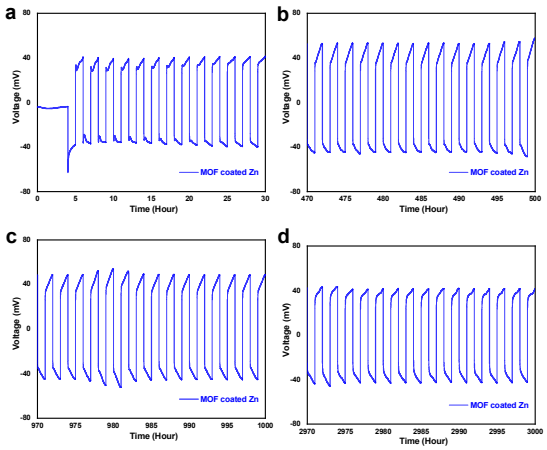

Figure 3.13 Over-potential evolution of symmetric Zn||Zn cell with ZIF-7 coated Zn anode.

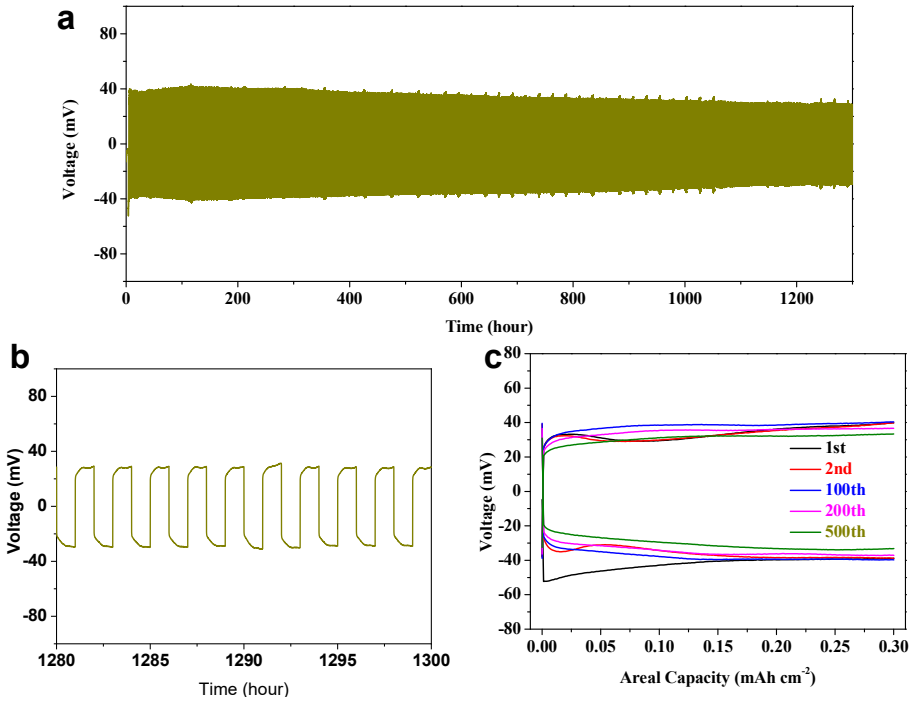

Figure 3.14 Symmetric Zn||Zn cells with ZIF-7 coated Zn plate under the test condition of 0.3 mA cm^{-2}/0.3 mAh cm^{-2}. (a) Cyclic performance with voltage profile over 1300 hours. (b) The enlarge voltage profile from 1280 to 1300 hours. (c) Over-potential profiles of different cycles.

Further decreasing the current density and areal capacity to 0.3 mA cm^{-2}/0.3 mAh cm^{-2}, the over-potential maintains at 28 mV for at least 1300 hours (**Figure 3.14**). However, it should be noted that ZIF-7 protected Zn cannot withstand reversible plating/stripping cycles at high current density (>1 mA cm^{-2}). The cell soon

changes into short-circuit (**Figure 3.15**), which might be caused by the much-reduced ionic diffusion within ZIF-7 layer. In brief, the ZIF-7 coating is proved effective to enhance Zn anode stability and prolong Zn battery life under low current density.

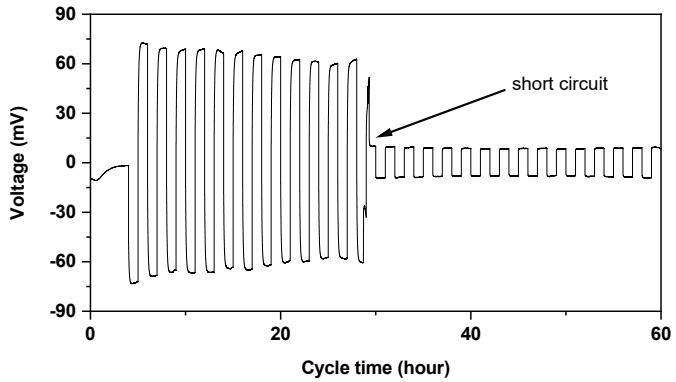

Figure 3.15 Symmetric Zn||Zn cells with ZIF-7 coated Zn plate under the test condition of 1 mA cm^{-2}/1 mAh cm^{-2}.

We then tried to find out the factor to determine the cyclic stability. The SEM image can intuitively reflect the evolution of Zn anode surface. We the collected Zn plates after 20 cycles (40 hours) for SEM observation. Prior to SEM observation, the absorbed components including ZIF-7 coating are removed. In collected images, Zn foil cycled in blank group exhibited the typical flake morphology, where most of Zn anode prefers growth direction <100> plane (**Figure 3.16a-b**).[68] The highly directional growth of Zn platelet morphology is consistent with previous literatures.[69-70] Because of the higher Young`s modulus of Zn metal, the uncontrollable dendrite would cause a rapid short-circuit and cell failure when compared with other metal anodes.[71] With the assistance of ZIF-7 coating, the Zn plate showcased a smooth and uniform morphology, which is neither slender fiber nor typical flake dendrite for Zn anode (**Figure 3.16c-d**). The Zn anode surface is occupied by a round-edged Zn electrodeposit, which is highly different from conventional growth direction according to <100> plane. Moreover, the dense electrodeposit morphology also favors the electronic transport in the Zn anode

surface.[72]

To prove the long-term stability, we checked the Zn plate morphology after 2000 hours. The large-scale region does not observe obvious dendrite growth. The surface maintained a good structure stability without noticeable crack or void (**Figure 3.17a**). With close observation, we find out that the round-edged morphology of Zn anode is well-maintained even after long-term cycling (**Figure 3.17b**).

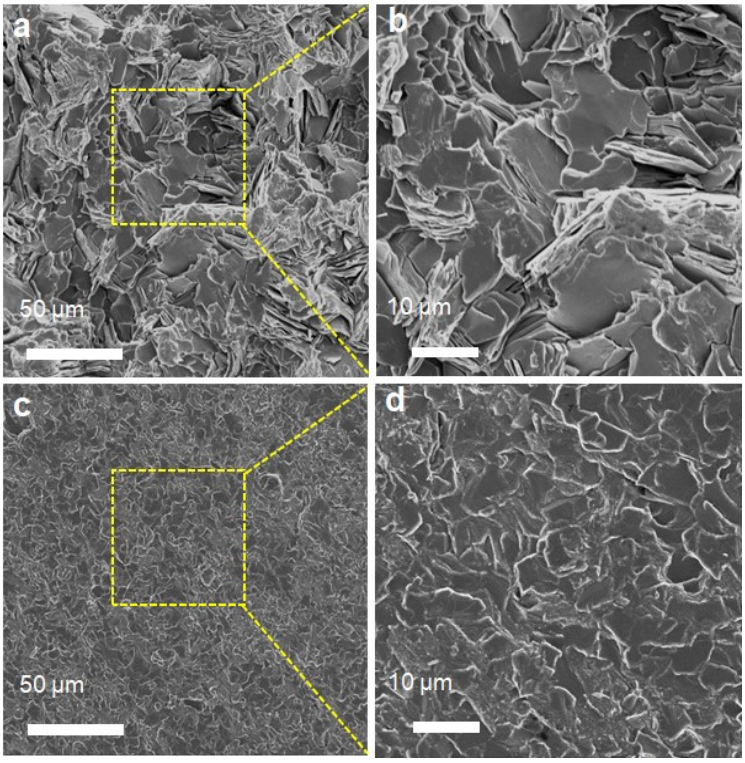

Figure 3.16 SEM images of Zn plates after 20 cycles. (a-b) Zn plate cycled in blank group. (c-d) Zn plate cycled in ZIF-7 coated group.

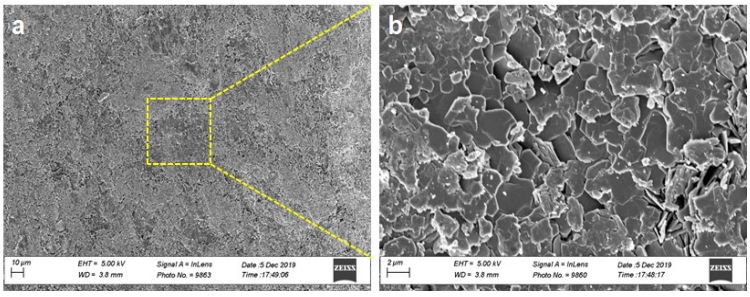

Figure 3.17 SEM images of Zn plates cycled in ZIF-7 coated group after 2000 hours. (a) at large-scale region. (b) at small-scale region.

Moreover, we checked the ZIF-7 morphology after long-term cycling. After 2000 hours, we confirm that the ZIF-7 coating maintains the typical morphology and has negligible structural change (**Figure 3.18**). In brief, we selected an aqueous-stable ZIF-7 as coating to enhance Zn anode stability.

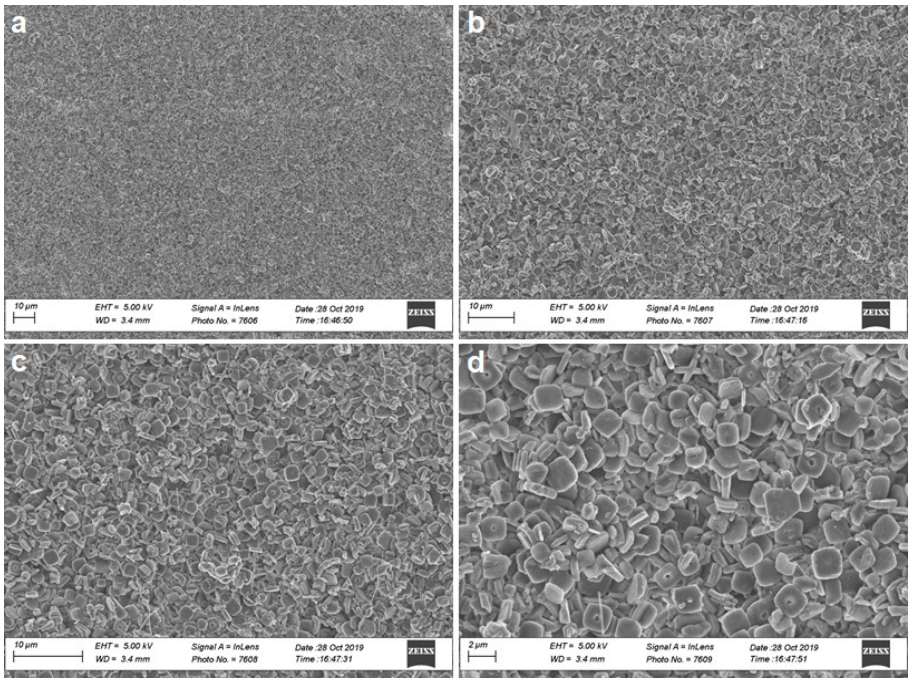

Figure 3.18 SEM images of ZIF-7 coating from ZIF-7 coated Zn anode after 2000 hours.

3.6 Decomposition component analysis on Zn anode surface

To further explore the factor to determine the Zn anode stability, we firstly carried micro-infrared (IR) to dig out the surface component and structure of side-reaction. Generally, the Zn metal anode involves passivation from water molecular and generates ZnO and $Zn(OH)_2$ side-product. The distribution and structure of side-product determines the ion and electron transport in the Zn anode surface. The cycled Zn plate cycled in blank group presents a dominated peak (O-H stretch, 3683 cm^{-1}), which can be attributed to $Zn(OH)_2$ side-product (**Figure 3.19a**).[73] Moreover, the micro-IR is equipped with ion sputtering devices to remove

the surface component, which is beneficial to analyze the in-depth component distribution. With several etching, the sharp peak of O-H stretch remains, which substantiates a thick passivation layer.

In comparison, the cycled Zn plate from ZIF-7 coating group presents a tiny O-H stretch, which indicates relatively small fraction of $Zn(OH)_2$ side-product (**Figure 3.19b**). Moreover, the related peak soon disappears after several etching times, which proves a very shallow passivation layer on the Zn anode surface.

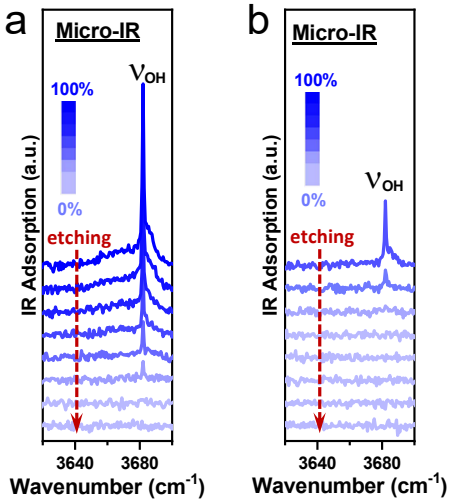

Figure 3.19 Micro-IR characterizations for cycled Zn plates. (a) Zn plate from blank group. (b) Zn plate from ZIF-7 coating group.

To distinguish the ZnO and $Zn(OH)_2$ species, we further employed micro-Raman spectroscopy to further reveal the component on Zn anode surface. For cycled Zn plate from blank group, Raman spectra exhibits typical ZnO peak, including E_2(h) mode at 437 cm^{-1} and E_2(h-l) mode at 329 cm^{-1} (**Figure 3.20a**).[74] It indicates that by-product ZnO crystal growth has no preferred orientation and accumulates owing to widely dispersed water molecular on bare Zn anode surface. Moreover, the related peaks of ZnO and $Zn(OH)_2$ side-product still maintains even after several etching times. In a sharp comparison, the Raman spectra of cycled Zn plate from ZIF-7 coated group only showcases single E_2(h) mode for ZnO crystal formation, which clearly

indicates a perpendicular growth direction to the Zn plate surface (**Figure 3.20b**). Besides, the Raman spectra of side-product soon disappears, which proves the slight thickness of passivation layer in ZIF-7 coated Zn metal anode. In brief, because of the super-concentrated front layer, ZIF-7 coated Zn anode involves less side-reaction from water attack.

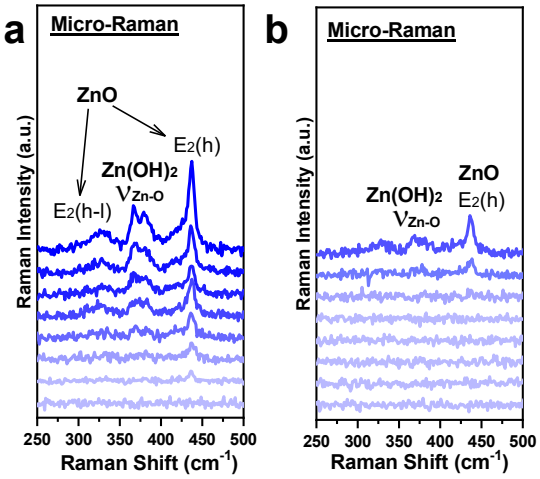

Figure 3.20 Micro-IR characterizations for cycled Zn plates. (a) Zn plate from blank group. (b) Zn plate from ZIF-7 coating group.

In conclusion, we analyzed the Zn metal failure mechanism from the perspective of de-solvation process in rechargeable Zn batteries. First, the most common solvated SSIP and CIP ion-pairs undergo a de-solvation process, with reactive water molecular release (**Figure 3.21a**). The de-solvation process happened in electric double layer would soon absorb on Zn anode surface and induces severe decomposition. Therefore, Zn anode surface accumulates lots of side-product, leaving poor ion and electron transport of Zn^{2+}. Consequently, the dendritic Zn growth would soon exacerbate and pierce through separator. The rechargeable Zn battery failure can be approximately ascribed to the degradation of Zn metal anode during plating/stripping process.[75]

With the assistance of ZIF-7 layer, the solvation structure inside coating layer evolves into a highly aggressive ion-pairs because of its unique pore structure. Most of reactive water molecular from de-solvation process are rejected to migrating

through ZIF-7 channel. The uniform and compact ZIF-7 coating functions as an effective artificial layer for de-solvation process in advance (**Figure 3.21b**). With the aid of ZIF-7 coating, a super-concentrated front layer on Zn anode surface is developed. Thus, less water molecular and less side-product generates during the final de-solvation on Zn anode surface.

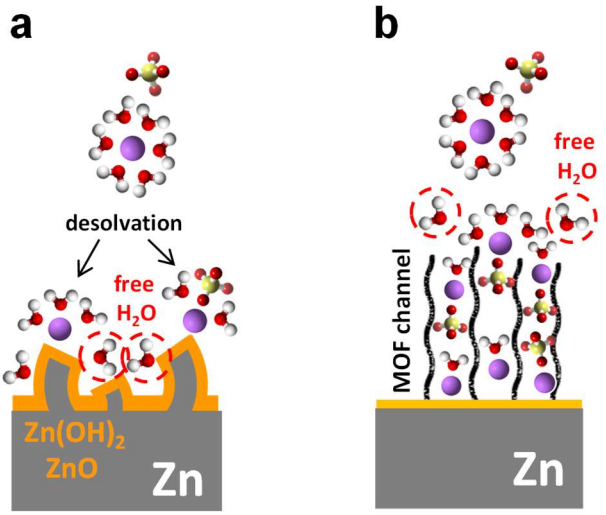

Figure 3.21 Schematic illustration of desolvation process. (a) At bare Zn anode surface. (b) At the ZIF-7 coated Zn anode surface.

3.7 Electrochemical performance of Zn-MnO_2 battery

To showcase the function of ZIF-7 coating, we selected MnO_2 as cathode and evaluated Zn-MnO_2 battery performance. Herein, we would like to highlight the superiority of Zn-MnO_2 battery system among the extensive family of Zn batteries. Firstly, the high element abundance of manganese (Mn) favors low-cost and large-scale application of Zn-MnO_2 battery.[76] Secondly, compared with other types of cathodes, Mn element is non-toxicity and can be operated without high-level safety protection. Lastly, the Zn-MnO_2 battery system is the most promising alternative for high-energy aqueous battery system because of its high-capacity and high operating voltage.

$MnO_2+H^++e^-\rightarrow MnOOH$ Equation (3)

$MnO_2+xZn^{2+}+2xe^-\rightarrow ZnxMnO_2$ Equation (4)

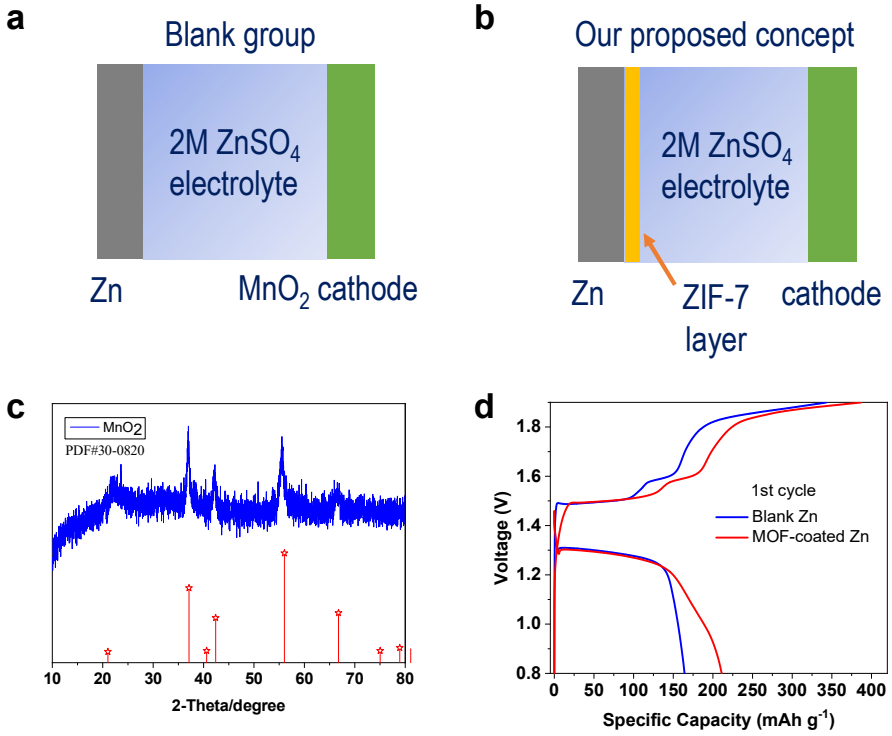

Figure 3.22 Schematic illustration of Zn-MnO_2 battery system. (a) Blank group with bare Zn plate. (b) Experimental group with ZIF-7 coated Zn plate. (c) XRD pattern of electrolytic MnO_2 cathode. (d) Voltage profiles of initial cycles for Zn-MnO_2 cells.

As schematically illustrated in **Figure 3.22a** and **3.22b**, the difference lies in the ZIF-7 coating on Zn anode in experimental group when pairing MnO_2 cathode. The electrolyte is used the same, 2 mol $ZnSO_4$+0.2 mol $MnSO_4$ to replenish the Mn^{2+} for MnO_2 cathode. In this experiment, electrolytic MnO_2 cathode was used because of it accessibility (**Figure 3.21c**). The MnO_2 cathode loading is ca. 4.2 mg cm^{-2} towards the high-capacity Zn batteries. Generally, the electrolytic MnO_2 cathode shares the classic co-intercalation mechanism by consequent H^+ and Zn^{2+} in both blank and experimental groups (**Figure 3.22d**).[76]

We then cycled Zn-MnO_2 battery to evaluate its electrochemical stability. The voltage profiles of Zn-MnO_2 batteries from 20th to 150th cycles are selected (**Figure 3.23a**). The blank group with bare Zn plate shows a gradual capacity declining in

comparison with the almost overlapped profiles in ZIF-7 coating group. The capacity decay might derive from the Zn anode degradation because of the large areal capacity (0.8 mAh cm^{-2}). We clearly observe the capacity fading from 188.4 mAh g^{-1} (the highest value in the 20th cycle after activation) to 129.1 mAh g^{-1} (the final cut-off 180th cycles) and only maintain 67.3% capacity retention in blank group (**Figure 3.23b**). In comparison, the capacity showcases a good electrochemical stability with a high retention of 94.4% over 180 cycles.

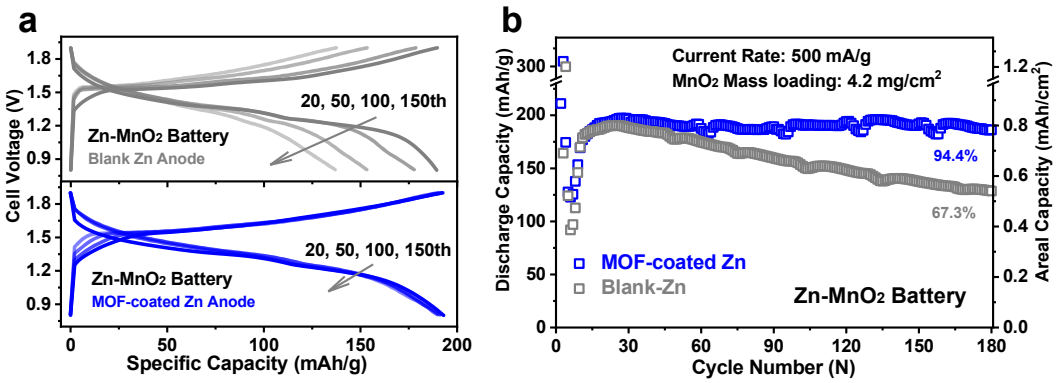

Figure 3.23 The discharge/charge voltage profiles of Zn-MnO_2 batteries. (a) In unprotected Zn anode (upper) and ZIF-7 coated Zn anode (lower). (b) The cycle life stability of Zn-MnO_2 cells.

After 180 cycles, we then disassembled the cells (at fully charged state) and then checked the Zn anode surface morphology. The digital photo of Zn plate from blank group after 180 cycles turns out gray surface and has noticeable cracks (**Figure 3.24a**). Then, SEM images can be observed lots of flake-like Zn dendrite and large voids (**Figure 3.24b**). The cycled Zn anode without any protection turned into uneven and porous structure, which was not simply induced by passivation process (**Figure 3.25a-b**). The severe shape change in bare Zn anode surface not only results in thick passivation layer, but also causes poor ion transport in the surface.

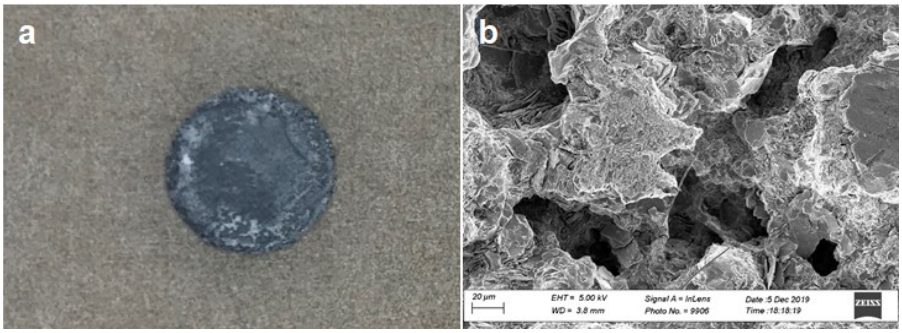

Figure 3.24 Zn plate from blank group. (a) Optical observation. (b) SEM observation.

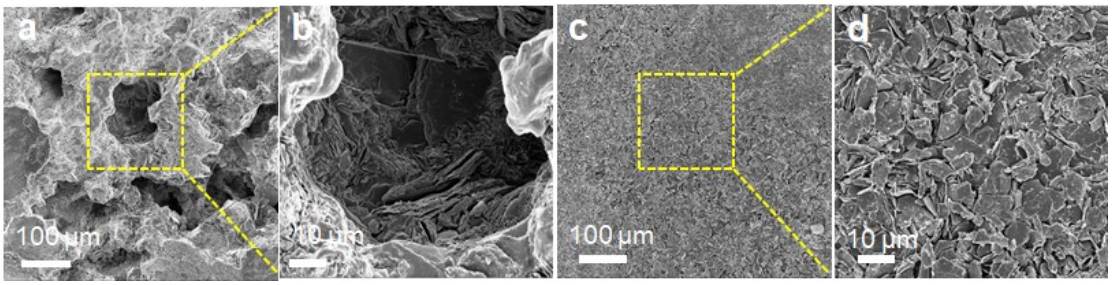

Figure 3.25 The SEM images of Zn plate. (a-b) From blank group after 180 cycles. (c-d) From ZIF-7 coating group after 180 cycles.

In compared with porous structure with flake-like dendrite formation, we found that the ZIF-7 coated Zn anode has no obvious cracks or voids (**Figure 3.25c-d**). In a sharp comparison, the ZIF-7 coated Zn after 180 cycles exhibited much more homogeneous surface and negligible voids on the Zn plane. It reveals that the ZIF-7 serves a functional layer to shield the attack of passivation reaction and suppress the shape change of Zn metal. In this pattern, Zn electrodeposit evolves into a dense and dendrite-free morphology.

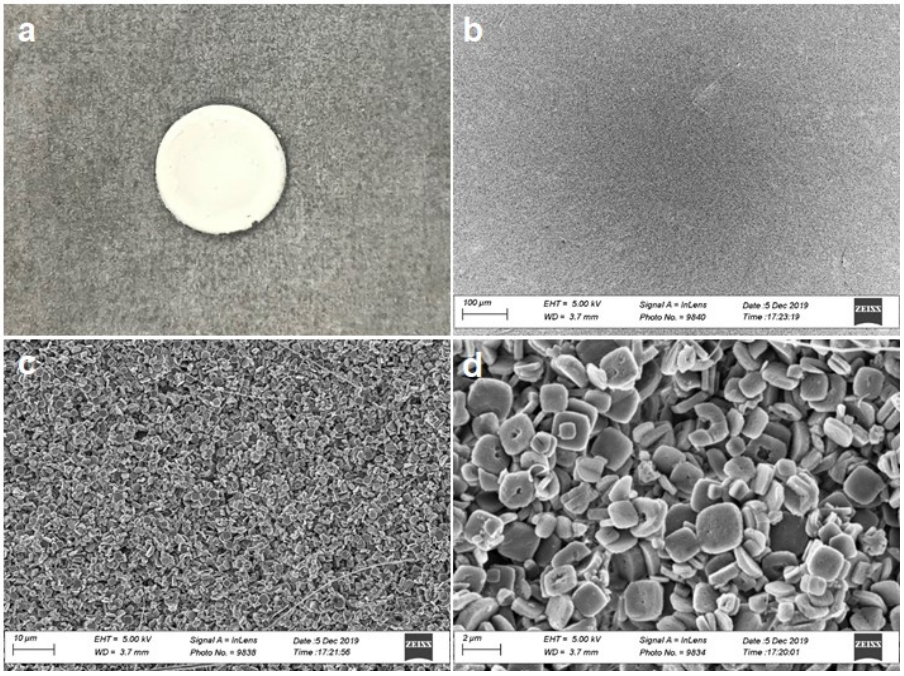

Figure 3.26 Images of ZIF-7 coated Zn anode harvested from Zn-MnO_2 cell. (a) Digital photo. (b-d) The SEM images of ZIF-7 layer surface after cycling.

Moreover, we checked the morphology of ZIF-7 layer after cycling. The ZIF-7 coated Zn plate has a uniform surface without obvious crack from optical observation (**Figure 3.26a**). The SEM images were also collected and turned out a homogeneous and uniform ZIF-7 layer (**Figure 3.26b-d**). The unique morphology of ZIF-7 particle after long-term cycling did not sacrifice and enabled its protection for Zn anode.

Futhermore, we boosted the rate to 700 mA g^{-1} for longer lifespan for Zn-MnO_2 battery with ZIF-7 layer. The specific capacity after electrochemical activation gradually recovered to 180 mAh g^{-1} and maintained 160 mAh g^{-1} over 600 cycle, which indicated a high retention of 88.9% (**Figure 3.27**). To highlight its superiority for Zn anode protection, we made a suvery for Zn-MnO_2 batteries using different strategies (**Table 3.2** and **3.3**).

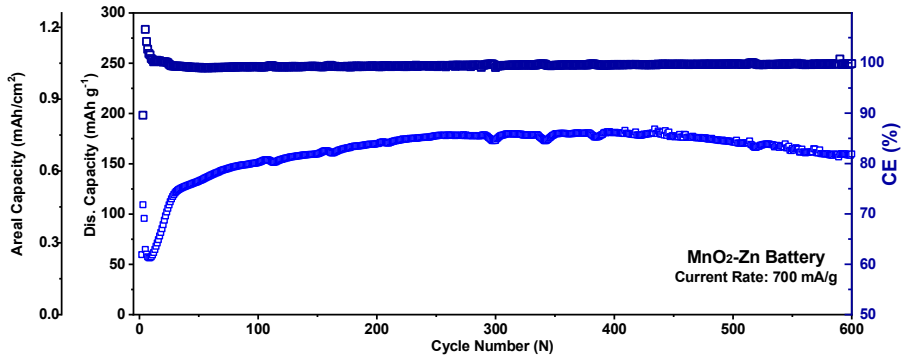

Figure 3.27 The cyclic stability and efficiency of Zn-MnO2 cell with ZIF-7 coated Zn anode at current density of 700 mA g^{-1}.

Table 3.2 Literature survey of previous reports of high concentrated electrolyte systems and our super-saturated electrolyte front surface in rechargeable Zn batteries

Electrolyte formula	**Symmetric cell performance**	**Full cell performance**			**reference**
		Cathode Loading (mg cm^{-2})	Performance	Current density	
1 M $Zn(TFSI)_2$ + 20 M LiTFSI/H_2O	0.2 mA cm^{-2} for 170 hours	$LiMn_2O_4$ /	28 mAh g^{-1}, 4000 cycles	600 (mA g^{-1})	44
30 M $ZnCl_2/H_2O$	0.2 mA cm^{-2} for 600 hours	$Ca_{0.20}V_2O_5{\cdot}_{0.80}H_2O$ (3~4 mg cm^{-2})	290 mAh g^{-1}, 1000 cycles	1600 (mA g^{-1})	54 77
0.5 M $ZnSO_4$ + 21 M LiTFSI/ H_2O	/	$LiMn_{0.8}Fe_{0.2}PO_4$ 5 mg cm^{-2}	110 mAh g^{-1}, 150 cycles	51 (mA g^{-1})	78
1 M $Zn(OTf)_2$ + 21 M LiTFSI/ H_2O	/	V_2O_5 /	110 mAh g^{-1}, 2000 cycles	2000 (mA g^{-1})	79
1 M $Zn(OTf)_2$ + 21 M LiTFSI/ H_2O	/	$VOPO_4$ 2 mg cm^{-2}	75 mAh g^{-1}, 1000 cycles	1000 (mA g^{-1})	80
2 M $ZnSO_4$+0.2 M $MnSO_4$	0.5 mA cm^{-2} for 3000 h	MnO_2 4.2 mg cm^{-2}	160 mAh g^{-1} 600 cycles	700 (mA g^{-1})	57 This work

Table 3.3 Literature survey of previous reports of modified strategies and our super-saturated electrolyte front surface in rechargeable Zn-MnO_2 batteries

Modified strategies	Symmetric cell performance	Full cell performance			reference
		Cathode Loading (mg cm^{-2})	Performance	Current density	
Nano-CaCO3 coating	0.25 mA cm^{-2} 0.05 mAh cm^{-2} for 800 hours	1 mg cm^{-2}	177 mAh g^{-1}, 1000 cycles	1000 (mA g^{-1})	[81]
3D carbon nanotube (CNT) framework	2 mA cm^{-2} 2 mAh cm^{-2} for 200 hours	4.3 mg cm^{-2}	167 mAh g^{-1}, 1000 cycles	4650 (mA g^{-1})	[82]
3D Porous Copper Skeleton framwork	0.5 mA cm^{-2} 0.5 mAh cm^{-2} for 350 hours	0.9-1.1 mg cm^{-2}	173 mAh g^{-1}, 300 cycles	400 (mA g^{-1})	[83]
Super-saturated electrolyte front surface	0.5 mA cm^{-2} 0.5 mAh cm^{-2} for 3000 h	4.2 mg cm^{-2}	160 mAh g^{-1} 600 cycles	700 (mA g^{-1})	[57] This work

3.8 Summary and conclusions

Herein, in this work, we contributed to revealing the Zn anode degradation mechanism and an effective strategy for high-performance rechargeable aqueous Zn battery. By thorough study on the de-solvation process, we highlighted the reactive water released from de-solvation process and its consequence of severe passivation on Zn metal anode surface. To minimize the side-effect of strong water activity, we proposed an efficient electrolyte solvation structure regulation strategy bypass the conventional high concentrated aqueous electrolyte (adding salts to form saturated electrolyte). The MOF with abundant pores and caves can be employed to accommodate ion-pairs of electrolytes and reject migration of most of large ion-pairs. A water-stable ZIF-7 (2.94 Å) coating was demonstrated a front layer on Zn metal surface and inhibited the decomposition of aqueous electrolyte. The Raman spectroscopy revealed that water activity in ZIF-7 channels was highly suppressed

and the Zn^{2+}-H_2O ion-pairs was signficantly enhanced. It indicates that ZIF-7 channels realized a super-saturated electrolyte in ZIF-7 channel under electric field. Benefitted from supersaturated front surface on Zn anode surafec, the lifespan of symmetric Zn half cell was promoted to 3000 hours at 0.5 mA cm^{-2} without obvious voltage fluctiation. The lifespan of Zn-MnO_2 battery was also prolonged up to 600 cycles, with a high retention of 88.9%.

Besides, we found that the Zn electrodeposit with ZIF-7 coating protection presented a a compact and smooth morpholohy. This flat deposition structure is extremely different flake-like dendrite growth morphology in previous literatures. Moreober, we carried out advanceed spectroscopy characterizations to prove less side-product accumulation on Zn anode surface. In brief, this work enlagres the applications of MOF or other porous materials (nano or micro-size) for rechargeable batteries. For example, in aqeuous Li-ion batteries, the strong water activity might induces severe hydrogen evolution reaction on negative electrode. We anticipate that this concept can be widely extended to other types aqueous and non-aqueous rechargeable batteries.

Chapter 4. Metal-organic framework as multi-functional ionic sieve membrane for long-life aqueous zinc-iodide batteries

4.1 Introduction

The employment of ZIF-7 coating on Zn metal anode surface has been confirmed effective to enhance electrode stability, by alleviating the water molecular corrosion and passivation. However, this approach remains infeasible at higher current density (>1 mA cm^{-2}) owing to the narrow MOF pore size (ZIF-7, 2.94 Å). Chapter 3 reveals the significance of pore size of MOF for electrolyte solvation structure regulation. In brief, the size dispersion of MOF channel severs as tool to determine the degree of de-solvation process by rejecting the water molecular. The small size distribution of MOF channel guarantees less water passivation, but simultaneously seems like a burden for fast-charging batteries. Besides, the working mechanism of Zn-MnO_2 battery also encumbers the fast-charging working and cannot enables long-term cycling performance. Therefore, it is necessary to develop a fast-charging and long-life rechargeable Zn batteries.

In the extensive family of rechargeable aqueous Zn batteries, Zn-iodine (Zn-I_2) battery is a competitive alternative for advanced Zn battery towards practical applications. Firstly, the Zn-I_2 battery system has a good prospect for scale-up application owing to the high natural element abundance in land or ocean (0.0075% earth crust for Zn element and 55 μg_{iodine} L_{ocean}^{-1} for iodine element).[84] In

consequence, the low-cost battery system based on aqueous electrolyte would be a safe choice.[85] Zn metal anode involves a two-electron plating/stripping reaction process and delivers -0.76 V *vs.* SHE electrode). Iodine cathode generally undergoes a liquid-liquid conversion ($I^-/I_2/I_3^-$ pathway) and contributes a theoretical capacity of 211 mAh g^{-1} based on the iodine mass. Therefore, the redox couple between Zn/Zn^{2+} and iodine species nowadays attracts extensive attention and becomes a safe and efficient rechargeable Zn batteries. Nonetheless, the employment of Zn-I_2 batteries still remains a problem because of the short cyclic life. Herein, we attribute the short lifespan to mainly the shuttle of iodine species and Zn anode degradation.

Similar to the dissolution of lithium polysulfide in lithium-sulfur battery, the I_3^- also has a high solubility in aqueous environment.[86-87] In the bulk electrolyte, the uncontrollable dissolution and migration of iodine species would cause severe shuttle effect, namely the directional transport of iodine species across concentration gradient. Therefore, the shuttle of iodine species would cause considerable capacity loss, low Coulombic efficiency, and poor cyclic life. The commonly used glass fiber separator is hardly to restrict and manipulate the free migration of iodine species. Most of previous literatures dedicated to artful host/substrate designs, which can accommodate and restrict the dissolution of iodine species.[88-91] For separator/membrane design, researchers have developed ion exchange membranes (such as Nafion) or solid-state electrolyte to cut-off the shuttle of iodine species for rechargeable lithium or sodium battery.[92-93] However, in our research topic of rechargeable aqueous Zn-I_2 batteries, the parasitic side-reaction from water molecular still remains a significant challenge.

Not just limited the shortcoming in iodine cathode side, the Zn anode in aqueous environment also faces severe Zn dendrite growth and surface passivation. The pristine Zn metal anode working in aqueous environment would simultaneously induce side-reaction and generate side-products such as $Zn(OH)_2$ and ZnO. Besides, the shuttle of iodine species also causes some unexpected results on Zn metal anode side. The free diffusion of iodine species to Zn anode might induce reaction with these side-products. The complex interplay between iodine species with side-product on Zn anode surface might cause some negative influence, such as more severe corrosion. However, this fundamental topic is still under elusive and urges a detailed analysis.

Chapter 3 proposed an effective and efficient approach to restrain the dendrite growth by developing a MOF protective coating on Zn anode surface. According to the detailed illustration, using MOF coating can effectively block the attack from water molecular and enhance Zn metal stability. Herein, in this work, we contributed a dual-functional MOF membrane to simultaneously resolve the problems in iodine cathode and Zn anode.[94] Inspired by the ionic sieve property of MOF channel and its degree of de-solvation process on MOF pore size, we demonstrated a Zn-BTC ($Zn_3(BTC)_2$) membrane for rechargeable aqueous Zn-I_2 batteries. As schematically illustrated in **Figure 4.1**, this MOF membrane has to resolve the free diffusion of iodine species and mitigate the Zn dendrite growth, by fully exploiting its pore size. First, the MOF membrane can shield the migration of I_3^- based on the physical restriction. Moreover, by tightly adhere the MOF membrane on Zn anode surface, this special membrane can also function as a layer to regulate the solvation structure and

then enhance Zn anode stability.

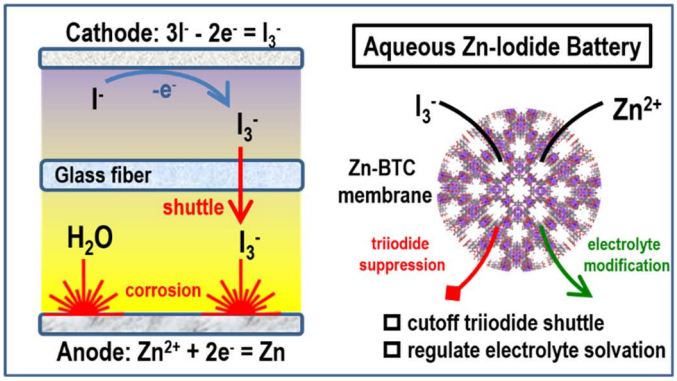

Figure 4.1 Schematic illustration of complex interplay in Zn-I_2 cells with conventional glass fiber separator and Zn-BTC membrane in our study.

4.2 Preparation of Zn-BTC membrane

To allow relatively larger ion-pairs to migrate through and enhance the tolerance on high current density, herein, we selected Zn-BTC material owing to its large pore size (~9 Å).[47] Zn-BTC also has a very good stability in aqueous environment, just like ZIF-7. The detailed preparation method of Zn-BTC powder is introduced in Chapter 2.2. Prior to a series of physical and electrochemical characterizations, Zn-BTC powder has to remove DMF solvent in the vacuum oven. The process of maintaining at 160ºC for 24 hours in vacuum oven can effectively remove the absorbed solvent in pores and caves. As shown in **Figure 4.2a**, Zn-BTC has a uniform pore size and caves, which serves as place to sieve and store electrolyte ion pairs. The XRD patterns of Zn-BTC is consistent with that from literature (**Figure 4.2b**).[45, 48] We then checked its morphology by SEM observation, which shown uniform and highly ordered particles (**Figure 4.2c-d**).

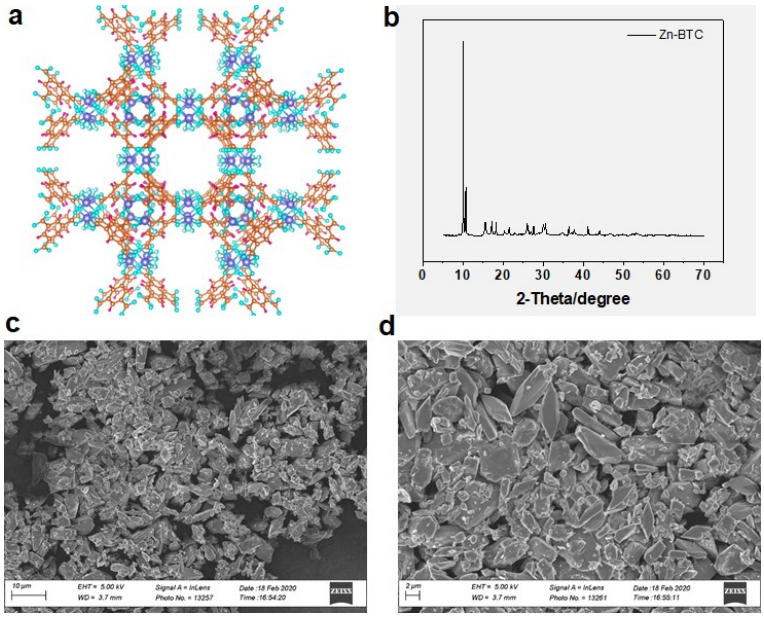

Figure 4.2 XRD and SEM characterization of as-synthesized Zn-BTC powder. (a) Schematic structure; (b) XRD characterization; (c, d) SEM images.

The as-prepared Zn-BTC power was mixed with PVDF slurry in DMF (mass ratio 3:1) and then dripped on glass fiber substrate by a simple blast-cast method. The composite was then coated on Zn metal anode surface and formed a compact membrane. The as-prepared Zn-BTC membrane maintains a typical morphology of Zn-BTC particle (**Figure 4.3**).

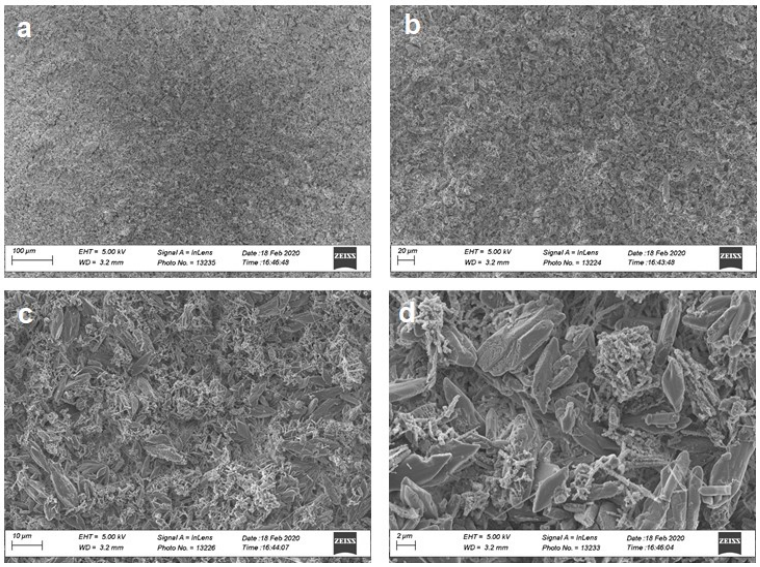

Figure 4.3 SEM images of Zn-BTC membrane without cracks voids at different scales.

Herein, we would like to highlight the selection of Zn-BTC membrane. The prepared Zn-BTC membrane is closely adhered on Zn plate surface without obvious gap (**Figure 4.4b**). One the one hand, the Zn-BTC membrane is proposed to physically block the free diffusion of iodine species, especially the I_3^-. One the other hand, the Zn-BTC membrane can also enhance Zn anode stability by developing a highly aggressive ion-pairs in Zn anode surface (**Figure 4.4a**).

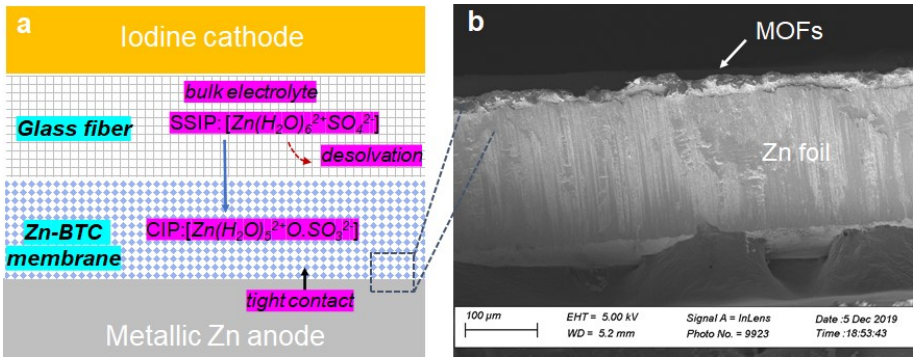

Figure 4.4 (a) Schematic illustration of assembled Zn-I_2 battery with Zn-BTC membrane; (b) The cross-section SEM image of Zn foil with Zn-BTC membrane.

4.3 Shuttle of iodine species

A home-designed V-type glass was used to visually monitor the shuttle of polyiodide species. The catholyte chamber composes of brown polyiodide, which is prepared by 1 mol LiI and 0.1 mol I_2 in aqueous environment. The 0.5 mol Li_2SO_4 aqueous solution is the colorless anolyte, which would become colorful as the invasion of polyiodide. For the V-type glass with common glass fiber separator, the anolyte color soon becomes light yellow only after 5min in the connected place and then fully turns brown deep yellow only after 8h (**Figure 4.5a**). The clear color change strongly certificates the rapid shuttle of polyiodide species across the glass fiber even without outside electric field. On the contrary, the V-type glass with Zn-BTC membrane did not observe obvious color change, neither in the joint place nor the bulk anolyte. After resting for 7 days, the anolyte remains colorless, which

strongly confirms the benign resistance property against shuttle of polyiodide species.

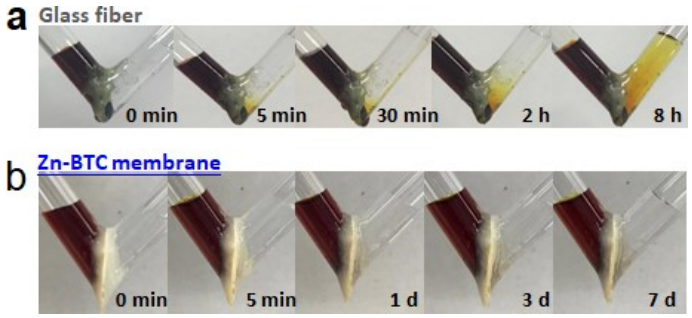

Figure 4.5 Optical observation of home-made V-type glass with anolyte. (a) With glass fiber separator. (b) With Zn-BTC membrane.

We then carried out an electrochemical aging process to characterize its self-discharge process. When fully charging the Zn-I_2 cell up to 1.6 V, almost iodine species would convert into brown polyiodide. After the galvanostatic charge process, the cells are idled at different time for free migration of iodine species. Firstly, we checked the galvanostatic discharge-charging process of Zn-I_2 cells with different separators after resting time. Comparatively, the over-potential in glass fiber separator group is much lower than that in Zn-BTC membrane group, which might be caused by the increased resistance in the interface (**Figure 4.6**). With the interval time ranging from 0.5 to 5 hours, the specific capacity of glass fiber separator group exhibits a noticeable fading, which can be attributed to active iodine species loss during the resting time (**Figure 4.6**). Moreover, we defined the Coulombic efficiency by the ratio of discharging capacity to charging capacity (Equation 5). Generally, the discharge capacity is lower than the charging capacity owing to the loss of active material into the bulk electrolyte. We found that the glass fiber separator group delivers a lower Coulombic efficiency of 95% when setting the resting time at 0.5 hour, which indicates about 5% active materials lost. Further prolonging the rest time to 5 hours, the Coulombic efficiency only remains about 80%.

$$\text{Coulombic efficiency} = \frac{\text{Discharge capacity}}{\text{Charge capacity}} \times 100\% \qquad \text{Equation (5)}$$

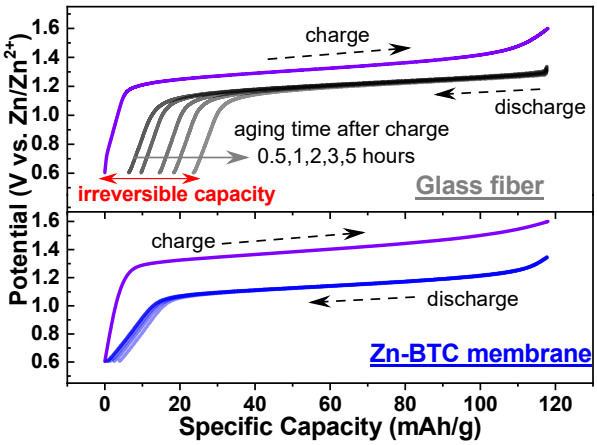

Figure 4.6 Electrochemical aging test (from 0.5 to 5 hours resting after fully charge state) for Zn-I_2 batteries with GF separator (upper) and Zn-BTC membrane (lower).

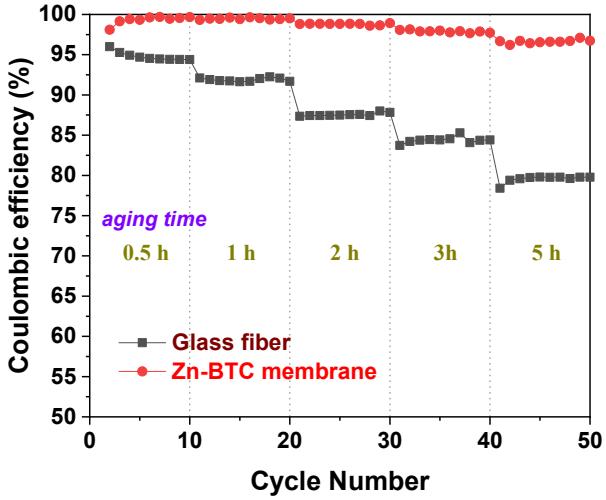

Figure 4.7 Coulombic efficiency of Zn-I_2 cells with different separators after resting time ranging from 0.5 to 5 hours.

We then checked the galvanostatic discharge-charging process cell with Zn-BTC membrane. The profiles of discharge process after different resting time are almost overlapped without obvious capacity fading, which indicates negligible active material loss during idling time (**Figure 4.7**). Similarly, we calculated the Coulombic efficiency for Zn-I_2 cell with Zn-BTC membrane. It was found that the Zn-BTC membrane group maintains a high Coulombic efficiency near 100% when setting the resting time at 0.5 hour, which indicates almost no active materials lost. Further prolonging the rest time to 5 hours, the Coulombic efficiency still delivers about 98%

(**Figure 4.7**). In brief, the Zn-BTC membrane is proved effective to shield the migration of iodine species, not only in the static home-made V-type glass, but also in the cycled Zn-I_2 cells.

We then carried out Raman spectra to further prove the shuttle of iodine species shuttle to Zn anode by a home-made cell (**Figure 4.8**). The separators (both glass fiber and Zn-BTC membrane) surface can be easily detected a sharp peak locating at 981 cm^{-1}, which is ascribed to ν-SO_4^{2-} band (**Figure 4.9**).[58] For glass fiber separator, there is a distinct peak at 122 cm^{-1}, which is attributable to liner triiodide species.[95-96] Moreover, the peak still maintained even with the detection depth, which indicates the glass fiber inside was occupied by the triiodide species, from the surface to internal space.

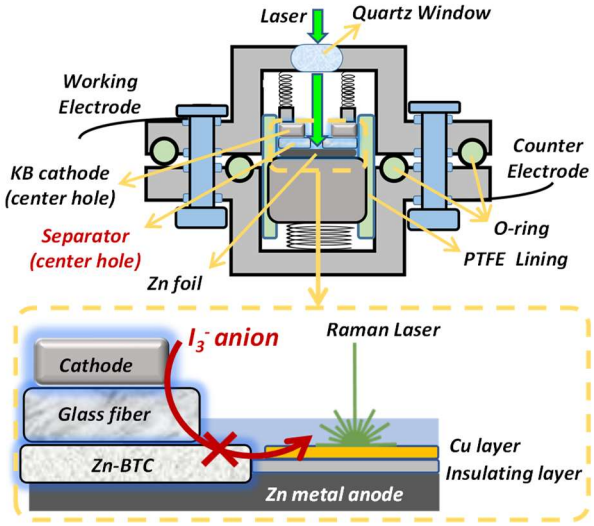

Figure 4.8 A home-made Zn-I_2 cell equipped with Raman spectroscopy.

During the charge process, iodine species would continuously convert into I_3^-. When the soluble I_3^- migrate through separator and would been detected by Raman laser. In cell with glass fiber separator, the large amount of I_3^- shuttle would be easily mobile to Cu layer and be confirmed by Raman laser (**Figure 4.9a**). In comparison, Raman laser cannot detect the signal of I_3^- in the Cu layer with Zn-BTC membrane (**Figure 4.9b**).

Similarly, Zn-BTC membrane obtained from cycled Zn-I_2 cell did not observe the spectra of triiodide both in the surface and inside region. The in-depth analysis substantiated that glass fiber is infeasible to cut-off the permeation of triiodide. In comparison, Zn-BTC membrane can effectively eliminate the permeation of iodine species.

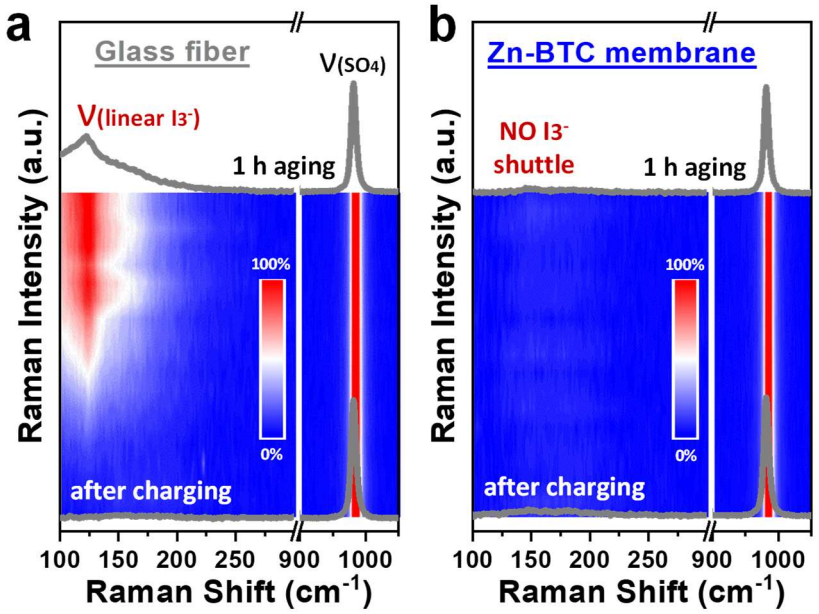

Figure 4.9 Raman spectroscopy characterization to detecting the components in different separators harvested from Zn-I_2 cells after 1 hour aging. (a) With glass fiber separator. (b) With Zn-BTC membrane.

4.4 Side-effect of shuttled iodine species

Besides the active material loss owing to the shuttle effect, we then carefully studied the side-effect of shuttled iodine species on Zn anode. The migration of iodine species and complex interplay on Zn anode surface remains elusive. Generally, we have a basic background that the shuttled polysulfide species involves a complex reaction with Li metal anode in rechargeable Li-sulfur batteries.[86, 97-99] The extensive accumulation of lithium polysulfide would generate a thick passivation layer, which is generally ionic insulator and would cause negative impact for ion transport and Li

metal deposition.

Herein, we would like to systematically study Zn anode surface component by advanced operando Raman and micro-infrared (IR) spectroscopy characterizations, which is harvested from cycled Zn-I_2 cells. The obtained Zn plates were fully rinsed by DME solution to remove the precipitated salts and attached glass fiber, which also washed the attached soluble iodine species. Generally, Zn metal anode surface involves a side-reaction from water molecular, leaving a passivation layer consisting of ZnO and $Zn(OH)_2$. Firstly, we checked the Zn plate harvested from Zn-I_2 cell with glass fiber separator. There is a typical spectrum of ZnO crystals, which consists of A1(TO) mode at 380 cm^{-1}, E_2(h) mode at 437 cm^{-1}, E_2(h-l) mode at 329 cm^{-1}, respectively (**Figure 4.10a**).[96] The varied spectrum indicated that ZnO crystal deposit has no preferred orientation. However, we did not detect any *v*-OH band, which is a typical spectra of $Zn(OH)_2$. The Raman spectroscopy was then equipped with ion sputtering measurement to etch the Zn anode surface and check the component distribution. With several etching times, these typical spectrum of ZnO crystal still remained unchanged, which indicated the severe corrosion from water molecular from surface to in-depth (**Figure 4.10a**). However, the thick side-product on Zn anode surface is not consistent with no observation of $Zn(OH)_2$ component. Further etching the Zn plate, we found both ZnO and $Zn(OH)_2$, which generally are common side-products in neat aqueous electrolytes. The existence of $Zn(OH)_2$ inside Zn plate not only proves the severe corrosion Zn metal, but also indicates a $Zn(OH)_2$-conusmption reaction process in iodine-contained electrolyte. Micro-IR spectroscopy provides a supporting proof, where $Zn(OH)_2$ can only be found in the in-depth Zn plate (**Figure 4.10b**). In the surface and shallow layer of Zn plate, ZnO species is the only side-product. Herein, we assume that most of $Zn(OH)_2$ in the shallow surface was reacted by the iodine species.

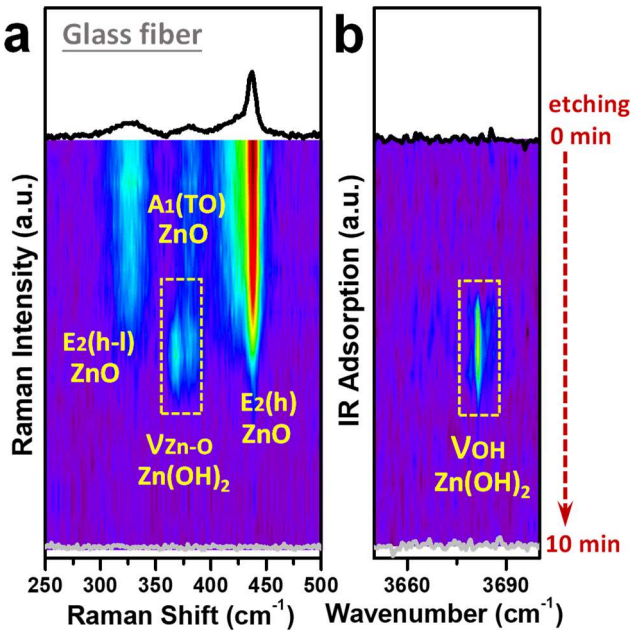

Figure 4.10 In-depth spectroscopy characterizations of Zn plate harvested from Zn-I_2 cells after cycling with glass fiber separator. (a) Raman spectroscopy. (b) Micro-IR spectroscopy.

We then checked the Zn plate surface harvested from the cell with Zn-BTC membrane. The Zn plate surface occurred typical spectra of ZnO and $Zn(OH)_2$, which is sharply different with that in glass fiber group. The three typical spectra can be attributed to ZnO crystal, which is same with that in blank group (**Figure 4.11a**). Micro-IR gives a sharp peak of $Zn(OH)_2$ at ca. 3861 cm^{-1}, which substantiates almost no consumption of $Zn(OH)_2$ (**Figure 4.11b**). Moreover, these spectra soon disappeared after several etching and confirmed the shallow side-product layer.

By comparison with the spectroscopy results from Zn-BTC membrane group, we assume the disappearance and re-appearance of $Zn(OH)_2$ on Zn plate in blank group remains elusive and a very interesting topic. First, the thick side-product layer on Zn plate surface and uneven distribution of ZnO and $Zn(OH)_2$ from glass fiber group might derives from the side-reaction between triiodide species with $Zn(OH)_2$.

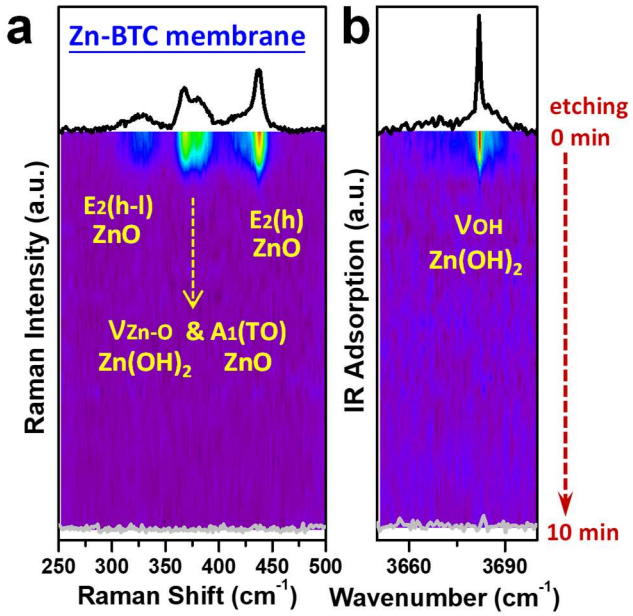

Figure 4.11 In-depth spectroscopy characterization of Zn plate harvested from Zn-I_2 cell after cycling with Zn-BTC membrane. (a) Raman spectroscopy. (b) Micro-IR spectroscopy.

We then carried out in-situ differential electrochemical mass spectrometry (DEMS) and ex situ Gas chromatography–mass spectrometry (GC–MS) measurements to study the inhomogeneous distribution of side-product on Zn anode surface. The in-situ DEMS was equipped with Zn-I_2 home-made cells for monitoring the gas evolution. Generally, Zn cell in aqueous electrolyte only releases hydrogen (H_2), which derives from side-reaction of water molecular on Zn anode side with pH change and side-product accumulation.[96] This H_2 evolution was proved in our experimental (**Figure 4.12**). However, the extra oxygen (O_2) is elusive because of low charging potential (<1.6 V *vs.* Zn/Zn^{2+}). Therefore, this strange O_2 evolution is hardly coming from water splitting but originate from the complex interplay between $Zn(OH)_2$ with iodine species. This complex interplay is similar with that in lithium-oxygen batteries, where LiOH reacts with I_3^- with a clear O_2 evolution.[100] In our case, the complicated aqueous environment consists of water molecular, iodine, and lots of polyanions, which involves a reaction with $Zn(OH)_2$.[101-102] Therefore,

based on the component analysis of Zn metal anode and GC-MS measurement, we concluded that O_2 evolution derives from reaction of IO^- species with $Zn(OH)_2$ (Equation 6).

$$I_3^- + Zn(OH)_2 \rightarrow IO^- \rightarrow I^- + O2\uparrow \qquad \text{Equation (6)}$$

Herein, we assume a reaction mechanism for Zn anode degradation process. The shuttled triiodide from negative electrode, involves a complex reaction with $Zn(OH)_2$ in Zn anode surface with a clear O_2 evolution. This interplay can well illustrates the disappearance of $Zn(OH)_2$ in the shallow layer of Zn plate. For the group with Zn-BTC membrane, there is no obvious O_2 and H_2 evolution (**Figure 4.12**). The restrained O_2 evolution might derives from the cut-off of iodine species and subsequent reaction with $Zn(OH)_2$. As for the diminished H_2 evolution, we assumed that Zn-BTC membrane also favors the Zn anode reversibility by suppressing water molecular activity. This would be deliberately illustrated in next part.

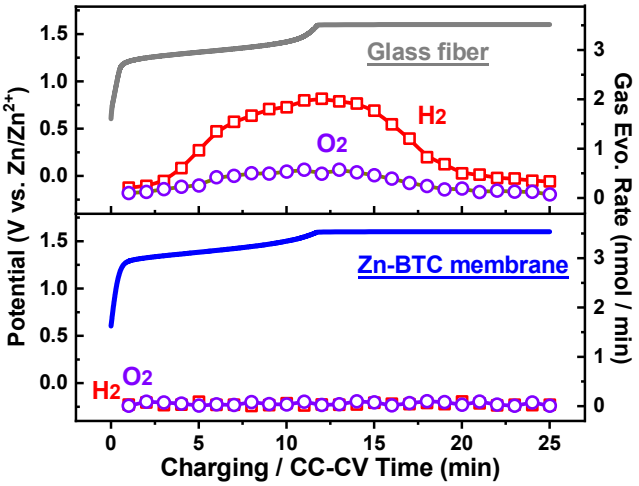

Figure 4.12 Gas evolution rate of H_2 and O_2 on the Zn-I_2 cells charging with GF separator and Zn-BTC membrane.

We then carried out SEM observation on Zn plates after cycled in Zn-I_2 cells. The Zn plate harvested from blank group can be detected lots of cracks and voids even in large-scale observation (**Figure 4.13a**).[103] Further close observation finds the dendrite growth occupied the cracks, which might be caused by gas evolution from Zn

anode side (**Figure 4.13b**). The release of gas might deconstruct the Zn anode stability and leave pore structure.[104] In a sharp comparison, we also observed the Zn plate obtained from cycled Zn-I_2 cells with Zn-BTC membrane. The morphology turns out homogeneous and uniform without obvious cracks or voids (**Figure 4.13c**). This integral structure favors fast ion and electron migration in the Zn anode surface.

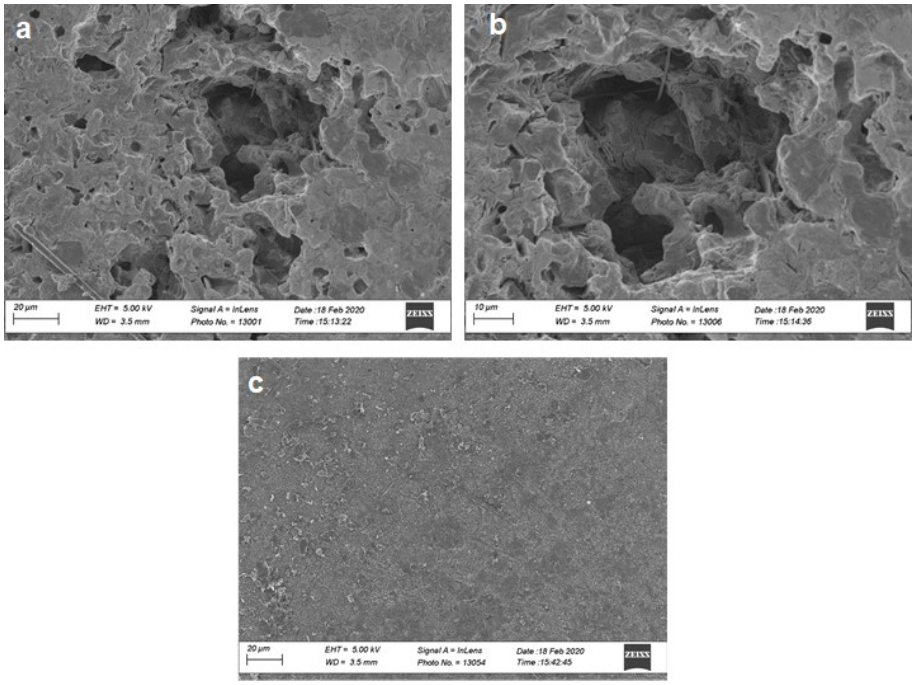

Figure 4.13 The SEM images of Zn plates after cycled Zn-I_2 cells. (a-b) with GF separator. (c) with Zn-BTC membrane.

In brief, we would like to conclude the failure mechanism of Zn-I_2 system (**Figure 4.14a**). First, the uncontrollable shuttle of soluble iodine species would induce irreversible iodine loss, capacity drop and low efficiency. Moreover, Zn anode stability in aqueous electrolyte also induces severe water passivation, with side-product accumulation and H_2 evolution. More critically, the diffused iodine species would react with $Zn(OH)_2$, which not only causes an uneven component distribution of Zn anode surface, but also releases O_2 evolution. This complex interplay negatively destructs the Zn anode stability and exacerbates Zn anode reversibility. We believe the comprehensive Zn anode degradation mechanism cannot

enable its long-term working.

In the case with Zn-BTC membrane, the free migration of iodine species was firstly blocked and then also inhibited the complex interplay with $Zn(OH)_2$ (**Figure 4.14b**). Therefore, the Zn anode surface component distribution has a thin and uniform ZnO and $Zn(OH)_2$. Moreover, the diminished gas evolution including O_2 and H_2 would benefit the benign maintenance of Zn anode structure. Therefore, the Zn plate did not suffer lots of attack coming from both iodine species and water molecular with the shield of Zn-BTC membrane.

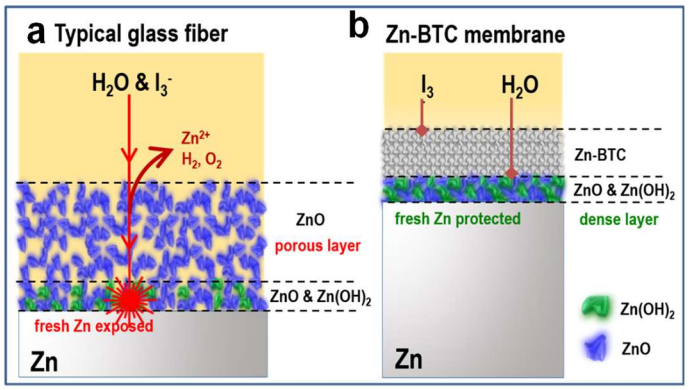

Figure 4.14 Schematic illustration of degradation of Zn-I_2 cell, coming from active material loss, water molecular attack on Zn metal anode surface and the complex interplay between iodine species with side-product on Zn anode surface. (a) system with glass fiber separator. (b) system with Zn-BTC membrane.

4.5 Raman spectroscopy study on electrolyte solvation structure

Besides the above detailed study on Zn anode degradation from the perspective of shuttled iodine species, herein, we would like to emphasize the advantages of Zn-BTC membrane in Zn anode protection aspect. Similar to the illustration in Chapter 3, we firstly studied the Raman spectra of conventional liquid $ZnSO_4$ solutions (**Figure 4.15**). The common solvated ion-pairs can be split into SSIP and CIP, according to their association degree. With the increase of concentrations, the

Zn-OH_2 vibration at390 cm^{-1} was diminished and the Zn-O vibration envolved into [Zn^{2+}·OSO_3^{2-}] (ca. 260 cm^{-1}). Besides, the *v*-SO_4^{2-} band at ~984 cm^{-1} also evidenced an blue-shift. Moreover, the O-H stretch vibration for water molecular was highly suppressed and proved a blue-shift for "HOH-OSO_3^{2-}" vibration.[63-64]

Comparatively, the spectra in Zn-BTC channels displayed a highly aggressive ion-pairs (**Figure 4.15**). In detail, the Zn-OH_2 vibration was signficantly suppressed and most of Zn^{2+} evolved into [Zn^{2+}·OSO_3^{2-}]. The solvation of *v*-SO_4^{2-} band then became into a fully CIP mode, which indicates all water molecualr was coordinated with Zn^{2+}. Besides, the water molecular interaction was greatly suppressed and a signficant blue-shift of "HOH-OSO_3^{2-}" vibration. In all, the unique Raman spectra indicated a super-concentrated electrolyte solvation sturtcure in Zn-BTC channels.

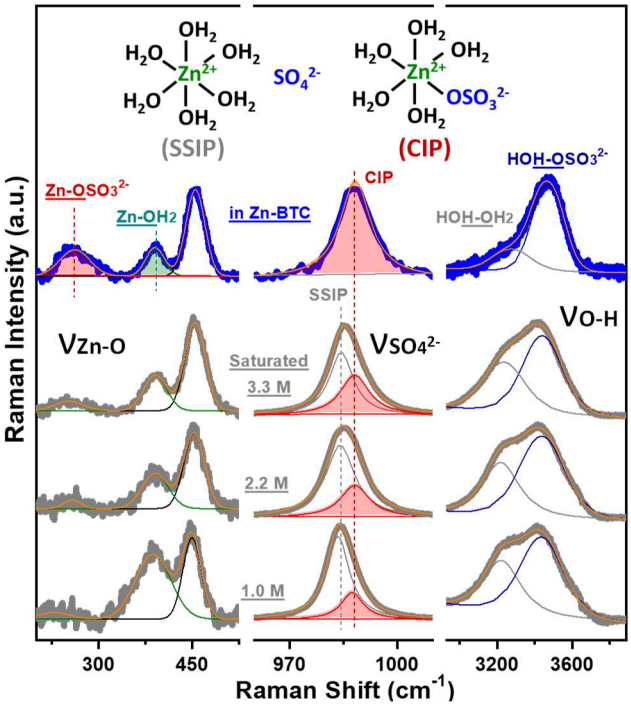

Figure 4.15 Raman spectroscopy for aqueous $ZnSO_4$ solutions and solvation configuration in Zn-BTC channels.

We would like to compare the solvated degree with that in saturated electrolyte (3.3 mol). The saturated liquid electrolyte has two solvation mode, SSIP and CIP, where most of water molecular belongs to free water (**Figure 4.16a**). The

accomodation of ion-pairs into Zn-BTC channel fully coordinated all free water molecular and evolved the SSIP mode to fully CIP mode (**Figure 4.16b**). In brief, most of water molecular in SSIP and free state changed into CIP mode, which mitigated the Zn anode corrosion.[60]

Therefore, in our case with Zn-BTC membrane, the ion-pairs under electric field completed a partical de-solvation process. The region near to Zn anode surface reaches a highly concentrated ion-pairs, which is differernt from the loose structure in the bulk electrolyte (**Figure 4.17**).

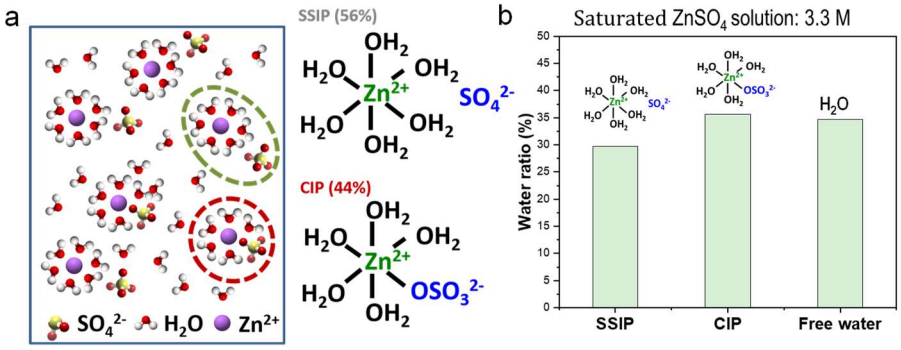

Figure 4.16 Study of solvated structure for saturated $ZnSO_4$ solution. (a) Solvation sheath in SSIP and CIP mode and their ratios; (b) Water molecular distribution in saturated $ZnSO_4$ solution.

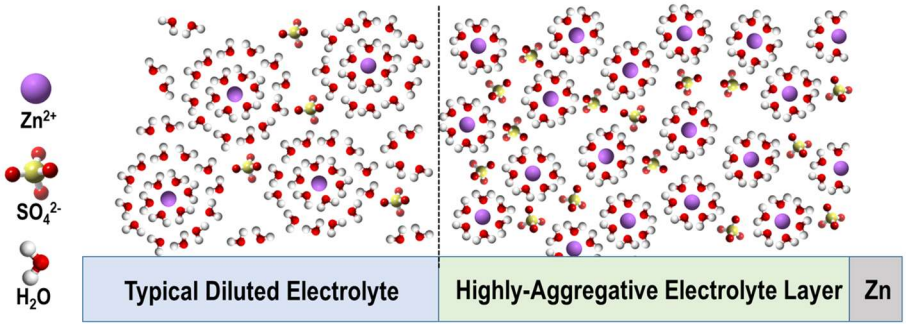

Figure 4.17 The loose solvation configurations of $ZnSO_4$ solutions and high-aggregative electrolyte layer on Zn anode in MOF channels.

4.5 Study on Zn anode stability

We then carried out symmetric Zn||Zn cells with different separators under the

test condition of 0.5 mA cm^{-2}/0.5 mAh cm^{-2} in conventional 2 mol $ZnSO_4$ electrolyte. In the blank group, the voltage profiles maintained stable before 100 hours and soon fluctuated after that (**Figure 4.18**). The instable voltage evolution profile indicates uncontrollable Zn dendrite formation on bare Zn plate. Soon, the symmetric Zn||Zn cell is short-circuit owing to the final Zn dendrite piercing through the glass fiber.

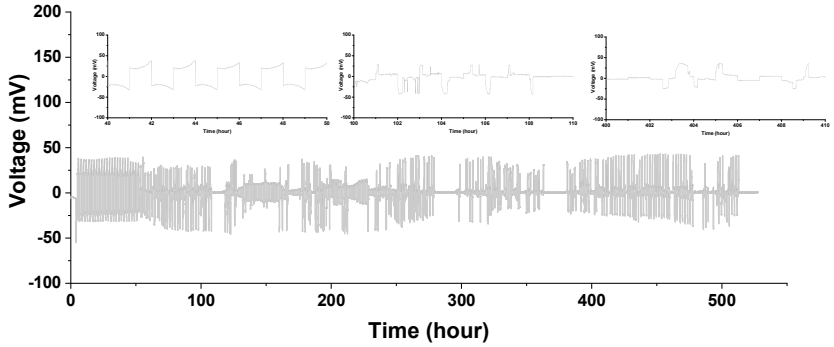

Figure 4.18 Symmetric Zn half-cells of Zn plates with glass fiber separator.

We then examined the stability in symmetric Zn||Zn cell with Zn-BTC membrane. We observed a extremely stable voltage evolution profile up to 3000 hours without significant fluctuation (**Figure 4.19a**). The much-extended lifespan proved the effectiveness of Zn-BTC membrane to Zn anode. The over-potential at initial state reached ca. 60 mV and gradually reached a stable state ca. 40 mV (**Figure 4.20**). Moreover, the over-potential profile does not have obvious movements to the end of test time. We then attributed the enhanced stability to the CIP solvation mode in Zn-BTC channels, which would release less reactive water molecular.

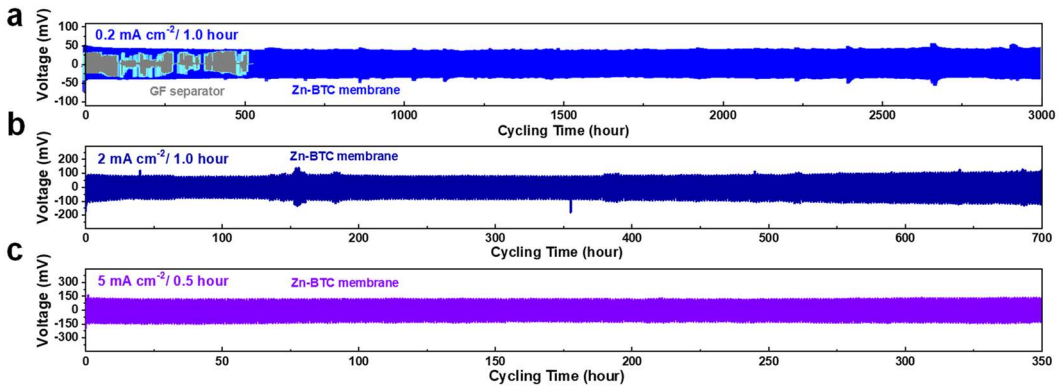

Figure 4.19 The cyclic life of symmetric Zn half-cells with Zn-BTC membrane under different test conditions. (a) 0.2 mA cm^{-2}/0.2 mAh cm^{-2}. (b) 2 mA cm^{-2}/2 mAh cm^{-2}. (c) 5 mA cm^{-2}/2.5 mAh cm^{-2}.

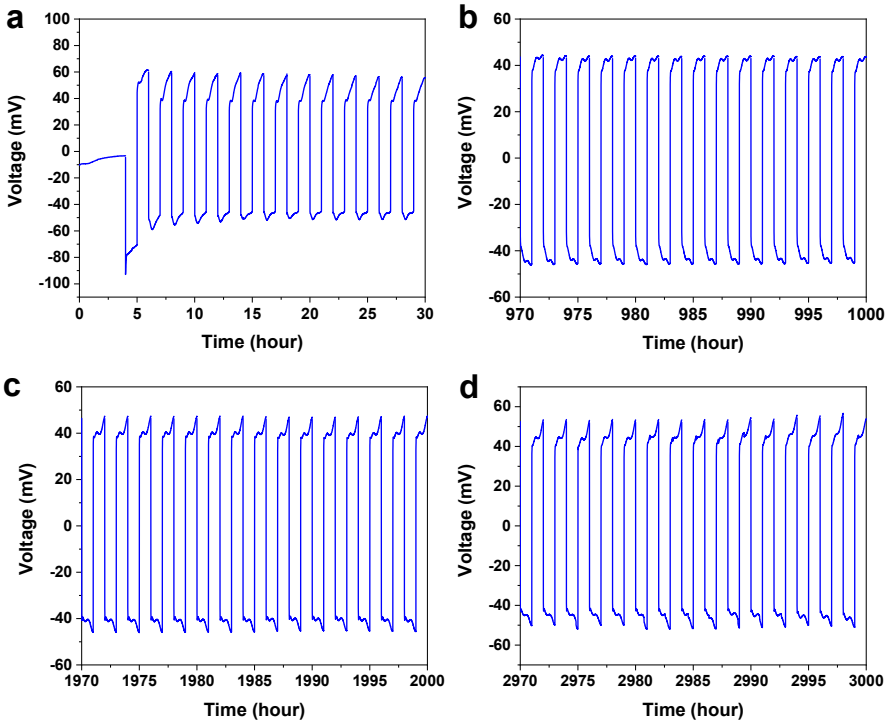

Figure 4.20 The over-potential evolution profiles of symmetric Zn half-cell with Zn-BTC membrane under the test condition of 0.2 mA cm^{-2}/0.2 mAh cm^{-2}.

To exclude the possibility of PVDF function, we then separately prepared PVDF-coated Zn plate for symmetric Zn||Zn cell. We found that the over-potential of PVDF-coated Zn began fluctuated after near 150 hours (**Figure 4.21**). It indicated that PVDF-coating cannot significantly improved the lifespan but only serves as the binder to connect the Zn-BTC powder.[105]

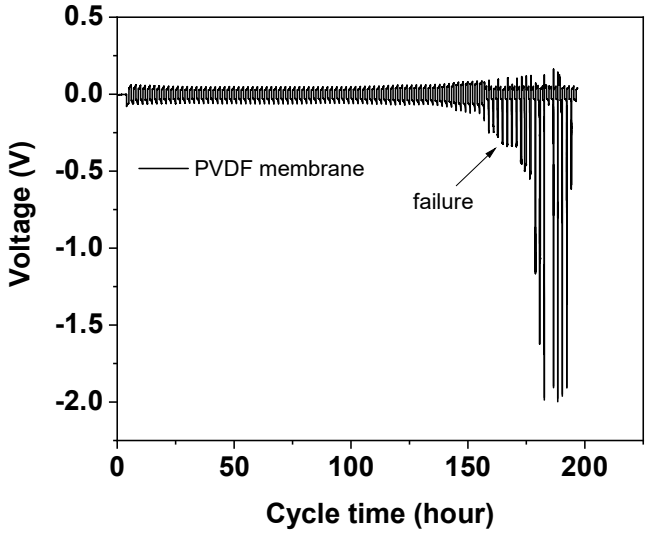

Figure 4.21 The over-potential evolution of symmetric Zn half-cells with PVDF membrane at current density under the test condition of 0.2 mA cm^{-2}/0.2 mAh cm^{-2}.

Based on the benign electrochemical behaviors at 0.2 mA cm^{-2}/0.2 mAh cm^{-2}, we tried to change the test condition into 2 mA cm^{-2}/2 mAh cm^{-2}. With the assistance of Zn-BTC membrane, the symmetric Zn cell maintained stable cycle up to 700 hours without obvious voltage fluctuation (**Figure 4.19b**). At the end of test, the over-potential maintained ca. 100 mV, which was almost overlapped with previous cycles (**Figure 4.22**).

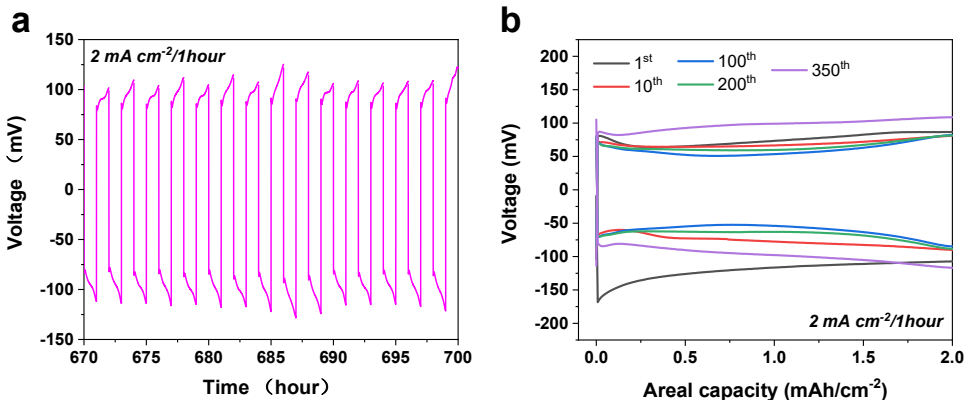

Figure 4.22 The over-potential evolution of symmetric Zn half-cell with Zn-BTC membrane under the test condition of 2 mA cm^{-2}/2 mAh cm^{-2}. (b) Voltage hysteresis of different cycles.

We then tried to boost the current density to 5 mA cm^{-2} with an areal-capacity of

2.5 mAh cm^{-2}, which is an important parameter towards practical application. The symmetric Zn cell extended the lifespan to 350 hours (**Figure 4.19c**). The over-potential is ca. 125 mV even after the end of test (**Figure 4.23**). To emphaize the advantages of Zn-BTC membrane strategy, we summarized a table to compare its lifespan (**Table 4.1**).

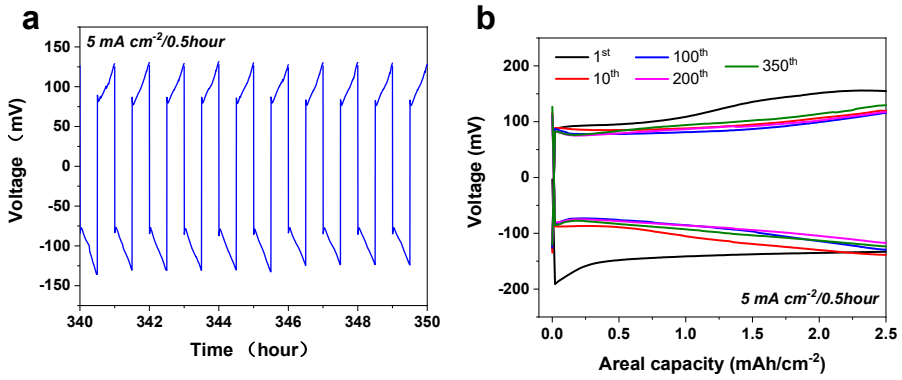

Figure 4.23 (a) The over-potential evolution of symmetric Zn half-cell with Zn-BTC membrane under the test condition of 5 mA cm^{-2}/2.5 mAh cm^{-2}. (b) Voltage hysteresis of different cycles.

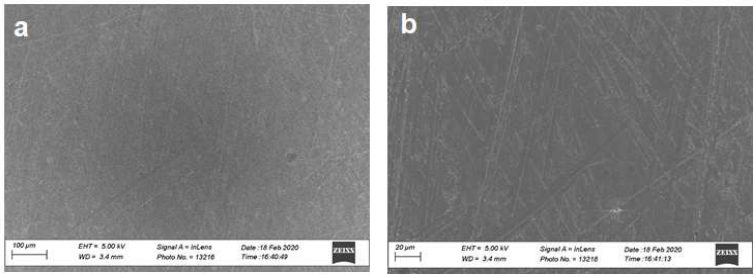

Figure 4.24 (a-b) The SEM images of pristine Zn plate surface.

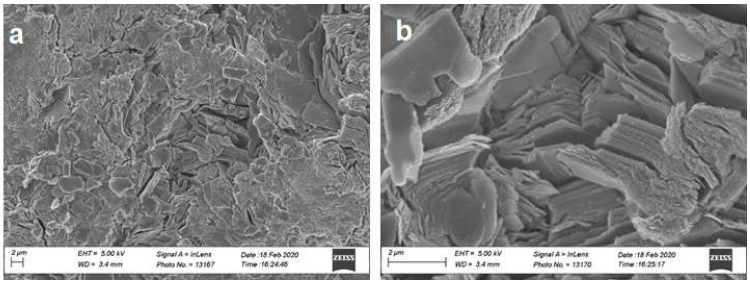

Figure 4.25 (a-b) The SEM images of Zn plate surface after cycling with glass fiber separator.

Table 4.1 Literature survey of previous strategies to prolong lifespan of symmetric Zn cells.

Strategies	Electrolyte formulation	Electrochemical behaviors	Areal capacity	Ref.
High concentrated electrolyte	1 M $Zn(TFSI)_2$ + 20 M LiTFSI/ H_2O	0.2 mA cm^{-2} for 170 hours	/	44
High concentrated electrolyte	30 M $ZnCl_2/H_2O$	0.2 mA cm^{-2} for 600 hours	0.033 mAh cm^{-2}	54
Nanoporous $CaCO_3$ Coatings	3 M $ZnSO_4$ + 0.1 M $MnSO_4$	0.25 mA cm^{-2} for 800 hours	0.05 mA cm^{-2}	81
Organic electrolyte	0.5 M $Zn(OTf)_2$/TEP 0.5 M $Zn(OTf)_2$/TMP	0.5 mA cm^{-2} for 3000 hours 1.0 mA cm^{-2} for 2400 hours	0.5 mAh cm^{-2} 1.0 mAh cm^{-2}	33 32
3D-matrix and electrolyte additive	1 M $ZnSO_4$ + 0.5 M Na_2SO_4 + 1 g/L polyacrylamide	1.0 mA cm^{-2} for 180 hours 20 mA cm^{-2} for 100 hours	1 mAh cm^{-2} 1 mAh cm^{-2}	106
3D-cooper matrix	2 M $ZnSO_4$	0.5 mA cm^{-2} for 350 hours	0.5 mAh cm^{-2}	83
3D-CNT matrix	2 M $ZnSO_4$	2.0 mA cm^{-2} for 200 hours 5.0 mA cm^{-2} for 100 hours	2.0 mAh cm^{-2} 2.5 mAh cm^{-2}	82
3D-ZnO coating	2 M $ZnSO_4$	5.0 mA cm^{-2} for 500 hours	1.25 mAh cm^{-2}	53
Zn-BTC membrane	2 M $ZnSO_4$	0.2 mA cm^{-2} for 3000 hours 2 mA cm^{-2} for 700 hours 5.0 mA cm^{-2} for 350 hours	0.2 mAh cm^{-2} 2 mAh cm^{-2} 2.5 mAh cm^{-2}	94 This work

The Zn anode morphology change was observed by comparing the uniform pristine Zn surface without damage (**Figure 4.24**). The Zn plate cycled in cell with glass fiber separator turns out inhomogeneous structure (**Figure 4.25a**). The typical flake-like dendrite growth occupied the whole region, which is similar with previous literatures (**Figure 4.25b**). We then carefully studied the Zn morphology, which harvested from cycled cell with Zn-BTC membrane. The large-scale observation is uniform and smooth surface, without large dendrite growth (**Figure 4.26a-b**). Further observation turns out uniform and well-distributed flake-like Zn deposits on the whole region (**Figure 4.26c-d**). This nano-sized three-dimensional Zn deposits is similar to

that in organic electrolytes. In organic electrolytes, the much lower water activity significantly enhanced its thermodynamic activity with Zn metal. Herein, by reducing the water activity, Zn-BTC membrane also favors the three-dimensional Zn deposits.

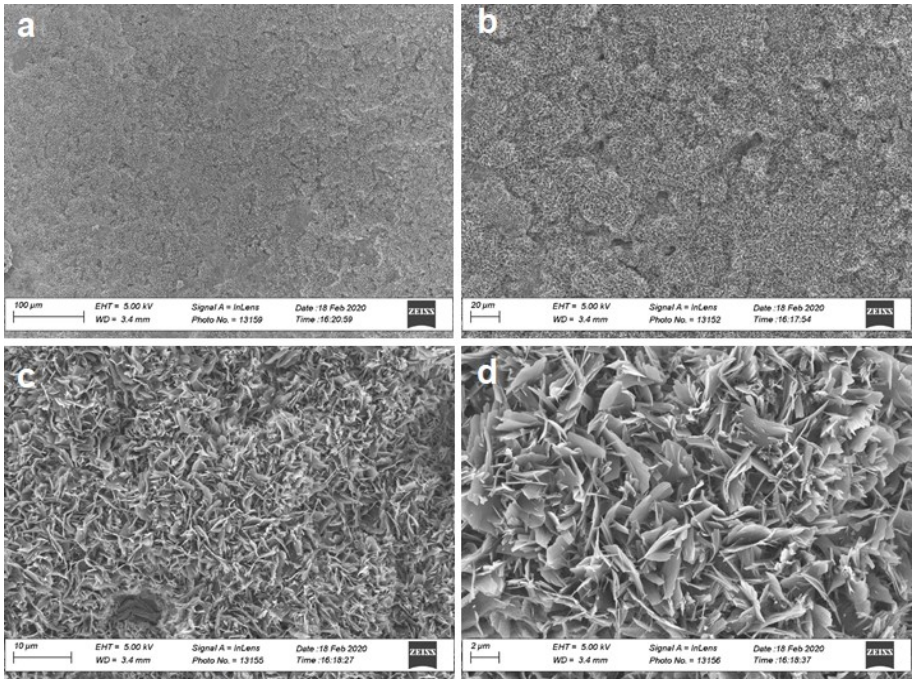

Figure 4.26 (a-d) The SEM images of Zn plate surface after cycling with Zn-BTC membrane at 2 mA cm^{-2}/2 mAh cm^{-2} after 700 hours.

4.6 Electrochemical performance of Zn-I_2 battery

Then, we evaluated the Zn-I_2 coin-cells by electrochemical characterizations. All specific capacity and current density in this work is calculated based on mass of iodide species. The cell with glass fiber separator delivered a capacity of 194 mAh g^{-1} at current density of 160 mA g^{-1}, with a iodine utilization approaching 92% after several initial cycles (**Figure 4.27a**). However, the specific capacity then dropped to 156 mAh g^{-1} within 100 cycles. The Coulombic efficiency is also crucial parameter to moniteor the shuttle of iodine species. The Coulombic efficiency only maintained ca. 94% for each cycle (**Figure 4.27b**). It indicated that ca. 6% iodine species loss during each cycle, which would considerably despair the advantages of Zn-I_2 battery.

In comparsion, the cell equipped with Zn-BTC membrane exhibits a more stable capacity profile with a high retention of 99% within 100 cycles, delivering high-capacity of 201.1 mAh g^{-1} and high iodine utilization of 95.3% (**Figure 4.27a**). More importantly, the The Coulombic efficiency remains above 99% for each cycle (**Figure 4.27b**). The electrochemical performance is highly consistent with above-mentioned study on battery degradation.

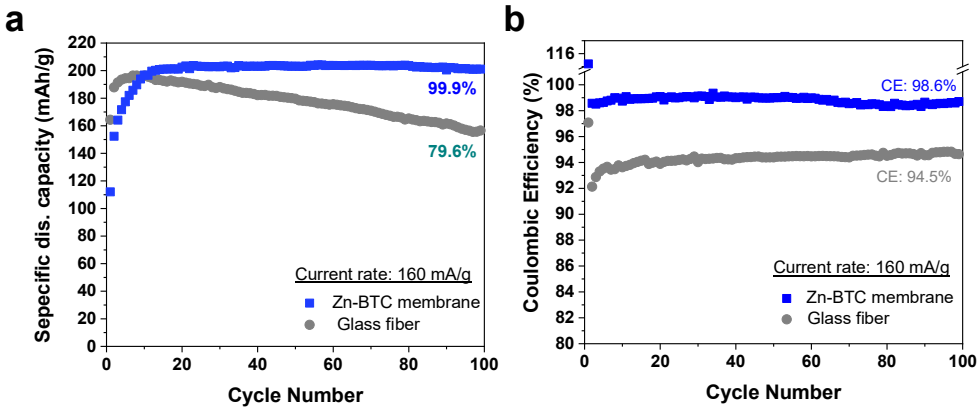

Figure 4.27 (a) Cyclic performance of Zn-I_2 cells at 160 mA g^{-1} with different separators. (b) Corresponding Coulombic efficiency of Zn-I_2 cells.

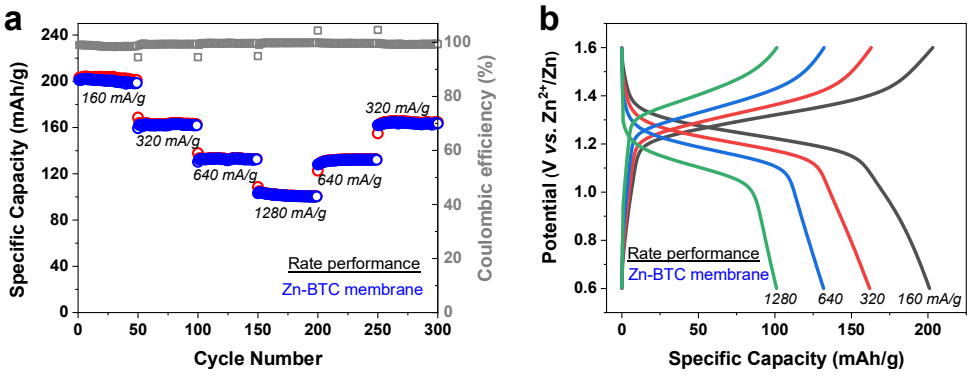

Figure 4.28 (a) The rate behavior of Zn-I_2 cells with Zn-BTC membrane. (b) Corresponding charge/discharge voltage profile under different current densities.

For Zn-I_2 battery with Zn-BTC membrane, we then characterized its rate performance. The specific capacity delivered much lower capacity as the increase of rate (**Figure 4.28a**). Moreover, the specific capacity almost entirely recovered to high-capacity when the rate recover back, which indicated the intact redox reaction of iodine species at high rates (**Figure 4.28a**). The corresponding discharge/charge

potential profiles still remain the typical reaction of iodine cathode (**Figure 4.28b**).

Then, we conducted cyclic voltammetry (CV) measurment for Zn-I_2 battery with Zn-BTC membrane. The CV profile at 0.04 mV s^{-1} displayed a oxidation and reduction potential at 1.32 and 1.23 V, respectively (**Figure 4.29a**). With the increase of sweep rate ranging from 0.04 to 0.24 mV s^{-1}, the potential polarization also enlarged. We then depicted the correlation between peak current with sweeping rate. The relationship obeyed the typical diffusion-controlled routine, where peak current has a good linearity to with square root of sweeping rate (**Figure 4.29b**).

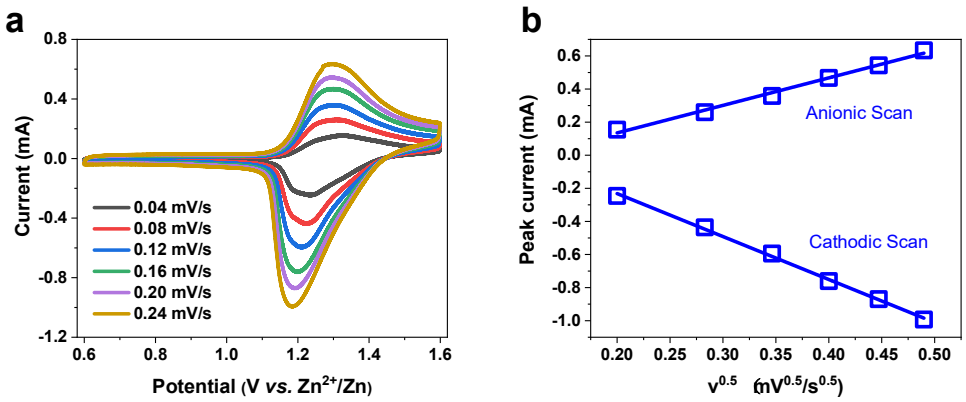

Figure 4.29 (a) The CV profiles with sweeping current density ranging from 0.04 to 0.24 mV s^{-1}. (b) Liner fits of peak currents with square root of sweeping current density.

Based on the benign rate capability, we then evaluated the performance of Zn-I_2 batteries with Zn-BTC membrane at high-current of 1920 mA g^{-1}. After initial capacity drop, the specific capacity maintained an ultra-stable profile over 6000 cycles, with a specific capacity of 85 mAh g^{-1} and high average Coulombic efficiency of 99.65% (**Figure 4.30a**). Moreover, the discharge/charge cycles exhibited almost overlapped voltage profiles (**Figure 4.30b**). Comparatively, Zn-I_2 cell with glass fiber separator presented a fast capacity declining owing to comprehensive electrode degradation (**Figure 4.30a**).

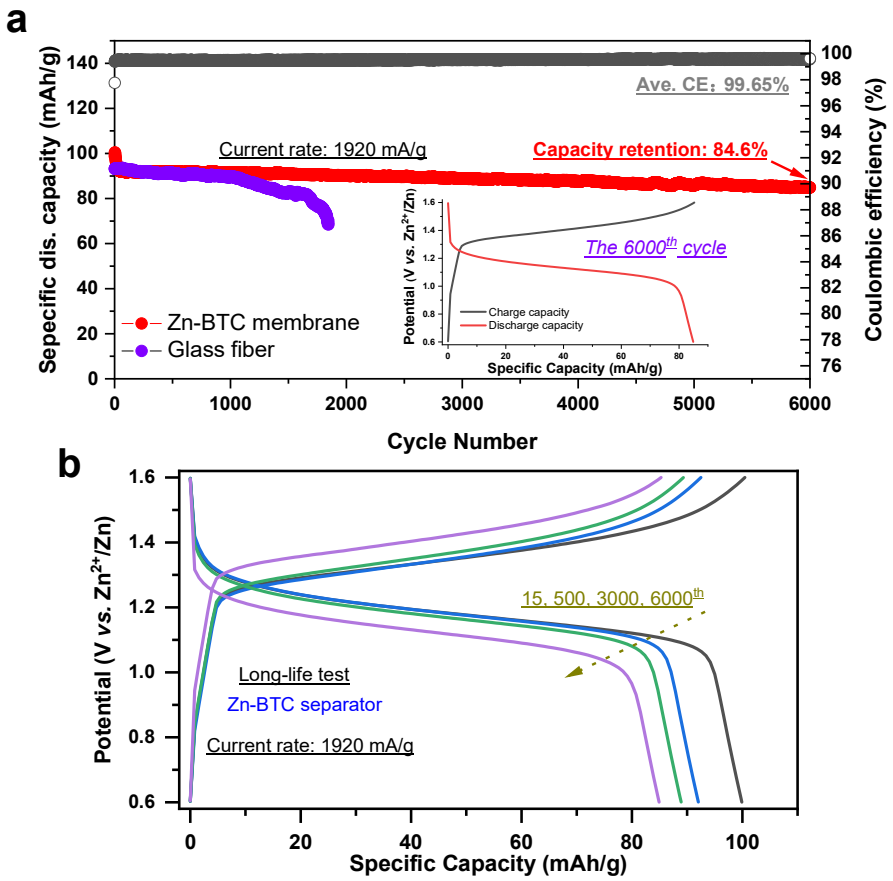

Figure 4.30 (a) The Zn-I_2 cell cycled at current density of 1920 mA g^{-1} with different separators. (b) The discharge/charge voltage profiles of Zn-I_2 cell with Zn-BTC membrane.

4.7 Summary and conclusions

In conclusion, in this work, we contributed to reveal the electrode degradation mechanism and a multifunctional Zn-BTC membrane for Zn-I_2 battery system. By advanced space-resolution characterizations, we originally discovered the negative impact of water molecular and iodine species to the Zn metal anode. Firstly, water molecular involves a passivation reaction, leaving ZnO and $Zn(OH)_2$ layer. Besides, the free migration of I_3^- species would participate a complex interplay with $Zn(OH)_2$, which not only deconstruct the side-product layer on Zn metal surface, but also induce O_2 evolution.

Herein, the adoption of Zn-BTC membrane can effectively shield the shuttle of iodine species, which was proved by visual observation, electrochemical self-discharge test and Raman spectroscopy characterization. Moreover, the introduction of Zn-BTC membrane provided ample pores and caves for electrolyte storage and ion-pairs regulation. Based on its unique pore structure, Raman spectra revealed a highly aggressive solvation sheath. Based on the simultaneous progress on both electrodes, aqueous Zn-I_2 batteries with Zn-BTC membrane displayed an ultra-long cyclic life of 6000 cycles, high retention of 84.6% and high average Coulombic efficiency of 99.65%.

Chapter 5. General conclusions and perspectives

5.1 General conclusions

In this dissertation, we dedicated to in-depth analysis on Zn metal anode degradation mechanism and propose a MOF coating/membrane strategy to prolong Zn battery lifespan. The routine liquid electrolyte consists of lots of free water molecular and ion-pairs with loose solvated structure. Especially, the Zn^{2+} with hexahydrate would finally de-solvate the water molecular prior to redox reaction, which would induce severe passivation on Zn anode surface. We emphasized the threat of strong water activity to poor Zn anode reversibility. Inspired by the good Zn metal anode stability in highly concentrated aqueous electrolyte and the unique property of ionic sieve of MOF materials, we demonstrated a MOF coating/membrane strategy to construct a highly aggressive ion-pairs layer on Zn anode surface. Our original findings highlight the role of strong water activity for Zn anode degradation mechanism and contribute to a MOF coating/membrane strategy to resolve the related concerns. We believe that the comprehensive study in this dissertation would enlighten more insight and discovery in future better Zn batteries.

Chapter 3 systematically discussed the reactive water releasing from de-solvation process and its side-effect for Zn metal anode. Based on the in-depth understanding on electrolyte solvation structure, we proposed an effective electrolyte solvation structure regulation approach. The method using MOF materials bypasses the disadvantages (poor ionic conductivity and high viscosity) for conventional high concentrated aqueous electrolyte. We the proved the MOF with abundant pores and caves can be employed to accommodate ion-pairs of electrolytes and reject migration of most of large ion-pairs. Raman spectroscopy revealed that water activity in ZIF-7 channels was highly suppressed and the Zn^{2+}-H_2O ion-pairs was signficantly

enhanced. It indicates that ZIF-7 channels realized a highly aggressive solvation confirguation in ZIF-7 channel under electric field. Benefitted from supersaturated front surface on Zn anode surafec, the lifespan of symmetric Zn half cell was promoted to 3000 hours at 0.5 mA cm^{-2} without obvious voltage fluctiation. The lifespan of Zn-MnO_2 battery was also prolonged up to 600 cycles, with a high capacity-retention of 88.9%. However, this approach cannot satisfy for high-rate and fast-charging batteries.

Therefore, we modified the MOF channel to larger pore size, which can accomodate larger ion-pairs in Chapter 4. In this work, we demonstrate a multifunctional Zn-BTC membrane for Zn-I_2 battery system and contributed to reveal the electrode degradation mechanism. For the Zn metal anode protection, the Zn-BTC channel realized a fully CIP solvation mode, which enables highly reversible Zn electrodeposit and improve the current density to 5 mA cm^{-2}. For cathode, the liquid-liquid conversion mechanism favors fast-charging property. Moreover, the Zn-BTC membrane was proved effective to shield the shuttle of soluble iodine active species.

In all, this dissertation concentrates on the electrolyte solvation structure regulation by MOF strategy and demonstrates two types of representative aqeuous Zn batteries. One is rechargeable Zn-MnO_2 battery, which is not only the successor of primary dry cell, but also is one of the most promising for high-energy aqueous batteries. Another is aqueous Zn-I_2 battery, which can satisfy for fast-charging demands. We anticipate that this concept can be widely extended to other types aqueous and non-aqueous rechargeable batteries.

5.2 Perspectives

This dissertation reveals the side-effect of strong water activity and employs the

concept in aqueous Zn batteries. We believe this approach can have more promising applications in other types of aqueous batteries, such as safe aqueous Li-ion batteries or aqueous sodium-ion batteries. For example, in aqeuous Li-ion batteries, the strong water activity might induces severe hydrogen evolution reaction on negative electrode. Moreover, for better illustration of the Raman spectra, we used simple ZnSO4 aqueous solution for the baseline electrolyte. In the future, more investigations based on aqueous/non-aqueous hybrid baseline electrolyte can be developed.

Besides, in consideration the complicated preparation process and high cost of MOF materials, other types of porous materials (nano or micor-size) can be utilized and studied for the host materials. The requriments lie in chemical and electrochemical stability for the battery system, and portable pore size to accomodate the solvated ion-pairs. For example, the water-stable zeolite molecular sieve has a much lower cost, which favors its extensive application in the future.

In brief, as an efficient concept, the electrolyte solvation structure regulation strategy based on porous materials can be extend to a wide-spectrum energy storage system.

List of Publications

(The first two papers are related to this Ph.D. thesis.)

1. **Huijun Yang**[+], Zhi Chang[+], Yu Qiao*, Han Deng, Xiaowei Mu, Ping He, Haoshen Zhou*. Constructing a super-saturated electrolyte front surface for stable rechargeable aqueous zinc batteries. *Angewandte Chemie International Edition*, 2020, 59, 9377-9381.

2. **Huijun Yang**, Yu Qiao*, Zhi Chang, Han Deng, Ping He, Haoshen Zhou*. A metal-organic framework as a multifunctional ionic sieve membrane for long-life aqueous zinc-iodide batteries. *Advanced Materials,* 2020, 32, 2004240-2004247.

3. **Huijun Yang**, Yu Qiao*, Zhi Chang, Han Deng, Ping He, Haoshen Zhou*. A safe and sustainable lithium-ion-oxygen battery based on a low-cost dual-carbon electrodes architecture. *Advanced Materials,* 2021, 33, 2100827. DOI: 10.1002/adma.202100827.

4. **Huijun Yang**[+], Yu Qiao[+], Zhi Chang, Han Deng, Xingyu Zhu, Ruijie Zhu, Zetao Xiong, Ping He, Haoshen Zhou*. Reducing water activity by zeolite molecular sieve membrane for long-life rechargeable zinc battery. *Advanced Materials,* 2021, 2102415. DOI: 10.1002/adma.202102415.

5. **Huijun Yang**[+], Yu Qiao[+], Zhi Chang, Ping He, Haoshen Zhou. Designing cation-solvent fully coordinated electrolyte for high-energy-density lithium-sulfur full cell based on solid-solid conversion. *Angewandte Chemie International Edition*, 2021, 60, 17726-17734.

Acknowledgements

I have to admit the life in University of Tsukuba (Japan) and AIST is grinding and challenging, not because of academic pressure, but the threat of Covid-19 virus. The emergence and rapid spread of Covid-19 virus tremendously reshapes my PhD life. I wear mask to cut-off the spread the Covid-19 virus but cannot suppress mental tension in my mind. Therefore, I would like to start by thanking myself because of my endurance against changes.

I would like to express my sincere appreciation to my supervisor Professor Haoshen Zhou (University of Tsukuba and AIST). One of the most fortunate moment in my life so far was to be admitted by Prof. Zhou. In the past years, Prof. Zhou devoted himself to Lab life, consisting of day-to-day companionship and face-to-face guidance. As an experienced scholar, Prof. Zhou is keen to share his viewpoint and thinking in our regular monthly group meetings. His support in both financial and mental saved me from the tough and rambling life.

Then, I would like to thank my vice-supervisors, Prof. Masayoshi Ishida and Associate Prof. Hirohisa Aki for their care in University of Tsukuba. I also appreciate Dr. Hirokazu Kitaura and Dr. Yoo Eunjoo for discussion in PhD defense. Their suggestion indeed makes the PhD thesis and PhD defense presentation much better. Besides, I also appreciate the assistance from my group members in AIST, including Dr. Eunjoo Yoo, Mr. Jun Okagaki, Ms. Yoko. Okita, Dr. Hirokazu Kitaura, and Dr. Hirofumi Matsuda. Yoo-san, the group leader, paid most of time in Lab management and helped us a clean Lab for study. Okagaki-san is always patient when I turn to him for machine repairing. Especially, I also appreciate the help from Okita-san, who serves as secretary and helps me a lot in daily matter.

Besides, I also want to thank my fellow apprentices in AIST, Dr. Yarong Wang,

Dr. Yu Qiao, Dr. Xiang Li, Dr. Yibo He, Dr. Zhi Chang, Dr. Han Deng, Dr. Min Jia, Mr. Xin Cao, Mr. Xingyu Zhu, Mr. Jianming Sun, Mr. Ziyang Lu. They offer a peaceful atmosphere for better lab-life. Especially, I am grateful for Dr. Yarong Wang`s help in writing scholarship application in Japanese and daily matters. I also thank Dr. Qiao for his assistance in spectroscopy study. Besides, I appreciate Bro-Zhi for sincere sharing his attitudes toward everything with me when we ride around the villages, rivers, and lakes in Tsukuba and Tsuchiura.

Moreover, I am also very grateful for the assistance from my former colleagues in Shanghai Jiao Tong University, Prof. Jiulin Wang, Mr. Jiahang Chen, Dr. Zhixin Xu, Dr. Jingyu Lei and Mr. Huichao Lu for their help and discussion in my research. My gratitude also goes to my friends, Mr. Hancheng Yuan, Mr. Bin Lei, Mr. Cheng Guo, Mrs. Xiaoyan Hou and Mrs. Xin Zhou for your outspoken chat. I am also thankful for Mr. Ruijie Zhu from Hokkaido University. Bro-Jie always unstintingly share with me his knowledge and understating on research.

Lastly, my deepest gratitude belongs to my family. My parents, Mr. Daohuan Yang and Mrs. Shuizhen Yang offer me care, support and love through the childhood and my student-career life. Their invaluable qualities, such as reliability, perseverance, optimism, and humor have greatly impressed me and shaped me. For my grandmother, Meirong Wang, I believe she is a unique educator because of her genial personality and benevolent of saving me from an ignorant child to a strong man. I pray for him a peaceful and well-being life in her twilight years. Besides, I cannot wait to share the happiness with my siblings and my little nephew when I return to my home country. Life is hard, but never in the time with my girlfriend. I am looking forward to embracing changes with you in the future.

Writing in Tsukuba, Japan, 2021-06-20

References

1. York, R., Do alternative energy sources displace fossil fuels? *Nat. Clim. Change* **2012,** *2* (6), 441-443.

2. Martins, F.; Felgueiras, C.; Smitkova, M.; Caetano, N., Analysis of fossil fuel energy consumption and environmental impacts in European countries. *Energies* **2019,** *12* (6), 964.

3. Galloway, W. E.; Hobday, D. K., *Terrigenous clastic depositional systems: applications to fossil fuel and groundwater resources*. Springer Science & Business Media: 2012.

4. Leonard, M. D.; Michaelides, E. E.; Michaelides, D. N., Energy storage needs for the substitution of fossil fuel power plants with renewables. *Renew. Energy* **2020,** *145*, 951-962.

5. Deese, D. A., Energy: economics, politics, and security. *Int. Secur.* **1979,** *4* (3), 140-153.

6. Lund, H., Renewable energy strategies for sustainable development. *Energy* **2007,** *32* (6), 912-919.

7. Dincer, I., Renewable energy and sustainable development: a crucial review. *Renew. Sust. Ener. Rev.* **2000,** *4* (2), 157-175.

8. Yang, Y.; Bremner, S.; Menictas, C.; Kay, M., Battery energy storage system size determination in renewable energy systems: A review. *Renew. Sust. Ener. Rev.* **2018,** *91*, 109-125.

9. Bhatia, R. S.; Jain, S.; Jain, D. K.; Singh, B. In *Battery energy storage system for power conditioning of renewable energy sources*, 2005 International Conference on Power Electronics and Drives Systems, IEEE: 2006; pp 501-506.

10. Amrouche, S. O.; Rekioua, D.; Rekioua, T.; Bacha, S., Overview of energy

storage in renewable energy systems. *Int. J. Hydrog. Energy* **2016,** *41* (45), 20914-20927.

11. Aneke, M.; Wang, M., Energy storage technologies and real life applications–A state of the art review. *Appl. Energy* **2016,** *179*, 350-377.

12. Xu, K., Nonaqueous liquid electrolytes for lithium-based rechargeable batteries. *Chem. Rev.* **2004,** *104* (10), 4303-4417.

13. Xu, K., Electrolytes and Interphases in Li-Ion Batteries and Beyond. *Chem. Rev.* **2014,** *114* (23), 11503-11618.

14. Verma, P.; Maire, P.; Novák, P., A review of the features and analyses of the solid electrolyte interphase in Li-ion batteries. *Electrochim. Acta* **2010,** *55* (22), 6332-6341.

15. Sun, Y.; Liu, N.; Cui, Y., Promises and challenges of nanomaterials for lithium-based rechargeable batteries. *Nat. Energy* **2016,** *1* (7), 16071.

16. Bruce, P. G.; Freunberger, S. A.; Hardwick, L. J.; Tarascon, J.-M., Li-O-2 and Li-S batteries with high energy storage. *Nat. Mater.* **2012,** *11* (1), 19-29.

17. Lu, Y.; Chen, J., Prospects of organic electrode materials for practical lithium batteries. *Nat. Rev. Chem.* **2020,** *4* (3), 127-142.

18. Doughty, D. H.; Roth, E. P., A general discussion of Li ion battery safety. *Electrochem. Soc. Interface* **2012,** *21* (2), 37.

19. Tarascon, J.-M., Is lithium the new gold? *Nat. Chem.* **2010,** *2* (6), 510-510.

20. Glicksman, R., The Performance of Zinc, Magnesium and Aluminum Primary Cell Anodes. A Review. *J. Electrochem. Soc.* **1959,** *106* (5), 457.

21. Wranglén, G., Dendrites and growth layers in the electrocrystallization of metals. *Electrochim. Acta* **1960,** *2* (1-3), 130-143.

22. Despic, A.; Diggle, J.; Bockris, J. M., Mechanism of the formation of zinc dendrites. *J. Electrochem. Soc.* **1968,** *115* (5), 507.

23. Bockris, J. M.; Nagy, Z.; Damjanovic, A., On the deposition and dissolution of

zinc in alkaline solutions. *J. Electrochem. Soc.* **1972,** *119* (3), 285.

24. Song, M.; Tan, H.; Chao, D.; Fan, H. J., Recent Advances in Zn-Ion Batteries. *Adv. Funct. Mater.* **2018,** *28* (41), 1802564.

25. Mertens, J., Shocks and sparks: the voltaic pile as a demonstration device. *Isis* **1998,** *89* (2), 300-311.

26. Grønneberg, T.; Kvittingen, L.; Eggen, P.-O., Small-scale and low-cost galvanic cells. *J. Chem. Educ.* **2006,** *83* (8), 1201.

27. Jenson, G.; Singh, G.; Bhama, J. K.; Ratner, A., Hydrogel Leclanché Cell: Construction and Characterization. *Energies* **2020,** *13* (3), 594.

28. Coleman, J. J., Dry Cell Dynamics: The Bobbin. *Trans. Electrochem. Soc.* **1946,** *90* (1), 545.

29. Cheng, J.; Zhang, L.; Yang, Y.-S.; Wen, Y.-H.; Cao, G.-P.; Wang, X.-D., Preliminary study of single flow zinc–nickel battery. *Electrochem. Commun.* **2007,** *9* (11), 2639-2642.

30. Parker, J. F.; Chervin, C. N.; Nelson, E. S.; Rolison, D. R.; Long, J. W., Wiring zinc in three dimensions re-writes battery performance—dendrite-free cycling. *Energy Environ. Sci.* **2014,** *7* (3), 1117-1124.

31. Xu, C.; Li, B.; Du, H.; Kang, F., Energetic zinc ion chemistry: the rechargeable zinc ion battery. *Angew. Chem. Int. Ed.* **2012,** *51* (4), 933-935.

32. Naveed, A.; Yang, H.; Shao, Y.; Yang, J.; Yanna, N.; Liu, J.; Shi, S.; Zhang, L.; Ye, A.; He, B., A Highly Reversible Zn Anode with Intrinsically Safe Organic Electrolyte for Long-Cycle-Life Batteries. *Adv. Mater.* **2019,** *31* (36), 1900668.

33. Naveed, A.; Yang, H.; Yang, J.; Nuli, Y.; Wang, J., Highly Reversible and Rechargeable Safe Zn Batteries Based on a Triethyl Phosphate Electrolyte. *Angew. Chem. Int. Ed.* **2019,** *58* (9), 2760-2764.

34. Wang, N.; Dong, X.; Wang, B.; Guo, Z.; Wang, Z.; Wang, R.; Qiu, X.; Wang, Y.,

Zinc-Organic Battery with a Wide Operation-Temperature Window from -70 to 150 degrees C. *Angew. Chem. Int. Ed.* **2020,** *59* (34), 14577-14583.

35. Cao, L.; Li, D.; Pollard, T.; Deng, T.; Zhang, B.; Yang, C.; Chen, L.; Vatamanu, J.; Hu, E.; Hourwitz, M. J.; Ma, L.; Ding, M.; Li, Q.; Hou, S.; Gaskell, K.; Fourkas, J. T.; Yang, X. Q.; Xu, K.; Borodin, O.; Wang, C., Fluorinated interphase enables reversible aqueous zinc battery chemistries. *Nat. Nanotechnol.* **2021**. https://doi.org/10.1038/s41565-021-00905-4

36. Parker, J. F.; Chervin, C. N.; Pala, I. R.; Machler, M.; Burz, M. F.; Long, J. W.; Rolison, D. R., Rechargeable nickel–3D zinc batteries: An energy-dense, safer alternative to lithium-ion. *Science* **2017,** *356* (6336), 415-418.

37. Kundu, D.; Adams, B. D.; Duffort, V.; Vajargah, S. H.; Nazar, L. F., A high-capacity and long-life aqueous rechargeable zinc battery using a metal oxide intercalation cathode. *Nat. Energy* **2016,** *1* (10), 16119.

38. Pan, H.; Shao, Y.; Yan, P.; Cheng, Y.; Han, K. S.; Nie, Z.; Wang, C.; Yang, J.; Li, X.; Bhattacharya, P.; Mueller, K. T.; Liu, J., Reversible aqueous zinc/manganese oxide energy storage from conversion reactions. *Nat. Energy* **2016,** *1* (5), 16039.

39. Liu, Z.; Huang, Y.; Huang, Y.; Yang, Q.; Li, X.; Huang, Z.; Zhi, C., Voltage issue of aqueous rechargeable metal-ion batteries. *Chem. Soc. Rev.* **2020,** *49* (1), 180-232.

40. Tang, B.; Shan, L.; Liang, S.; Zhou, J., Issues and opportunities facing aqueous zinc-ion batteries. *Energy Environ. Sci.* **2019,** *12* (11), 3288-3304.

41. Zhang, N.; Chen, X.; Yu, M.; Niu, Z.; Cheng, F.; Chen, J., Materials chemistry for rechargeable zinc-ion batteries. *Chem. Soc. Rev.* **2020**, 49(13), 4203-4219.

42. Hao, J.; Li, X.; Zeng, X.; Li, D.; Mao, J.; Guo, Z., Deeply understanding the Zn anode behaviour and corresponding improvement strategies in different aqueous Zn-based batteries. *Energy Environ. Sci.* **2020,** *13* (11), 3917-3949.

43. He, P.; Chen, Q.; Yan, M.; Xu, X.; Zhou, L.; Mai, L.; Nan, C.-W., Building better

zinc-ion batteries: A materials perspective. *Energy Chem* **2019,** *1* (3), 100022.

44. Wang, F.; Borodin, O.; Gao, T.; Fan, X.; Sun, W.; Han, F.; Faraone, A.; Dura, J. A.; Xu, K.; Wang, C., Highly reversible zinc metal anode for aqueous batteries. *Nat. Mater.* **2018,** *17* (6), 543-549.

45. Chang, Z.; Qiao, Y.; Wang, J.; Deng, H.; He, P.; Zhou, H., Fabricating better metal-organic frameworks separators for Li–S batteries: Pore sizes effects inspired channel modification strategy. *Energy Storage Mater.* **2020,** *25*, 164-171.

46. Jantscher, W.; Binder, L.; Fiedler, D. A.; Andreaus, R.; Kordesch, K., Synthesis, characterization and application of doped electrolytic manganese dioxides. *J. Power Sources* **1999,** *79* (1), 9-18.

47. Yaghi, O.; Li, H.; Groy, T., Construction of porous solids from hydrogen-bonded metal complexes of 1, 3, 5-benzenetricarboxylic acid. *J. Am. Chem. Soc.* **1996,** *118* (38), 9096-9101.

48. Xu, L.; Choi, E.-Y.; Kwon, Y.-U., Ionothermal synthesis of a 3D Zn–BTC metal-organic framework with distorted tetranuclear [Zn_4(μ4-O)] subunits. *Inorg. Chem. Commun.* **2008,** *11* (10), 1190-1193.

49. Dong, H.; Li, J.; Guo, J.; Lai, F.; Zhao, F.; Jiao, Y.; Brett, D. J. L.; Liu, T.; He, G.; Parkin, I. P., Insights on Flexible Zinc-Ion Batteries from Lab Research to Commercialization. *Adv. Mater.* **2021**, *33* (20), e2007548.

50. Han, C.; Li, W.; Liu, H. K.; Dou, S.; Wang, J., Principals and strategies for constructing a highly reversible zinc metal anode in aqueous batteries. *Nano Energy* **2020,** *74*, 104880.

51. Zheng, J.; Archer, L. A., Controlling electrochemical growth of metallic zinc electrodes: Toward affordable rechargeable energy storage systems. *Sci. Adv.* **2021,** *7* (2), eabe0219.

52. Hao, J.; Li, B.; Li, X.; Zeng, X.; Zhang, S.; Yang, F.; Liu, S.; Li, D.; Wu, C.; Guo,

Z., An In-Depth Study of Zn Metal Surface Chemistry for Advanced Aqueous Zn-Ion Batteries. *Adv. Mater.* **2020**, *32* (34), e2003021.

53. Xie, X.; Liang, S.; Gao, J.; Guo, S.; Guo, J.; Wang, C.; Xu, G.; Wu, X.; Chen, G.; Zhou, J., Manipulating the Ion-Transference Kinetics and Interface Stability for High-Performance Zinc Metal Anode. *Energy Environ. Sci.* **2020**, *13* (2), 503-510.

54. Zhang, C.; Holoubek, J.; Wu, X.; Daniyar, A.; Zhu, L.; Chen, C.; Leonard, D. P.; Rodriguez-Perez, I. A.; Jiang, J. X.; Fang, C.; Ji, X., A $ZnCl_2$ water-in-salt electrolyte for a reversible Zn metal anode. *Chem. Commun.* **2018,** *54* (100), 14097-14099.

55. Chen, C. Y.; Matsumoto, K.; Kubota, K.; Hagiwara, R.; Xu, Q., A Room-Temperature Molten Hydrate Electrolyte for Rechargeable Zinc–Air Batteries. *Adv. Energy Mater.* **2019,** *9* (22), 1900196.

56. Qiu, H.; Du, X.; Zhao, J.; Wang, Y.; Ju, J.; Chen, Z.; Hu, Z.; Yan, D.; Zhou, X.; Cui, G., Zinc anode-compatible in-situ solid electrolyte interphase via cation solvation modulation. *Nat. Commun.* **2019,** *10* (1), 5374.

57. Yang, H.; Chang, Z.; Qiao, Y.; Deng, H.; Mu, X.; He, P.; Zhou, H., Constructing a Super-Saturated Electrolyte Front Surface for Stable Rechargeable Aqueous Zinc Batteries. *Angew. Chem. Int. Ed.* **2020,** *59* (24), 9377-9381.

58. Hayes, A. C.; Kruus, P.; Adams, W. A., Raman spectroscopic study of aqueous $(NH_4)_2SO_4$ and $ZnSO_4$ solutions. *J. Solution Chem.* **1984,** *13* (1), 61-75.

59. Rudolph, W. W.; Brooker, M. H.; Tremaine, P. R., Raman spectroscopy of aqueous ZnSO 4 solutions under hydrothermal conditions: solubility, hydrolysis, and sulfate ion pairing. *J. Solution Chem.* **1999,** *28* (5), 621-630.

60. Rudolph, W. W.; Pye, C. C., Zinc (II) hydration in aqueous solution. A Raman spectroscopic investigation and an ab-initio molecular orbital study. *Phys. Chem. Chem. Phys* **1999,** *1* (19), 4583-4593.

61. Li, Y.; Liang, F.; Bux, H.; Yang, W.; Caro, J., Zeolitic imidazolate framework

ZIF-7 based molecular sieve membrane for hydrogen separation. *J. Membr. Sci.* **2010,** *354* (1-2), 48-54.

62. Gautam, M.; Verma, M.; Misra, G., Structural and optical properties of ZnO nanocrystals. *J. Biomed. Nanotech.* **2011,** *7* (1), 161-162.

63. Rudolph, W. W.; Brooker, M. H.; Tremaine, P., Raman-and infrared spectroscopic investigation of aqueous $ZnSO_4$ solutions from 8ºC to 165ºC: inner-and outer-sphere complexes. *Z. Phys. Chem.* **1999,** *209* (2), 181-207.

64. Wang, X.; Wan, Y.; Hu, W.; Chou, I.-M.; Cao, J.; Wang, X.; Wang, M.; Li, Z., In situ observations of liquid–liquid phase separation in aqueous $ZnSO_4$ solutions at temperatures up to 400°C: Implications for Zn^{2+}-SO_4^{2-} association and evolution of submarine hydrothermal fluids. *Geochim. Cosmochim. Acta* **2016,** *181*, 126-143.

65. Kruus, P.; Hayes, A. C.; Adams, W. A., Determination of ratios of sulfate to bisulfate ions in aqueous solutions by Raman spectroscopy. *J. Solution Chem.* **1985,** *14* (2), 117-128.

66. Maeda, Y.; Katsuta, A.; Nagasaki, K.; Kamiyama, M., Electrochemical and Thermal Behavior of Polyaniline in Aqueous Solution Containing SO_4^{2-} Ions. *J. Electrochem.l Soc.* **1995,** *142* (7), 2261.

67. Lu, W.; Xie, C.; Zhang, H.; Li, X., Inhibition of Zinc Dendrite Growth in Zinc-Based Batteries. *ChemSusChem* **2018,** *11* (23), 3996-4006.

68. Diggle, J.; Despic, A.; Bockris, J. M., The mechanism of the dendritic electrocrystallization of zinc. *J. Electrochem. Soc.* **1969,** *116* (11), 1503-1514.

69. Wang, K.; Xiao, Y.; Pei, P.; Liu, X.; Wang, Y., A phase-field model of dendrite growth of electrodeposited zinc. *J. Electrochem. Soc.* **2019,** *166* (10), D389.

70. Jäckle, M.; Helmbrecht, K.; Smits, M.; Stottmeister, D.; Groß, A., Self-diffusion barriers: possible descriptors for dendrite growth in batteries? *Energy Environ. Sci.* **2018**, *11* (12): 3400-3407.

71. Zheng, J.; Zhao, Q.; Tang, T.; Yin, J.; Quilty, C. D.; Renderos, G. D.; Liu, X.; Deng, Y.; Wang, L.; Bock, D. C., Reversible epitaxial electrodeposition of metals in battery anodes. *Science* **2019,** *366* (6465), 645-648.

72. Tang, Y.; Liu, C.; Zhu, H.; Xie, X.; Gao, J.; Deng, C.; Han, M.; Liang, S.; Zhou, J., Ion-confinement effect enabled by gel electrolyte for highly reversible dendrite-free zinc metal anode. *Energy Storage Mater.* **2020,** *27*, 109-116.

73. Zhou, H.; Alves, H.; Hofmann, D.; Kriegseis, W.; Meyer, B.; Kaczmarczyk, G.; Hoffmann, A., Behind the weak excitonic emission of ZnO quantum dots: ZnO/Zn $(OH)_2$ core-shell structure. *Appl. Phys. Lett.* **2002,** *80* (2), 210-212.

74. Huang, Y.; Liu, M.; Li, Z.; Zeng, Y.; Liu, S., Raman spectroscopy study of ZnO-based ceramic films fabricated by novel sol–gel process. *Mater. Sci. Eng. : B* **2003,** *97* (2), 111-116.

75. Zhang, Q.; Luan, J.; Tang, Y.; Ji, X.; Wang, H., Interfacial design of dendrite-free zinc anodes for aqueous zinc-ion batteries. *Angew. Chem. Int. Ed.* **2020,** *59* (32), 13180-13191.

76. Sun, W.; Wang, F.; Hou, S.; Yang, C.; Fan, X.; Ma, Z.; Gao, T.; Han, F.; Hu, R.; Zhu, M.; Wang, C., Zn/MnO_2 Battery Chemistry With $H(^{+})$ and $Zn(^{2+})$ Coinsertion. *J. Am. Chem. Soc* **2017,** *139* (29), 9775-9778.

77. Zhang, L.; Rodríguez-Pérez, I. A.; Jiang, H.; Zhang, C.; Leonard, D. P.; Guo, Q.; Wang, W.; Han, S.; Wang, L.; Ji, X., $ZnCl_2$ "Water-in-Salt" Electrolyte Transforms the Performance of Vanadium Oxide as a Zn Battery Cathode. *Adv. Funct. Mater.* **2019,** *29* (30), 1902653.

78. Zhao, J.; Li, Y.; Peng, X.; Dong, S.; Ma, J.; Cui, G.; Chen, L., High-voltage Zn/$LiMn_{0.8}Fe_{0.2}PO_4$ aqueous rechargeable battery by virtue of "water-in-salt" electrolyte. *Electrochem. Commun.* **2016,** *69*, 6-10.

79. Hu, P.; Yan, M.; Zhu, T.; Wang, X.; Wei, X.; Li, J.; Zhou, L.; Li, Z.; Chen, L.; Mai,

L., Zn/V_2O_5 Aqueous Hybrid-Ion Battery with High Voltage Platform and Long Cycle Life. *ACS Appl. Mater. Inter.* **2017,** *9* (49), 42717-42722.

80. Wan, F.; Zhang, Y.; Zhang, L.; Liu, D.; Wang, C.; Song, L.; Niu, Z.; Chen, J., Reversible Oxygen Redox Chemistry in Aqueous Zinc-Ion Batteries. *Angew. Chem Int. Ed.* **2019,** *58* (21), 7062-7067.

81. Kang, L.; Cui, M.; Jiang, F.; Gao, Y.; Luo, H.; Liu, J.; Liang, W.; Zhi, C., Nanoporous $CaCO_3$ Coatings Enabled Uniform Zn Stripping/Plating for Long-Life Zinc Rechargeable Aqueous Batteries. *Adv. Energy Mater.* **2018,** *8* (25), 1801090.

82. Zeng, Y.; Zhang, X.; Qin, R.; Liu, X.; Fang, P.; Zheng, D.; Tong, Y.; Lu, X., Dendrite-Free Zinc Deposition Induced by Multifunctional CNT Frameworks for Stable Flexible Zn-Ion Batteries. *Adv. Mater.* **2019,** *31* (36), e1903675.

83. Kang, Z.; Wu, C.; Dong, L.; Liu, W.; Mou, J.; Zhang, J.; Chang, Z.; Jiang, B.; Wang, G.; Kang, F.; Xu, C., 3D Porous Copper Skeleton Supported Zinc Anode toward High Capacity and Long Cycle Life Zinc Ion Batteries. *ACS Sustain Chem. Eng.* **2019,** *7* (3), 3364-3371.

84. Turekian, K. K.; Wedepohl, K. H., Distribution of the elements in some major units of the earth's crust. *Geol. Soc. Am. Bull.* **1961,** *72* (2), 175-192.

85. Konarov, A.; Voronina, N.; Jo, J. H.; Bakenov, Z.; Sun, Y.-K.; Myung, S.-T., Present and future perspective on electrode materials for rechargeable zinc-ion batteries. *ACS Energy Lett.* **2018,** *3* (10), 2620-2640.

86. Mikhaylik, Y. V.; Akridge, J. R., Polysulfide shuttle study in the Li/S battery system. *J. Electrochem. Soc.* **2004,** *151* (11), A1969-A1976.

87. Ramette, R.; Sandford Jr, R., Thermodynamics of iodine solubility and triiodide ion formation in water and in deuterium oxide. *J. Am. Chem. Soc.* **1965,** *87* (22), 5001-5005.

88. Wang, F.; Liu, Z.; Yang, C.; Zhong, H.; Nam, G.; Zhang, P.; Dong, R.; Wu, Y.;

Cho, J.; Zhang, J.; Feng, X., Fully Conjugated Phthalocyanine Copper Metal-Organic Frameworks for Sodium-Iodine Batteries with Long-Time-Cycling Durability. *Adv. Mater.* **2019**, *32* (4), 1905361.

89. Ma, J.; Liu, M.; He, Y.; Zhang, J., Iodine Redox Chemistry in Rechargeable Batteries. *Angew. Chem. Int. Ed.* **2020**. DOI: 10.1002/anie.202009871

90. Xing, M.; Zhao, Z. Z.; Zhang, Y. J.; Zhao, J. W.; Cui, G. L.; Dai, J. H., Advances and issues in developing metal-iodine batteries. *Mater. Today Energy* **2020,** *18*, 100534

91. Zhao, Q.; Lu, Y.; Zhu, Z.; Tao, Z.; Chen, J., Rechargeable Lithium-Iodine Batteries with Iodine/Nanoporous Carbon Cathode. *Nano lett.* **2015,** *15* (9), 5982-7.

92. Wang, Z.; Huang, J.; Guo, Z.; Dong, X.; Liu, Y.; Wang, Y.; Xia, Y., A Metal-Organic Framework Host for Highly Reversible Dendrite-free Zinc Metal Anodes. *Joule* **2019**, *3* (5), 1289-1300.

93. Xie, C.; Liu, Y.; Lu, W.; Zhang, H.; Li, X., Highly stable zinc–iodine single flow batteries with super high energy density for stationary energy storage. *Energy Environ. Sci.* **2019,** *12* (6), 1834-1839.

94. Yang, H.; Qiao, Y.; Chang, Z.; Deng, H.; He, P.; Zhou, H., A Metal–Organic Framework as a Multifunctional Ionic Sieve Membrane for Long-Life Aqueous Zinc–Iodide Batteries. *Adv. Mater.* **2020,** *32* (38), 2004240.

95. Qiao, Y.; Wu, S.; Sun, Y.; Guo, S.; Yi, J.; He, P.; Zhou, H., Unraveling the Complex Role of Iodide Additives in Li-O_2 Batteries. *ACS Energy Lett.* **2017,** *2* (8), 1869-1878.

96. Andrews, L.; Prochaska, E. S.; Loewenschuss, A., Resonance Raman and ultraviolet absorption spectra of the triiodide ion produced by alkali iodide-iodine argon matrix reactions. *Inorg. Chem.* **1980,** *19* (2), 463-465.

97. Bauer, I.; Thieme, S.; Brückner, J.; Althues, H.; Kaskel, S., Reduced polysulfide

shuttle in lithium–sulfur batteries using Nafion-based separators. *J. Power Sources* **2014,** *251*, 417-422.

98. Cheng, X.-B.; Peng, H.-J.; Huang, J.-Q.; Zhang, R.; Zhao, C.-Z.; Zhang, Q., Dual-Phase Lithium Metal Anode Containing a Polysulfide-Induced Solid Electrolyte Interphase and Nanostructured Graphene Framework for Lithium-Sulfur Batteries. *ACS Nano* **2015,** *9* (6), 6373-6382.

99. Li, W.; Yao, H.; Yan, K.; Zheng, G.; Liang, Z.; Chiang, Y. M.; Cui, Y., The synergetic effect of lithium polysulfide and lithium nitrate to prevent lithium dendrite growth. *Nat. Commun.* **2015,** *6*, 7436.

100. Liu, T.; Leskes, M.; Yu, W.; Moore, A. J.; Zhou, L.; Bayley, P. M.; Kim, G.; Grey, C. P., Cycling Li-O_2 batteries via LiOH formation and decomposition. *Science* **2015,** *350* (6260), 530-533.

101. Bray, W. C.; Liebhafsky, H. A., Reactions involving hydrogen peroxide, iodine and iodate ion. I. Introduction. *J. Am. Chem. Soc.* **1931,** *53* (1), 38-44.

102. Lim, H. D.; Song, H.; Kim, J.; Gwon, H.; Bae, Y.; Park, K. Y.; Hong, J.; Kim, H.; Kim, T.; Kim, Y. H.; Lepro, X.; Ovalle-Robles, R.; Baughman, R. H.; Kang, K., Superior rechargeability and efficiency of lithium-oxygen batteries: hierarchical air electrode architecture combined with a soluble catalyst. *Angew. Chem. Int. Ed.* **2014,** *53* (15), 3926-31.

103. McBreen, J., Zinc electrode shape change in secondary cells. *J. Electrochem. Soc.***1972,** *119* (12), 1620-1628.

104. Schmitt, T.; Arlt, T.; Manke, I.; Latz, A.; Horstmann, B., Zinc electrode shape-change in secondary air batteries: A 2D modeling approach. *J. Power Sources* **2019,** *432*, 119-132.

105. Zhao, Z.; Zhao, J.; Hu, Z.; Li, J.; Li, J.; Zhang, Y.; Wang, C.; Cui, G., Long-life and deeply rechargeable aqueous Zn anodes enabled by a multifunctional

brightener-inspired interphase. *Energy Environ. Sci.* **2019,** *12* (6), 1938-1949.

106. Zhang, Q.; Luan, J.; Fu, L.; Wu, S.; Tang, Y.; Ji, X.; Wang, H., The Three-Dimensional Dendrite-Free Zinc Anode on a Copper Mesh with a Zinc-Oriented Polyacrylamide Electrolyte Additive. *Angew. Chem. Int. Ed.* **2019,** *131* (44), 15988-15994.